UNIVERSITÀ DEGLI STUDI DI PALERMO

Dottorato in Ingegneria dell'Innovazione tecnologica

Dipartimento di Ingegneria

Settore Scientifico Disciplinare ING-IND/26

Synthesis and characterization of magnesium compounds recovered from exhausted brines

IL DOTTORE

Dott. Daniele La Corte

IL COORDINATORE:

Prof. Ing. Salvatore Gaglio

IL TUTOR

Prof. Ing. Giorgio Micale

CO-TUTOR

Prof. Ing. Andrea Cipollina

CICLO XXXIV

ANNO CONSEGUIMENTO TITOLO 2023

Contents

Introduction

In the current context, where environmental sustainability has become a global priority, adopting practices that promote resource efficiency and waste reduction is of paramount importance. Waste management presents a significant challenge, but at the same time, it offers a tremendous opportunity to harness the added value of materials present in waste. In this regard, the concept of a circular economy emerges as an innovative and promising approach for sustainable resource management.

This thesis aims to address this challenge through the study and valorization of high-value materials derived from waste products. The main objective is to contribute to the transition towards a circular economy, where waste is transformed into valuable resources, thereby reducing environmental impact and promoting resource efficiency.

Throughout this research, various strategies and methodologies for recovering valuable materials from specific waste streams will be explored. In particular, the focus will be on the recovery of magnesium, a critically important element for human health and with numerous industrial applications. Magnesium hydroxide has a wide range of applications and can be sold as a final product for pharmaceutical, flame retardant, and environmental protection purposes, depending on its purity, morphology, and size distribution. Furthermore, magnesium is involved in various essential biological processes, and its deficiency can lead to various pathologies. Therefore, integrating magnesium through supplements or transforming it into pharmaceutical excipients represents a significant solution to address such deficiencies.

To achieve this goal, different waste sources will be examined, including industrial process effluents, brines, and mining extraction by-products. Various recovery techniques, including crystallization, membrane technology, and laboratory analysis, will be studied and applied. Furthermore, comprehensive

characterization will be conducted to assess the purity, morphology, and physical properties of the recovered materials.

The significance of this research lies in its ability to provide innovative solutions for waste management and sustainable production of high-value materials. The valorization of waste through the extraction of high-value materials will not only contribute to reducing environmental impacts but also create economic and employment opportunities.

This research is aligned with and supported by two prominent European projects, namely ZERO BRINE and SEArcularMINE, which are focused on the recovery of raw materials from waste solutions. The ZERO BRINE project aims to recover valuable materials from industrial process brines, such as those generated in water softening and coal recovery from mines. The project involves the utilization of the MF-PFR (Multiple Feed Plug Flow Reactor) technology, which enables continuous production of magnesium hydroxide from waste brines under various conditions and the utilization of the CrIEM (Crystallization with an Ion-Exchange Membrane) technology, which allows for the recovery of magnesium from brines using a membrane-based crystallization process. The SEArcularMINE project, on the other hand, focuses on the recovery of raw materials from saltworks, an ancient and still widely used technology where natural evaporation takes place in shallow seawater basins. This traditional method allows for the concentration and fractionated crystallization of salts, including valuable trace elements. By harnessing this process, the project aims to recover various raw materials, from mining extraction by-products. The mining industry generates significant amounts of waste solutions known as bittern, which contain concentrated minerals and trace elements. By utilizing innovative techniques such as fractionated crystallization, these bitterns can be processed to extract valuable elements, including magnesium.

By exploring the potential of waste materials and developing efficient recovery processes, in conjunction with the utilization of advanced technologies such as

MF-PFR and CrIEM, this research seeks to contribute to a more sustainable and resource-efficient future. It is expected that the findings and insights obtained from this study will provide valuable knowledge and encourage further advancements in waste management and circular economy practices.

Ultimately, this research endeavors to support the global transition towards a more sustainable and circular economy, where waste is no longer seen as a burden but rather as a valuable resource for the creation of a greener and more prosperous future. By embracing the principles of a circular economy and harnessing the potential of waste materials, we can pave the way for a more sustainable and resource-efficient society, ensuring a better future for generations to come.

This thesis is structured into five chapters. The first chapter presents an overview of brine treatment processes, their improvements, and the recovery of raw materials, with a focus on magnesium. The second chapter examines the crystallization and prototype systems used to obtain high-purity magnesium hydroxide from waste brine within the Zero Brine project. This chapter's main focus is on multiple feed plug flow reactors (MF-PFR) and the characterization of the products using analytical techniques such as SEM, XRD, TGA, IC, and more.

The third chapter concentrates on membrane crystallization WP3 of the Zero Brine Project. A patented prototype, the CriEM, was used to carry out an experimental campaign with brine sourced from coal mines. The main objectives were to evaluate the product's purity and the prototype's efficiency.

The fourth chapter showcases the SEarculaMINE project, which aims to valorize products coming from saltworks. It presents a new methodology to assess the potential of a waste brine from a saltwork (bittern) in the most precise and straightforward manner possible. Additionally, an experimental campaign for recovering lithium carbonate will be illustrated.

The fifth and final chapter focuses on producing magnesium-based nutraceutical and pharmaceutical products. Magnesium hydroxide is the primary reagent used in the synthesis procedures. It was obtained from the bittern with high purity. Finally, an analytical check is conducted to assess the quality of the synthesized products.

1 Waste saline streams: disposal issue or non-conventional resource?

Brine saline solutions are solutions that come from waste saline streams. They are high-concentration solutions where sodium chloride (NaCl) is the main compound in most cases. However, the composition of these solutions can be highly variable. While high-salinity solutions can be detrimental to the environment and require proper disposal treatment, they can also contain important elements, minerals, and raw materials. Periodically, the European Union (EU) identifies certain elements or compounds as critical raw materials, which are crucial to the EU's economy and include raw materials that are both of high importance and at high risk of supply disruptions. This chapter will explain how to obtain critical raw materials from waste and potentially hazardous industrial streams, and transform the waste solutions into a non-conventional resource while minimizing their environmental impact.

1.1 A global outlook of the brine production

Water is undoubtedly the source of life on our planet, and as human activities continue to advance, the demand for water increases, leading to the need for new and alternative sources of water. Anthropogenic activities require a significant amount of water, and the processes involved often alter the water in various ways. The effluent generated from these processes contains a range of compounds, such as heavy metals, organic compounds, and hypersalinity, which require proper disposal. Generally, inorganic mineral concentrations increase, unsafe and toxic compounds enter solutions, and numerous pollutants[1] may be present. In paraghraph 1.2, I will describe the treatment required to comply with regional environmental regulations for such solutions.

An alternative source of fresh water for human consumption, domestic or industrial uses, is the desalination process. This process removes salts from

Desalination is an alternative source of fresh water for human consumption, domestic, or industrial uses, which removes salts from high-salinity water such as seawater, brackish water, or wastewater-like feed. The process separates the feed into two streams, with one stream producing freshwater and the other producing concentrated brine. The brine is the by-product of the process, and it contains most of the starting salts[2]. There are over 15,000 operative desalination plants around the world, which produce about 95 million m^3/day of freshwater and 142 million m^3/day of brine[3]. Almost half of these plants are located in the Middle East and North Africa region, where the arid climate increases the need for alternative water sources. In these areas, thermal desalination plants have been the central technology, especially in the early stages, due to the abundant availability of oil. Two examples of thermal desalination plants are the Multi-Stage Flash (MSF) and Multi-Effect Distillation (MED) plants, which remove water through evaporation from the feed water. The state transition is promoted by a temperature rise and pressure drop, and once collected, the evaporated water is salt-free.

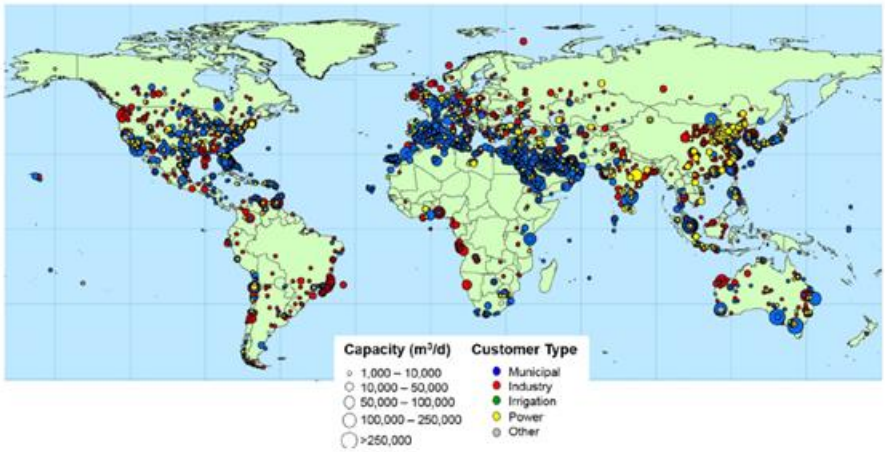

Figure 1-1: Global distribution of desalination plants with capacity higher than 1000 m^3 per day by sector user of produced water[4].

Reverse osmosis (RO) is the primary membrane technology used to produce freshwater, and since 1980, there has been a progressive shift towards this

technology. In the last twenty years, RO has grown exponentially to produce 69% of the total volume of desalinated water, with an absolute amount of 65.5 million m^3/day. RO accounts for 84% of all membrane desalination plants. The feed water passes through a specialized membrane that rejects most salts, resulting in low salinity water. High pressure is used to overcome the osmotic pressure, and dense, high-resistance membranes are necessary to withstand this process.

1.2 Disposal and environmental issue

As mentioned earlier, desalination is a solution to the global water scarcity problem, but it produces brine as a by-product. Therefore, the price to increase freshwater availability is a high salt concentration solution[4]. Improper disposal of brine can cause environmental damage. In 2015, Jin-Soo Chang[5] conducted a comprehensive analysis of the effects of desalination plants on marine pollution. Changing salt concentration or releasing chemicals used in the desalination plant can harm the marine ecosystem. Antiscalants, coagulants, biocides, and cleaning chemicals are just some of the chemicals required to operate desalination plants. Moreover, the concentrated plant stream can contain boron and heavy metals that exceed regional legal limits.

Furthermore, the main by-product is always a sodium chloride concentrated solution. Each of the compounds mentioned before can harm the marine ecosystem differently. For example, salinity reduces biodiversity, and coagulants may disturb photosynthesis. In general, the ecosystem health assessment is a potential indicator of possible water pollution from brines. The study of specific bioindicators indicates the damage caused by desalination plants, highlighting the need to dispose of these solutions properly. The most common disposal methods are surface water discharge, deep-well injection, sewer discharge, evaporation ponds, and land application[4–6]. Each method has its advantages and disadvantages in terms of costs and environmental impact,

and not all of them can be applied to high salinity solutions. In surface water discharge and deep-well injection, the effluent is discharged directly without particular pre-treatments, possibly resulting in harm to local fauna and flora. The high salinity of the brine may cause hypersaline stress, which interrupts ionic homeostasis[7]. Other methods, such as sewer discharge and soil application, cannot be used for excessively salty brines.

Evaporation ponds consist of lined earthen basins that enable the brines to evaporate through solar radiation. They are particularly suitable for managing brines with high Total Dissolved Solids (TDS). However, none of the methods mentioned, except for well-designed evaporation basins and land application, enables the recovery of resources.

Any industrial waste brine treatment process has a cost for the industry. Thus, proposing technologies able to treat brines and recover valuable materials from them is crucial nowadays because it would reduce disposal costs and implement a circular economy approach. This is why the interest in brine mining and valorization approach has rapidly increased in recent years[6,8–12].

1.3 Waste saline streams: from problem to resource

The necessity for raw materials is a vital aspect of each country's industrial sector. However, the global distribution of resources is often unequal, prompting governments to search for new resources constantly. High-value minerals are generally exploited using a traditional linear industrial approach. However, a shift towards a more sustainable use of available resources such as seawater and natural and anthropogenic brines can play an important role. These brines are generally rich in minerals, with Na^+, Mg^{2+}, Ca^{2+}, and K^+ being the most abundant, while traces of Li^+, Rb^+, and Cs^+ may also be present[13,14]. The composition of anthropogenic brines may be more variable than that of natural brines and seawater as they are usually much more saline and may contain organic compounds and heavy metals. For the most part, industrial brines are

wastes that should be disposed of appropriately, i.e., adequately treated before disposal to comply with regional environmental regulations and maintain environmental balance.

Given the considerations mentioned above, industrial waste, natural brine, and seawater can serve as alternative sources for extracting minerals such as magnesium, calcium, or trace elements. Magnesium extraction, in particular, should be taken into consideration due to its high added value. Recovering magnesium from these natural sources and waste brines is strategic for European countries, given the high supply risk and economic importance of the mineral. Additionally, the European Commission has identified magnesium as one of the 30 critical raw materials (CRMs)[15], as shown in Figure 1-2.

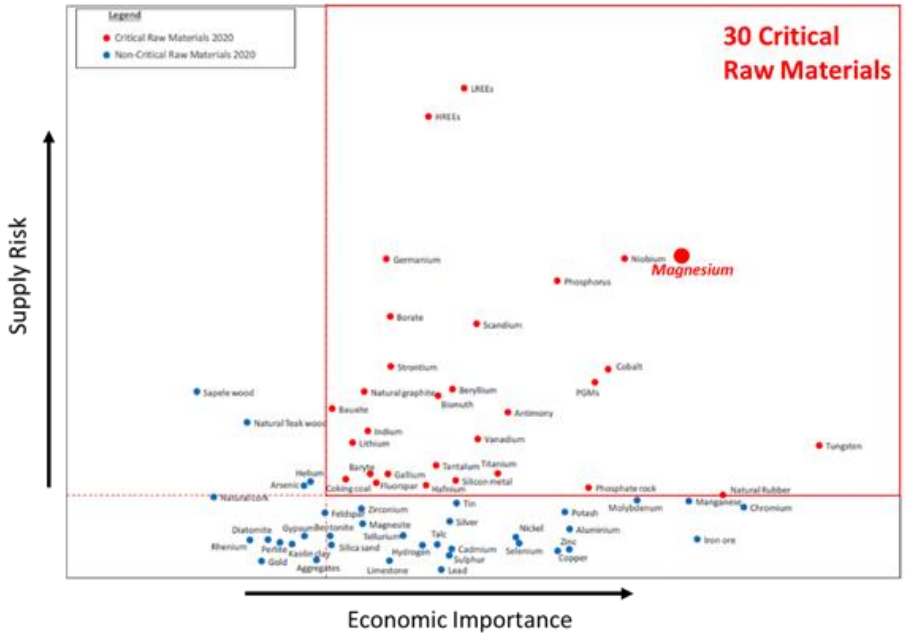

Figure 1-2:Critical raw material defined by the European Commission according to the supply risk and economic importance[15].

Table 1-1[16] presents the production of magnesium as kton of magnesium oxide equivalent in 2014. Magnesium is obtained by extracting dolomite or magnesite or derived from seawater or brine by precipitation. China, Turkey, and Russia

produce around 84% of the world's equivalent magnesium oxide production, with China alone accounting for approximately 67%. The Netherlands, the US, and Japan produce about 57% of the total equivalent magnesium oxide produced by the precipitation process from brine or seawater.

Table 1-1: Worldwide production of equivalent magnesium oxide in 2014[16].

	Magnesite		Seawater or brines		
Country	**Caustic-Calcined**	**Dead-Burned**	**Caustic-Calcined**	**Dead-Burned**	**Tot**
Australia	218	110			328
Austria	76	325			401
Brazil	96	380	12		488
Canada	100				100
China	**1440**	**2740**			4180
France			30		30
Greece	90	110			200
India	20	202			222
Iran	25	40			65
Ireland				90	90
Israel			10	60	70
Italy	25				25
Japan			**50**	**70**	120
Jordan			10	50	60
North Korea	25	100			125
Republic of Korea				40	40
Mexico			15	95	110
Netherlands			**10**	**205**	215
Norway			30		30
Poland		10			10
Russia	**380**	**2500**			2880
Saudi Arabia	39	32			71
Serbia		35			35
Slovakia		465			465
South Africa	12				12
Spain	150	70			220
Turkey	**106**	**544**			650
Ukraine		170	20	80	270
United States	140		**191**	**195**	526
Total	2940	7730	378	885	12000

Overall, the Mediterranean basin represents a promising source of magnesium hydroxide production through brine mining. This presents an opportunity for European countries to become significant global producers of magnesium compounds. magnesium hydroxide has a wide range of applications and can be sold as a final product for pharmaceutical, flame retardant, and environmental protection purposes, depending on its purity, morphology, and size

distribution. Additionally, it serves as an intermediate for producing other magnesium compounds, such as magnesium metal, magnesium oxide and organic salt of magnesium. However, to meet the purity requirements of pharmaceutical and flame retardant applications, magnesium hydroxide must be produced by precipitation from brine, making the use of industrial waste brine particularly attractive for the production of magnesium hydroxide in these industries. The current selling prices for magnesium hydroxide are approximately $2,700/tonne and $2,500/tonne for flame retardants and pharmaceuticals, respectively, making the production of magnesium hydroxide from industrial waste brine both potentially profitable and environmentally beneficial.

1.4 Strategies to recover raw materials from brine

In most cases, minerals are extracted from brine by increasing the concentration of dissolved salts until they become oversaturated and precipitate as crystals. This process involves various technologies, of which solar evaporation is undoubtedly the most common. It typically involves one or more shallow ponds where brine is gradually concentrated until minerals precipitate and can be harvested. This is essentially an elementary and approximate example of fractional crystallization. Solar evaporation has been used since ancient times, primarily to collect salt from seawater. However, this method only allows salts in high concentrations to be crystallized[8].

In the extraction of low-concentration minerals, adsorption and desorption can be employed. Selective binding of minerals can be achieved by various inorganic and organic compounds. Li, U, Sr, and Rb are important elements due to their economic value and scarcity, and their recovery has been extensively studied. Compounds like MnO_2, calcium alginate, and cobalt hexacyanoferrate have shown good adsorption capacity for these elements and can be used to recover them from seawater or industrial brine[17–19]. The common procedure involves

adsorbing the elements from the brine solution onto these compounds and then desorbing them in a small amount of solvent, followed by crystallization, usually through evaporation or reactive crystallization. While the adsorption/desorption method is relatively inexpensive, achieving good selectivity remains a challenge, and several adsorption steps may be required. Therefore, producing high-purity products is complex and expensive, particularly when dealing with high-salt brines.

Membrane-based technologies are also being adopted for recovering raw materials from pickles. In particular, Electrodialysis (ED) and Membrane Distillation Crystallization (MDC)[20–22] are the mostly studied. Both technologies take advantage of the membrane's selective properties to modify a solution's composition, usually concentrating a stream in the salts, thereby facilitating their recovery. ED uses suitably tailored Ion Exchange Membranes (IEM) and an external electrical field to facilitate ion migration. More precisely, IEMs, selective towards monovalent ions, are used to separate mono from divalent ions, thereby allowing them to be crystallized separately by a conventional method (evaporation or chemical precipitation). The high electrical power cost and scaling problems are the major technological limits[23].

Conversely, MDC uses hydrophobic microporous membranes and heat energy to obtain oversaturation conditions. Curcio et al.[24] were the first to name this MDC technology as "membrane crystallization". However, MDC is actually used to concentrate the solution, while massive crystallization is carried out in a conventional crystallizer following the MDC unit. It is a novel process derived from membrane distillation in which the solvent evaporates to increase the salt concentration. Different temperatures exist on both sides of the membrane. The solvent evaporates on the hot side and condenses on the chill side. The hydrophobic character of the membrane enables the steam to pass through itself and prevents the condensed water from coming back. This technology has been shown to ensure tight oversaturation control and consequent crystal size

distribution and morphology control[25]. Crystallization is done in a separate container to minimize the fouling of the membrane. MDC can only recover the salts exhibiting the highest concentration in the solution. Another special application of membrane crystallization involves the use of solvent/anti-solvent. Specifically, a crystallizing solution feeds the channel of the membrane module, whereas the anti-solvent is used to feed the other channel. It evaporates gradually and traverses the membrane. Once the antisolvent has reached the crystallization solution, the solubility decreases to crystallization[25,26].

Reactive crystallization is a valid alternative to recovering substances from saline solutions. It is particularly suitable to obtain sparingly soluble or insoluble compounds that may encounter a phase separation when reacting with an appropriate reactant. This method has effectively separated and recovered different ions such as AsH^{4+} and PO_3^{2-} ions, heavy metal ions, and alkaline earth metal (calcium and magnesium) ions[27–30]. Phosphates can be recuperated with magnesium as struvite, a crystal of magnesium ammonium phosphate ($(NH_4)MgPO_4{\cdot}6(H_2O)$) widely used as fertilizer. Sulphide and hydroxyl ions are suited to react with heavy metals to form a precipitate, which can be easily separated from the original solution. It is often important to remove them from effluents and brines before disposal to avoid biological accumulation and toxicity.

Many studies reported the possibility of recovering magnesium in the hydroxide form, from a saline solution by reactive crystallization[31–36] via a precipitation process driven by the addition of an alkaline reactant:

$$Mg^{2+}_{(aq)} + 2\,OH^{-}_{(aq)} = Mg(OH)_{2\,(s)}\downarrow \qquad (1\text{-}1)$$

Magnesium hydroxide has a vast market and can be sold as a final product for pharmaceutical, flame retardant and environmental protection purposes depending on its purity, morphology and size distribution. Also, it is an

intermediate for the production of other magnesium compounds (magnesium metal and magnesium oxide)[37].

In recent years, Mohammad[38] et al. and Dong et al.[39] proved the feasibility to recover magnesium hydroxide via the addition of ammonium hydroxide. They used two different artificial brines originating from a desalination plant. The main issue of this methodology is the low conversion percentage. In fact, ammonium hydroxide reacting with magnesium is transformed into ammonium forming the ammonia buffer solution. Therefore, an excess of ammonium hydroxide must be added to increase the pH and achieve a good conversion rate. An optimal NH_3/Mg molar ratio of 4.4 was found by Mohammad et al.[38]; conversely, Dong et al.[39] reported an NH_3/Mg ratio of 6.0 and a product purity of 93.5%. This over-stoichiometric amount of reactant clearly implies a significant increase in the operative cost. Moreover, the exhausted solution still contains a large amount of unreacted ammonium hydroxide, a toxic compound whose disposal is regulated by strict environmental laws, thus further increasing the cost of the recovery process and reducing its economic potential.

Cipollina et al.[36] demonstrated the recovery of magnesium from exhausted brines produced by the saltworks of Trapani, Italy. This brine is particularly rich in magnesium ions, containing about 20-30 times more magnesium than seawater. The researchers were able to recover the magnesium in the form of high-purity magnesium hydroxide by adding NaOH to the brine. They used a Continuous Stirred Tank Reactor (CSTR) to perform the reactive crystallization process, and the purity of the $Mg(OH)_2$ crystals was found to range from 98% to 100%.

In reactive crystallization, reactants are mixed together. Thus, high purity reactants are needed for this process in order not to contaminate the final product, but operating costs increase accordingly. In addition, being seawater and brines composed of many ions, choosing the most suitable alkaline reactant

is crucial to guarantee a high product purity: in the worst cases, undesired massive co-precipitations may occur[32].

Membrane technologies are also used for this purpose. In fact, a novel Ion Exchange Membrane Crystallizer (CrIEM) was developed and patented by Cipollina et al.[40] It allows the passage of ions of interest (i.e. OH^- ions) for crystallization, without the necessity of direct mixing between the two solutions, thus eliminating any problem of co-precipitation. This also allows low-cost and purity reactants or alkaline industrial waste to be used without the risk of decreasing the final product purity.

1.5 EU projects for the valorization of brines

The European Commission is funding several projects within the framework of the Horizon 2020 programme. Two of these projects are ZERO BRINE and SEArcularMINE, in which the University of Palermo (UNIPA) is a partner. The main goal of these projects is to improve research, technological development, and innovation. Part of this thesis has contributed to the completion of some sub-tasks. These projects will be described in more detail in the following sections.

1.5.1 ZERO BRINE project

The ZERO BRINE project aims to develop innovative solutions to recover resources and reduce the environmental impact of brines generated by various industries, such as water treatment, mining, and food production. By implementing circular economy principles, the project seeks to transform brines from waste streams into valuable resources, such as minerals, water, and energy. The project consortium includes 22 partners from academia, industry, and research organizations across Europe, with TU Delft leading the project.

The project aims to develop innovative technology for recovering industrial brine salts, minerals, and clean water while considering local market

specifications and reusing these resources in other areas. The goal is to facilitate a new industrial economic model that implements the circular economy concept and reduces the environmental impact of brine removal from industrial waste. Specifically, the project has several objectives: to provide economically and industrially affordable solutions with innovative technologies for recovering minerals from industrial brine, to recover at least 90% of salts, minerals, and water, to minimize disposal of solids in landfills to below 10% of the current volume, and to promote industrial symbiosis by recovering 60% of residual heat from meeting thermal energy needs. The project aims to develop different treatment chains for implementing the circular economy concept and overcoming environmental issues caused by the disposal of waste brine produced by various industrial processes. The project is structured into ten work packages (WPs), with WP2 analyzing treatment chains for the valorization of brine produced by the water industry.

WP2 focuses on the recovery and reuse of the two spent brines produced in the Demi Water Plant (Evides, Netherlands). The Demi Water Plant (Figure 1-3) includes dissolved air flotation, ion exchange resins (IXE), reverse osmosis, and mixed bed ion exchange.

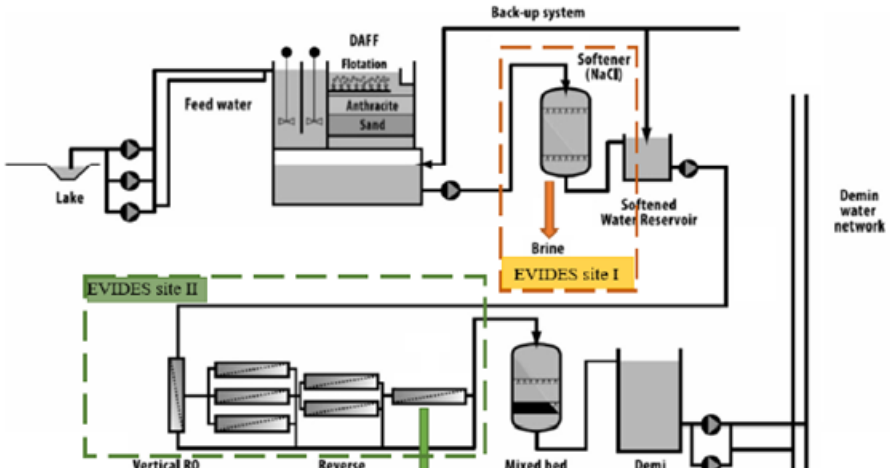

Figure 1-3: Treatment train of EVIDES demi water plant in the Botlek area. Illustration of the waste brine to be treated in ZERO BRINE PROJECT (Site One & Site Two).

During the production of demi water, the plant produces two different brines. The first one is generated during the regeneration of IEXs to reduce water hardness by removing magnesium and calcium, while the reverse osmosis process produces the second one. Therefore, the objective of WP2 is to implement two major processing lines for the valorization of these industrial brines.

The first treatment chain will treat the waste brine produced by the regeneration of ion exchange resins (IEXs) carried out by a sodium chloride solution at high concentration (from 2 up to 5 g/l). The processing chain aims to regenerate the spent brine by removing calcium and magnesium to be reused again for IXE regeneration. On the other hand, the second processing line will deal with the residual brine produced by the reverse osmosis unit. This latter treatment chain aims to exploit the waste brine by recovering minerals such as sodium bicarbonate ($NaHCO_3$), sodium sulfate (Na_2SO_4), and fresh water, to avoid any environmental release. Magnesium and calcium will be recovered as hydroxides, and the treatment chain will produce high-quality freshwater.

For EVIDES I, a schematic representation of the processing chain can be found in Figure 1-4.

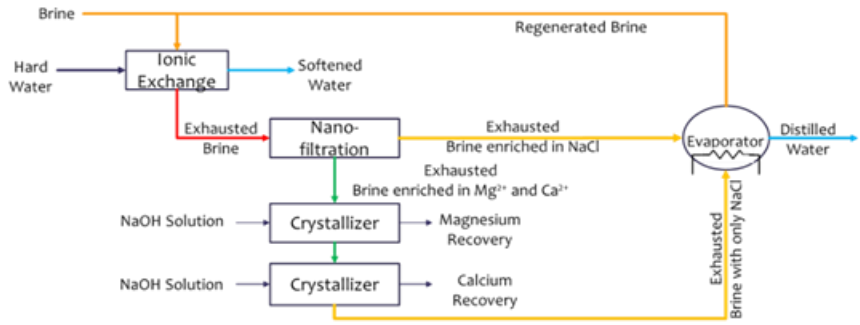

Figure 1-4: Schematics of the treatment chain proposed within the ZERO BRINE EU-H2020 project for the valorization of brines from IX water softening plants.

The process involves several units, including nano-filtration (NF), crystallization of magnesium (Mg) and calcium (Ca), and multi-effect distillation (MED), to produce permeate enriched with monovalent ions such as sodium chloride. The residual brine from the ion exchange resins (IEX) is fed to the NF unit, which produces a retentate enriched in bivalent ions such as magnesium and calcium. The retentate then undergoes selective recovery of magnesium and calcium hydroxide through chemical precipitation with an alkaline solution in a two-step crystallizer. The hydroxide slurry is separated through a continuous drum filter, and the resulting clarified brine, which is almost free of calcium and magnesium, is neutralized to pH=7 by adding hydrochloric acid. The clarified brine is then mixed with the permeate from the NF and fed to the MED unit to further concentrate the solution in sodium chloride until it reaches the appropriate target value for reuse in the IEX regeneration stage.

1.5.2 The SEArcularMINE project

The SEArcularMINE is a research and innovation project coordinated by UNIPA, and the consortium includes 12 partners from various industries, universities, and research centres. The project aims to provide the EU with raw materials through technological innovation from an alternative and internal source. One of the main challenges for the EU's economy is the continuous search for raw materials outside its borders, making it dependent on imports from third countries.

The core of this proposal is the use of saltworks, an ancient and still widely used technology where natural evaporation takes place in shallow seawater basins, allowing for fractionated crystallization. Sodium chloride is the final product, and the remaining solution at the end of the process, called bittern, is typically returned to the sea. Bittern is a solution with a high concentration of dissolved salts, with a concentration that can be up to 40 times that of seawater. During

the process, salts with lower solubility, such as calcium salts, precipitate, leaving the final solution without them. Thus, bittern is an ideal source for the recovery of valuable elements such as magnesium by reactive crystallization in the form of hydroxide, lithium, and trace elements with specific technologies developed within the project. The three technologies are:

- Reactive crystallization of $Mg(OH)_2$;
- Li-selective membrane separation;
- Selective sorption of trace elements.

The project aims to minimize the use of external resources and maximize energy efficiency to integrate the process into the circular economy approach (Figure 1-5). This approach increases financial performance with particular attention to environmental issues.

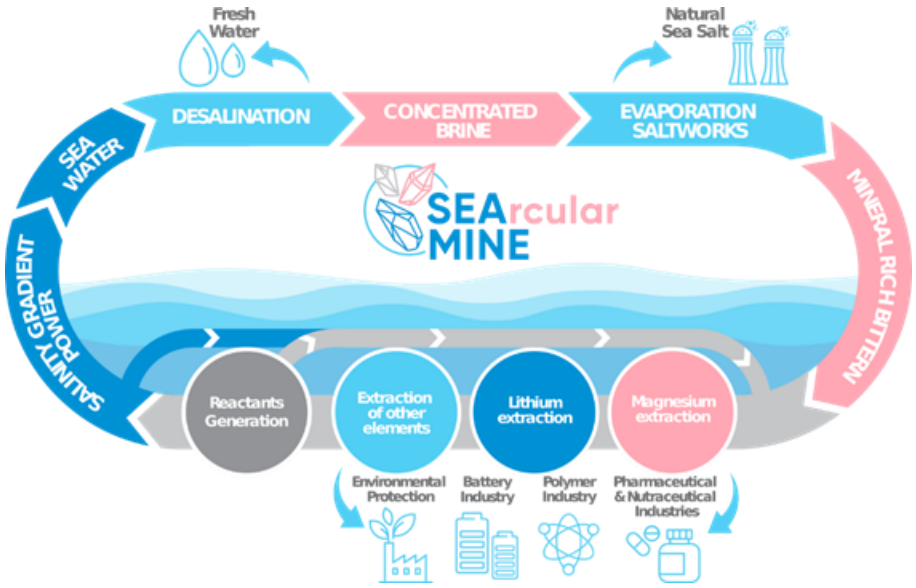

Figure 1-5: the concept of SEArcularMINE project.

The structure of the SEArcularMINE project is divided into eleven work packages (WPs). Part of this PhD thesis work contributed to the development of the objectives of WP2 and WP3. WP2 aims to search for brines or bitterns

available in the Mediterranean basin, and one of its goals is to develop a rapid procedure to evaluate the potential for mineral recovery from saline solutions, called the brine potential test. On the other hand, WP3 focuses on the study of the crystallization process for the recovery of magnesium as hydroxide and trace elements such as lithium.

1.6 Objectives of the PhD

The focus of this PhD work is to recover high-purity and quality magnesium hydroxide from exhausted brines through a reactive crystallization process, in line with the concept of an integrated cycle. The goal is to thoroughly characterize the product's morphological, chemical-physical, and microstructural properties and explore how these properties change depending on the method of production. Different technologies, reagents, and procedures were investigated, and post-processing and synthetic modifications were explored to transform magnesium hydroxide into commercially valuable derivative products, particularly organic salts.

Brines can be a valuable source of raw materials, and a quick evaluation of their potential for recovery allows for assessing their capacity. To this end, an analytical method called the Brine Potential Test (BPT) was developed, and a preliminary study on the recovery of lithium carbonate was conducted.

2 Characterization of magnesium hydroxide crystallization processes: techniques and methods

Magnesium hydroxide is an inorganic compound with slightly alkaline properties, and its solubility in water is very low. In fact, at 25°C, it is only 6.4 x 10^{-5} g/L. These characteristics make it ideal for separation from highly concentrated solutions using reactive crystallization. Many technologies utilize this principle to extract magnesium hydroxide from seawater and brine[36,41–43].

This chapter will describe several techniques used to analyze magnesium hydroxide obtained through different technologies. It will begin with the concept and theory of crystallization and then describe the technologies used to recover magnesium hydroxide, concluding with the techniques and methods used to analyze the product obtained. As will be seen later, the purity and morphology characteristics depend on the technologies and conditions used during reactive crystallization.

2.1 Crystallization theory

Crystallization is a process that involves the formation of solid particles within a homogeneous phase. This physical phenomenon can occur in various scenarios, such as the formation of particles in vapors, solidification of molten mixtures, or precipitation of species in aqueous solutions. Among the different unit operations of chemical engineering, crystallization is essential from a practical point of view. It provides a separation tool that is highly useful in the manufacturing of high-purity crystalline compounds with high industrial interest.

From a technical perspective, the product of crystallization is a suspension called magma, which is composed of a solid phase of crystals dispersed in a solution in the form of aggregates or polycrystals. The structure of a crystalline

solid, the most ordered organization of inorganic matter, is a result of the space repetition of a basic cell with a well-defined geometrical shape.

The necessary condition for the formation of a crystal within a solution is that the solute is supersaturated. This means that the species concentration must exceed its maximum solubility for its precipitation. The solubility of a substance is always a function of temperature. Many species increase their solubility with increasing temperature, while some show negligible variation with temperature. A third category of chemical species has inverse solubility, meaning that solubility decreases with increasing temperature. A solution can be supersaturated in different ways, such as by properly controlling the temperature, evaporating a fraction of the solvent, or adding a third component that alters the solubility of the solute.

Among the different methodologies that make a particular solution supersaturated, the common ion effect is worth highlighting because it is used in this PhD thesis. The common ion effect involves adding a third compound to the mother solution that has a common ion with the compound of interest that needs to be precipitated.

The physical processes responsible for the formation of a crystal in a saturated solution are nucleation and growth. Nucleation is responsible for the formation of the nuclei, which are the first stable aggregates of order above the tens units. Growth, on the other hand, is responsible for the continuous addition of solvated species in the solution and the growth of these nuclei. Both of these processes are driven by supersaturation, which is defined as the difference between the current concentration of the solution (expressed in any unit of technical use) and the equilibrium concentration.

$$\Delta C = C - C_{sat} \qquad (2\text{-}1)$$

The degree of supersaturation, which indicates when a solution is more concentrated than its equilibrium state, is given by the ratio between the actual

concentration of the solute and its saturation concentration:

$$S = \frac{C}{C_{sat}} = \frac{C_{sat}+\Delta C}{C_{sat}} = 1 + \frac{\Delta C}{C_{sat}} = 1 + s \qquad (2\text{-}2)$$

In the expression (2.2), the fractional supersaturation s is defined as a quantity that expresses the degree of supersaturation relative to a reference concentration, which is the saturation concentration[44].

Whether expressed in terms of ΔC, S, or s, the importance of supersaturation in a crystallization process can be understood by considering that solubility is a function of the particle size. This dependence is known by various names (Kelvin, Gibbs-Thomson, Gibbs-Kelvin, Ostwald-Freundlich) and shows a logarithmic relationship between the concentration and the size of the crystals:

$$\ln\left(\frac{C_{sat}(L)}{C^*_{sat}}\right) \propto \frac{1}{L} \qquad (2\text{-}3)$$

When considering particles of micrometric dimensions, it is important to note that they can be in equilibrium with a concentration $C_{sat}(L)$ that is higher than the maximum conventional solubility, denoted by C^*_{sat}. The Kelvin law reveals that to precipitate such particles, it is not sufficient to merely reach and exceed the saturation concentration C^*_{sat}. Rather, a certain degree of overcoming is required to make the equilibrium of micrometric and sub-micrometric particles unstable. However, it should be noted that as the crystal length tends towards infinity, the particle will return to equilibrium with the saturation concentration C^*_{sat} (though this mathematical infinity is physically represented by hundreds or thousands of microns).

The phenomenon responsible for the formation of crystal nuclei is nucleation. For a crystal to grow, microscopic aggregates known as nuclei must be present in solution to act as growth centres. Various types of nucleation can occur simultaneously during practical crystallization processes, including primary and secondary nucleation. Primary nucleation can be further subdivided into homogeneous or heterogeneous nucleation, depending on whether the

formation of nuclei is catalysed by the presence of solid bodies such as imported particles, the crystallizer walls, impeller blades, and so on.

Although homogeneous nucleation is the most spontaneous form of nucleation, it is rarely observed in isolation. The mechanism by which nuclei form involves continuous bimolecular collisions, where a new species is added to the lower order aggregates. As a result, the solvated particles in solution, typically clustered in structures of only a few units called clusters, transform into embryos. These embryos are unstable species that can break up and evolve into clusters or nuclei through the continuous addition of units.

However, the presence of a solid particle can act as a catalyst for the process, according to the mechanisms of heterogeneous nucleation. In this case, the process reduces the energy required due to the wetting angle formed by the nucleus and the solid phase. It is worth noting that atmospheric dust usually induces several particles in the order of 10^6, which can act as catalysts. Even with preventive filtration, this number is not less than 10^3, highlighting that nuclei formation is rarely due to simple primary nucleation.

Secondary nucleation is characterized by the presence of crystalline materials in the solution. This addition can be deliberate if the crystal size distribution needs to be controlled. However, it can also occur unintentionally due to tiny crystals dispersed in the atmosphere during collateral manufacturing activities such as transportation or solid handling. These particles act as promoters for the formation of new nuclei.

A third category, known as spurious nucleation, should be avoided in crystallization practice. Excessive supersaturation can lead to anomalous crystal growth in one direction rather than another, resulting in needle-like structures that can create new nuclei if they break. Another phenomenon to consider is the manufacture of crystals itself. The separation from the liquid phase takes place by filtration, which may leave traces of liquid on the crystals or into the crystals if they are aggregates. During the subsequent drying step, this liquid can lead

to the formation of solids on the surface of the crystals, which, when added to the solution, form new nuclei.

Regardless of their origin, each nucleus acts as a growth center during crystal formation. Theories that consider growth based on matter transport describe the phenomenon in two steps. In the first stage, the solute particle is transferred from the solution bulk to the crystal, followed by superficial diffusion towards a growth center where the ion is incorporated into the crystalline lattice.

Strictly speaking, particle growth is a function of its length. This is mainly due to the different terminal velocities with which particles of different diameters are stirred in a crystallizer. However, it is often used to approximate the crystal growth rate depending on the length. This hypothesis, known as the ΔL law, has a limited range of validity. A length greater than 500 μm affects particle fluid dynamics, resulting in a variation of the transport coefficient that is no longer negligible. On the other hand, particles with smaller dimensions than the Kolmogorov turbulent vortices are immersed in a laminar surrounding, reducing the supersaturation on the crystals (as explained by the Kelvin law)[44].

Given the complex kinetic phenomena that contribute to crystallization, mathematical modeling of nucleation and growth is often reduced to empirical relationships that assume a power supersaturation law. The nucleation relationship can be expressed as follows:

$$B^0 = k_n \cdot s^b \qquad (2\text{-}4)$$

The growth rate can be expressed in different ways. B^0 represents the nucleation speed, i.e., the number of nuclei created per unit time and volume, while k_n and the exponent n are experimentally determined parameters. The linear growth rate, defined as the variation in the crystal's length, also depends on the

supersaturation and follows a law similar to that of nucleation:

$$G = \frac{dL}{dt} = k_g \cdot s^g \qquad (2\text{-}5)$$

Alternatively, the growth rate can also be expressed as the amount of mass added to the crystals per unit time and exposed crystal area. This can be defined as the following equation:

$$R_G = \frac{1}{Ac}\frac{dm}{dt} \qquad (2\text{-}6)$$

The two expressions are linked by the volume factors vf and β, defined respectively as the ratio between the area and the square of a characteristic length of the crystal, and the relationship between the volume and the cube of the characteristic length. Substituting these expressions into the previous relation, we obtain the relationship between R_G and G

$$Ac = \beta \cdot L^2 \qquad (2\text{-}7)$$

$$m = \rho \cdot V = \rho \cdot Vf \cdot L^3 \qquad (2\text{-}8)$$

$$R_G = \frac{3\,Vf}{\beta} \cdot G \qquad (2\text{-}9)$$

The experimental values required by the kinetic equations were calculated by Alamdari et al.[45] for a batch crystallizer. The crystallizer consisted of 100 ml of a solution containing Mg^{2+} ions, to which a volume of 250 ml of 1M NaOH solution was added drop by drop. They developed a mathematical model to describe the system in terms of nucleation, growth, and agglomeration of the crystals, and compared it with experimental data. Table 2-1 presents the kinetic parameters for both real brines and synthetic solutions.

Table 2-1: Estimated kinetic parameters of growth, nucleation, and agglomeration rates of magnesium hydroxide precipitation from synthetic liquor and from sea bittern[45].

Parameter	Synthetic solution	Sea bittern
Growth rate coefficient, kg (μm s^{-1})		
Mean value	$3.01 \cdot 10^{-5}$	$3.01 \cdot 10^{-5}$
Standard error	$0.080 \cdot 10^{-5}$	$0.142 \cdot 10^{-5}$
Growth rate order with respect to supersaturation, g	1	1
Nucleation rate coefficient, k_n (# s^{-1} $g_{crystal}^{-1}$)		

Mean value	0.335	0.418
Standard error	0.0595	0.0764
Nucleation rate order with respect to supersaturation, b	3	3
Agglomeration rate coefficient, k_a ($g_{solution}$ $\#^{-1}$ s^{-1} μm^{-3})		
Mean value	$3.01 \cdot 10^{-5}$	$3.01 \cdot 10^{-5}$
Standard error	$3.01 \cdot 10^{-5}$	$3.01 \cdot 10^{-5}$
Agglomeration rate order with respect to supersaturation, a	1	1

During crystallization, nucleation and growth phenomena interact with each other, determining the final morphology and size distribution of the crystals. However, although the process can be controlled, the final result will be a population of crystals of different sizes.

The size distribution can be described through a quantity known as the crystal size distribution (CSD) function:

$$n = \lim_{\Delta L \to 0} \frac{\Delta N}{\Delta L} = \frac{dN}{dL} \qquad (2\text{-}10)$$

In the previous relation, the variable N is a crystals concentration (number of particles per unit of volume) while L is the characteristic length. The physical meaning of the newly defined population density variable is clear if it is considered the following relationship

$$n \cdot dL = dN \qquad (2\text{-}11)$$

The relation (2.10) $n = \lim_{\Delta L \to 0} \frac{\Delta N}{\Delta L} = \frac{dN}{dL}$ (2-10) is a rearrangement of (2.11) that allows for quantifying the crystal concentration with a length in the range of L and L + dL. The population density is, in turn, a function of the crystal length and can be precisely determined only in a simple crystallization process (such as in the MSMPR crystallizer). From a strictly theoretical point of view, if all the crystals have only one dimension, the function n = f(L) would be reduced to a line flattened at zero with a single peak corresponding to the diameter of the crystals. In real cases, however, this curve has a more or less restricted bell shape depending on the diameter distribution. The population density is, therefore, a sufficient function to describe the CSD. Since n(L) is only a measure of the crystal concentration at a given length, it is

useful to translate this information into a cumulative curve, i.e., to plot the integral of n, rather than n itself, as the dependent variable:

$$N(L) = \int_0^L n(L)dL \qquad (2\text{-}12)$$

This integral gives the number of particles with a diameter smaller than L and, by definition, is an increasing monotonic function. Note that in the limit, as L approaches infinity, the total number of particles is obtained:

$$N_{tot} = \int_0^\infty n(L)dL \qquad (2\text{-}13)$$

In the scientific and technical field, it is common practice to represent the cumulative curve not in absolute terms, but by comparing the quantity N(L) to the total number of particles N_{tot} and plotting the fractional quantity:

$$\frac{N(L)}{N_{tot}} = \frac{\int_0^L n(L)dL}{\int_0^\infty n(L)dL} \qquad (2\text{-}14)$$

Once again, in the ideal scenario of having a monodisperse population of particles, this curve would be reduced to a step from 0 to 1, corresponding to the characteristic length of the crystals.

The population density function and its derived magnitudes are useful as they describe the CSD and allow for the derivation of other information, such as the average characteristic length of the distribution or the coefficient of variation, which measures the amplitude of the cumulative curve.

The theory described above is important for a better understanding of the experimental results obtained in the research focused on developing new crystallizers for magnesium recovery through the crystallization process. To provide context for this work, some state-of-the-art studies on magnesium recovery from brine are described below.

2.2 Laboratory set-ups for magnesium hydroxide precipitation

A plethora of technologies and alkaline reactants have been reported in the scientific literature to obtain magnesium hydroxide[9,27,36,41–43,46–54]; as mentioned in Chapter 1, the magnesium ions react quickly with an alkaline reactant, and any source of them can be used to recover magnesium hydroxide. In fact, it has been known for a long time that an alkaline solution can precipitate magnesium hydroxide. However, the idea of recovering magnesium from saltwork waste brine is studied since 2012[9]. Cipollina et al. have demonstrated the concept feasibility using semi-batch tests. The apparatus is reported in Figure 2-1.

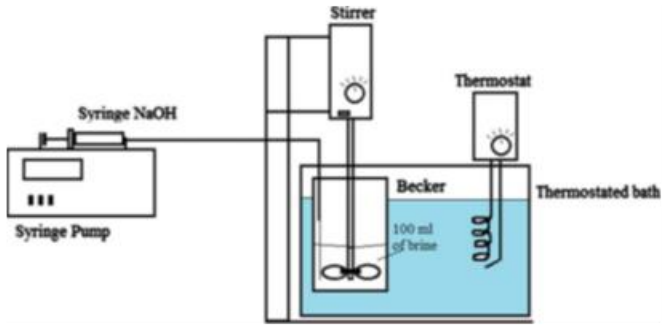

Figure 2-1: A schematic view of the experimental apparatus adopted for the reactive precipitation tests performed by Cipollina et al.[9]

The experimental configuration used by Cipollina et al.[9] was relatively simple but effective in proving the concept of recovering magnesium hydroxide from saltwork waste brine. Their reactor consisted of a 500 ml glass becher that was mechanically stirred by a small marine impeller. To perform a reactive crystallization, an over-stoichiometric NaOH solution was added to the brine using a syringe pump. All solutions were kept at a controlled temperature using a thermostatic bath. The researchers chose performance parameters such as the purity of magnesium salts produced, conversion, and filtration time, which is an indicator of crystal size. Larger crystals tend to give faster filtration times.

In their preliminary tests, Cipollina et al.[9] varied the concentration and flow rate of the alkaline solution as well as the stirring rate of the reaction medium to

investigate their effects on the purity and nucleation/growth rates of magnesium hydroxide crystals. The experiments were conducted at two different temperatures, 25°C and 40°C, to analyze the effect of temperature on the process.

Cipollina et al.[9] reported that the filtration time increased for low impeller speed, high NaOH concentration, and high temperature. They also found that the magnesium hydroxide purity was always higher than 90% with precipitation efficiency always higher than 99%. However, the primary nucleation rate was probably promoted at the expense of growth in all the cases reported.

Despite the success of the technology described above, the researchers still had to address some challenges. In particular, they needed to recover magnesium hydroxide under ZERO BRINE conditions, which have a high presence of calcium that can significantly lower the quality of the recovered magnesium hydroxide[55]. Although stoichiometric studies show that calcium and magnesium can be separated effectively, the colloidal nature of the magnesium hydroxide slurry that traps much of the mother fluid inside makes an effective recovery uncertain.

For this reason, preliminary experimental campaigns were carried out to study the feasibility of magnesium hydroxide recovery under ZERO BRINE conditions. In my PhD thesis, I first attempted to recover magnesium alone, then added calcium, and finally artificially reproduced the entire matrix with all the salts. This approach allowed us to assess the feasibility of the study and calibrate the operating conditions for continuous recovery using a prototype.

In the following section, we will examine the continuous technologies that have been employed to acquire magnesium hydroxide.

2.2.1 New crystallizers for the recovery of magnesium from brines

My PhD thesis work is not solely focused on the characterization part of the reactants or products, but it has also actively participated in the construction

and testing of various technologies. These technologies were used within the scope of the ZERO BRINE project and have been tested with real solutions. Therefore, I have gained valuable practical experience that complements the theoretical knowledge I have acquired throughout my research. In this section, I will provide a brief description of two continuous technologies used in the project.

The first technology, Multiple Feed - Plug Flow Reactor (MF-PFR)[43,51], has been the subject of two publications that attest to its functioning. The reactor was designed and tested to analyze the effect of several operative parameters. Ideally, inside a PFR reactor, the solution containing the reactants moves with a piston flow, i.e., with a speed without radial gradients, and the reaction occurs along the entire length of the reactor at a steady state, which is not a function of time but only of space. However, the piston flow hypothesis becomes only an approximation when passing from ideality to reality. The condition of no slip to the wall inevitably creates a velocity profile, and the flatness of this profile depends on the achieved fluid-dynamic regime (i.e., the size of the tube and the flow rate). Moreover, in this case, the reaction of the hydroxyl ions with the magnesium in the solution is practically instantaneous, so that the properties of the system are not a function of space but depend solely on the distribution of the reagents. Figure 2-2 shows a schematic representation of the MF-PFR reactor, where one can note the input of the feed (brine) and of the alkaline solution.

Figure 2-2: schematics of the MF-PFR reactor

The MF-PFR crystallizer, serving as the core unit for the recovery of magnesium and calcium, was meticulously designed and constructed to ensure its optimal performance. The construction process involved several technical steps. The assembly of the MF-PFR began by carefully selecting and integrating various components and instruments. These included:

- Magnetic drive centrifugal pumps: Two pumps, IWAKI mod. MD-40RZ-220 and IWAKI mod. MD-30RZ-220, were utilized. These pumps were specifically chosen for their resistance to chemical corrosion. The MD-40RZ-220 pump had a maximum flow rate of 22 L/min and a maximum head of 10 meters, while the MD-30RZ-220 pump had a maximum flow rate of 15 L/min and a maximum head of 8 meters. Both pumps operated on a 230 VAC electrical supply.

- Electric-motorized valves: Two valves, FIPNET mod. VDK/CE, were employed to precisely control the flow rates of the brine and alkaline solution.

- Magnetic inductive flow-meters: Flow measurement was facilitated by using two KHRONE mod. OPTIFLUX 4300 C magnetic inductive flow-meters. These flow-meters were calibrated to accurately measure the flow rates of the brine (0-8 L/min) and alkaline solution (0-4 L/min).

- Pressure transducers: Pressure drops in the brine and alkaline solution were monitored using two pressure transducers. The transducers used were Krohne mod. OPTIBAR P1010C and Vega mod. VegaBar 14, providing valuable feedback for process control.

- Resistance thermometer Pt100 sensors: The inlet temperatures of the brine and alkaline solution were monitored using KHRONE mod. TRA-C20 resistance thermometer Pt100 sensors. These sensors ensured precise temperature control during the process.

- pH-meter: The outlet pH was measured and monitored using a KHRONE mod. PH 8320 pH-meter, allowing for accurate pH control.
- Conductive meters: Two conductive meters, Krohne mod. PTSENS IND 1000, were employed to measure the electrical conductivity of the alkaline and brine solutions. These meters had an operational range of 0-2000 mS/cm and were equipped with resistance thermometer Pt1000.

The MF-PFR itself was constructed as a crystallizer unit, featuring coaxial plexiglass tubes (Figure 2-3). The internal tube housed the brine, while the annular section surrounding it contained the alkaline solution. The injection of brine into the annular section was facilitated through strategically positioned distributed holes, promoting efficient mixing of the reactants.

Figure 2-3: Picture of the MF-PFR crystallizer.

To ensure structural integrity and turbulence promotion, four pitch-blade-shaped spacers were positioned along the length of the inner tube. These spacers provided mechanical support, preventing deformation of the internal tube while promoting turbulent flow. All the components and instruments were meticulously connected using welded rigid PP-H (polypropylene homopolymer) pipes with an inner diameter of 16 mm and a thickness of 2 mm.

PP-H fittings were also used to maintain resistance to the highly corrosive brine and sodium hydroxide solution. The supporting structure, built using corrosion-resistant materials such as PVC sheets and aluminum-profiled bars, provided stability for the entire setup. Finally, an electrical cabinet was incorporated to house all the necessary electrical devices for the management and control of the pilot unit.

The construction of the MF-PFR involved precise selection and integration of components, ensuring durability, chemical resistance, and precise control over the process. All the sensors were electrically connected with chassis produced by National Instruments, and the computer was linked to the chassis using software such as NI Measurement & Automation Explorer (MAX). This allowed for seamless data acquisition and control.

The pipes and instrumentation were installed on a supporting structure built with corrosion-resistant materials, including PVC sheets and aluminum-profiled bars. This structure provided stability and support to the entire MF-PFR unit. It had dimensions of 116 cm in height, 98 cm in width, and 198 cm in length, accommodating the various components and instruments (Figure 2-4).

Figure 2-4: a) picture of MF-PFR in the UNIPA laboratory; b) picture of MF-PFR during the test in Netherlands.

The overall construction of the MF-PFR crystallizer involved meticulous attention to detail and adherence to material compatibility to ensure the system's reliability and longevity. By utilizing high-quality components and integrating precise control instruments, the MF-PFR was designed to facilitate the efficient recovery of magnesium and calcium through its specialized crystallization process. The successful construction of the MF-PFR prototype laid the foundation for future advancements in magnesium and calcium recovery, offering potential solutions for industrial processes and environmental sustainability.

The second technology is the Crystallizer with Ion Exchange Membrane (CrIEM)[40,42,53] (Figure 2-5). This membrane reactor separates the brine from the alkaline solution by means of an ionic exchange membrane. The OH^- ions move from the alkaline solution to the brine to alloy the precipitation of magnesium hydroxide, while the chlorides present in the brine move in the opposite direction to re-balance the electric charge. This reactor is patented[40] and has already aroused interest in many sectors of research. In the next Chapter, I will describe the CrIEM in more detail and report the results obtained with this new crystallizer. While the detailed description of these technologies is beyond the scope of my thesis, the experience I gained from their construction and operation has been invaluable to my research and adds a practical aspect to my analytical work.

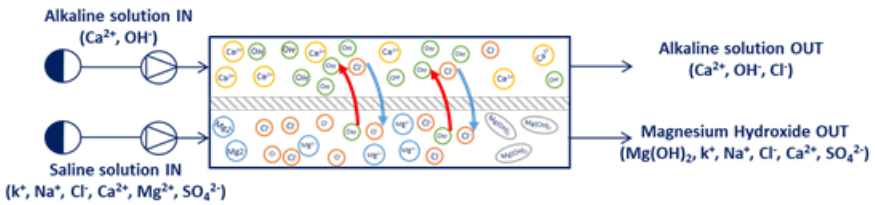

Figure 2-5: schematics of the CrIEM reactor.

2.3 Analytical techniques for the characterization of precipitated magnesium hydroxide

The technologies used to recover magnesium hydroxide were illustrated in the previous paragraph. However, the objective of this PhD thesis work is to ensure a full characterisation of the quality of the final product obtained from waste sources. Magnesium is typically obtained from a concentrated solution, which is often a waste product. This solution can come from seawater, waste brines resulting from water softening processes or coal extraction, and finally from the bittern, which is a solution resulting from the waste of saltwork processing and can contain up to 60 g/L of magnesium ions. The reaction with an alkaline reagent, typically sodium hydroxide, is effective in extracting magnesium in the form of hydroxide from this solution. However, the complex matrix of the starting material presents several problems such as co-precipitations, mother liquors trapped in the precipitated slurry, and other impurities, which may reduce the final quality of the magnesium hydroxide obtained. Therefore, after discussing the extraction technologies used, this work will illustrate the main analysis techniques used to ensure that the final product meets the required standards for the intended market.

The strategy used to derive essential information from the analysis equipment is shown in the diagram below. In the following sub-paragraphs, we will analyze the technologies used in detail, focusing on the information that can be obtained from each.

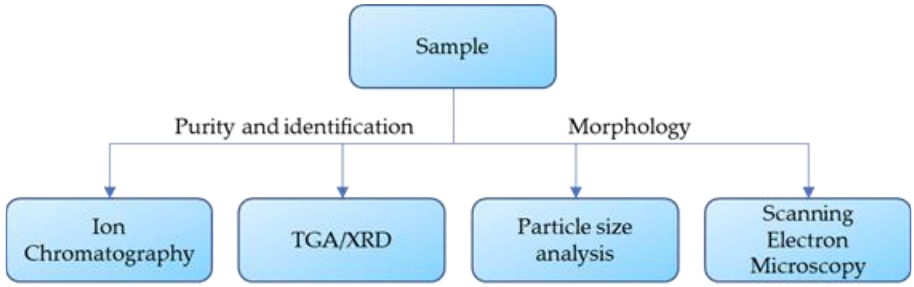

Figure 2-6: scheme of the strategy analysis used to magnesium hydroxide.

2.3.1 Ion chromatography

In the field of analytical chemistry, ion chromatography (IC) has become an increasingly popular technique for the determination of ionic solutes. The process is based on the separation of ions and polar molecules according to their charges, and it utilizes a liquid mobile phase, a separation column, and a detector to detect and measure the species eluted through the column. The Metrohm 882 Compact IC plus ion chromatography system was used to analyze the brine compositions and synthetic solutions in this study.

To achieve separation and quantification of cations and anions independently, ion exchange chromatography columns are used. These columns are filled with resins, which can be either anionic or cationic. The anionic resins possess negatively charged groups and attract positively charged species, while the cationic ones possess positively charged groups and attract negatively charged species. During the separation process, the charged species are retained on the active sites of the resin contained in the column, and the retention time increases as the charge/mass ratio increases. This means that ions with higher charges take longer to be eluted than those with lower charges.

The ion exchange chromatography process can be divided into four stages: loading of the eluent, injection of the sample to be analyzed, separation of the sample, and elution of the analytes at different times. The eluent, which is the solution used as a solvent in chromatography, is constantly pumped through

the column by means of a high-pressure pump. Once the sample is injected, it is transported by the eluent through the ion exchange column. The detector then measures the eluted species, and a computer processes the data and returns the results of the chromatographic analysis[56].

In this study, ion chromatography was used to investigate the composition of real brines and the corresponding synthetic solutions. The cationic purity of the solid obtained following filtration of the suspension produced by reactive crystallization was also evaluated using this technique. The cationic purity was calculated using equation (2.15)which takes into account the concentrations of the different cations present in the sample.

$$\frac{C_{Mg}^{S}}{\sum C_{i}^{S}} \times 100 \qquad (2\text{-}15)$$

where C_{Mg}^{S} represents the concentration of magnesium detected by ion chromatography from the dissolved solid sample, while C_{i}^{S} represent the concentration of any cation detected by ion chromatography.

The procedure for chromatographic analysis involves several steps. Firstly, the sample to be analyzed is prepared by diluting it with ultrapure water to ensure that the concentration of ions falls within the range detectable by the ion chromatograph with high precision. Next, a syringe is used to withdraw approximately 5 mL of the sample, which is then filtered using a 0.45 μm syringe filter. The filtered sample is then injected into the instrument, with 2 mL being the typical amount used for analysis. Although only 20 μL of the sample is necessary for injection, a larger quantity is preferred to ensure proper washing of the injection valve with the sample itself.

The computer connected to the instrument displays the results of the analysis. It is necessary to withdraw 5 mL initially to inject at the end of the first analysis, which uses 2 mL of the sample, and another 2 mL for repeating the analysis. The results of the two analyses are then compared, and the average value of the concentrations read by the two different analyses is calculated. In most cases,

the standard deviation is considered acceptable, and the absolute standard deviation is of the order of a few hundredths of a ppm. However, if this is not the case, further analyses of the same sample are required.

Ion chromatography was chosen for the purity analysis due to its ability to analyze the ions in a solution with high precision. The calibration results in Figure 2-7 show a correlation coefficient very close to 1, with a percentage error not exceeding 2.5%. The limit of detection, calculated as 3 times the white signal, is 0.1 ppm of the sample inserted, which needs to be multiplied by the dilution factor. Additionally, the sample's limit of quantification is 0.3 to 0.4 ppm, which also needs to be multiplied by the dilution factor.

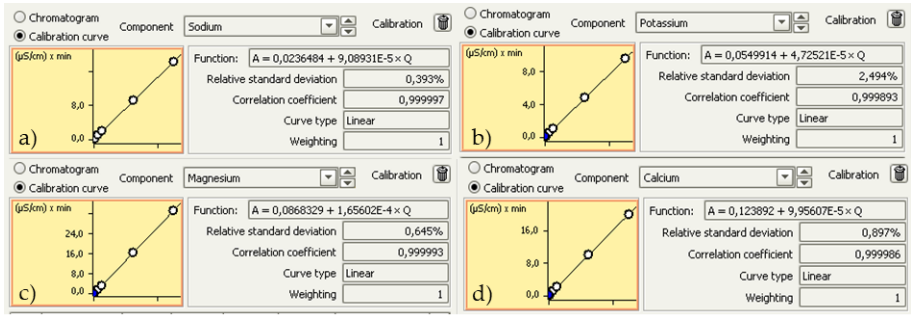

Figure 2-7: calibration curve of a) sodium ions; b) potassium ions; c) magnesium ions; d) calcium ions.

Overall, ion chromatography is an ideal technique for analyzing ions in a solution, and it does not pose any issues with starting solutions or final filtrates. By using IC, it able to obtain accurate and reliable data on the composition of the brines and synthetic solutions, as well as the purity of the resulting solid.However, for solid products like magnesium hydroxide, the solid must first be dissolved before analysis. The analysis of magnesium hydroxide will be further explored in the following paragraphs.

2.3.2 Particle size distribution analysis

The analysis of the particle size distribution of the magnesium hydroxide produced is a critical step in understanding its physical properties and behavior.

To achieve this, a Malvern Mastersizer 2000 laser granulometry is used[57]. This technique is based on the diffraction of a laser source, which encounters particles of varying sizes, causing different diffraction angles that indicate the size of each particle. The Mastersizer is designed to measure the particle size distribution of a given sample and is based on Mie theory, assuming that the particles are perfectly spherical, and the measured size is the diameter of the sphere.

To perform the measurement, the magnesium hydroxide is first dispersed inside a beaker containing distilled water using an impeller. The sample is then introduced into the optical chamber through tubes, where it is crossed by a laser beam. The interaction of the sample particles with the laser beam is detected by 51 detectors, which record the different diffraction angles. The data is then processed by the Malvern software and presented as histograms or graphs of the volumetric percentage of particles having a size less than or equal to a given measurement L as a function of dimension L or in the form of tables. The results of the particle size distribution analysis are shown in Figure 2-8.

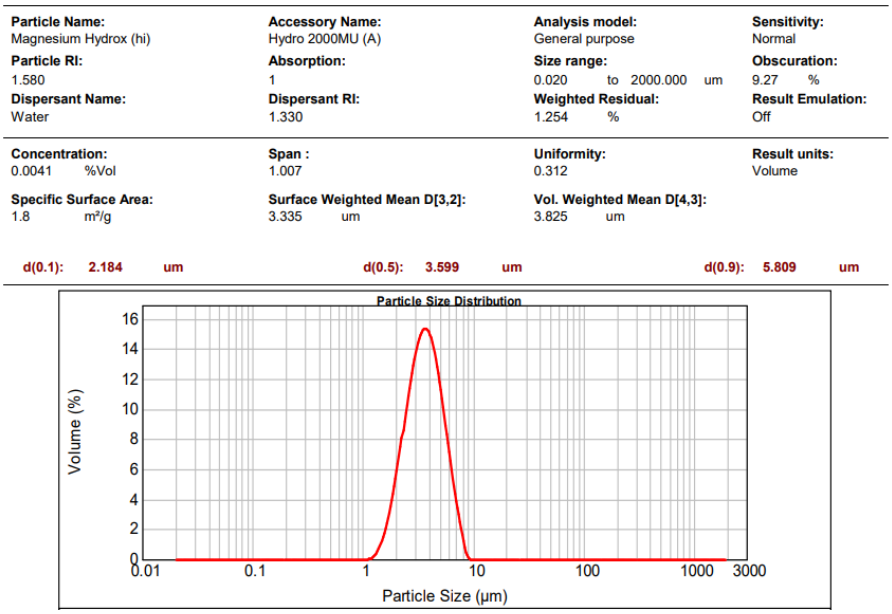

Figure 2-8: granulometric analysis of a magnesium hydroxide sample.

The granulometric distribution curve and the values D10, D50, and D90 are the main results of interest provided by the software. These values correspond to the analysis of 10%, 50%, and 90% by volume of the particles that are smaller than or equal to the corresponding values of D10, D50, and D90. In addition to these results, the software contains a database that includes the refractive indices, the absorption index of the sample, and the dispersant used (in this case, distilled water).

To ensure the accuracy of the chosen values for these quantities, it is important to verify how well the calculated data correspond to the actual measurements. This can be done by checking the residual, which should be less than 1%. If the residual is higher than 1%, it indicates that the chosen values for the refraction and absorption indices are incorrect.

Cleaning the cell is also crucial to obtaining accurate results. Any spots or dust can diffract the light and distort the measurements, so it is necessary to apply a correction by measuring the background before dispersing the sample. Additionally, the instrument must be washed with distilled water at the end of each measurement to ensure it is clean for the next use.

The software is also capable of monitoring the amount of sample present as it is added, which allows for controlling the sample concentration. This is done by monitoring the obscuration value, which represents the amount of light "lost" due to scattering or absorption when the sample is introduced relative to the entire light beam. The ideal measurement condition for the Mastersizer 2000 is when the obscuration is between 3% and 25%.

To carry out the measurement, the sample is added through a pipette until reaching an obscuration between 20% and 25% at the bottom of the machinery. The rotational speed of the impeller is set at 2000 rpm, and the analysis begins. After 5 minutes of ultrasound, further analysis is conducted since sonication tends to separate agglomerates into aggregates. One or more additional

sonication steps may be required, followed by respective acquisitions. Finally, the instrument is washed to prepare it for the next measurement.

This technique provides accurate and reliable data on the particle size distribution of the magnesium hydroxide, which is essential for understanding its behavior and performance in various applications. With this information, researchers and engineers can optimize the production process and improve the quality of the final product.

2.3.3 Thermogravimetric Analysis (TGA)

Thermogravimetry is a method used for measuring the mass variation of a material over time or as a function of temperature. This analytical technique provides a thermal decomposition curve, which is a graph that shows the changes in mass of the sample over the course of the analysis. By analyzing the curve, it is possible to determine the characteristic temperature and time at which the mass variation occurs for each substance in the sample, which in turn, enables the determination of the sample's composition.

The mass variation of a sample is associated with the reactions that the sample undergoes at certain temperatures. By measuring the mass variations, it is possible to trace the percentage by mass of certain compounds in the analyzed sample. The thermal decomposition of magnesium hydroxide is one such sample that has been extensively studied in the literature. It has been observed that the thermal decomposition of magnesium hydroxide results in a mass loss of typically between 26.8% and 28.5% over a temperature range of 200 °C to 450 °C, which is attributed to the decomposition of magnesium hydroxide $Mg(OH)_2$ into magnesium oxide MgO.

However, the measured mass drop is usually lower than the theoretical value of 30.9%, which is due to the presence of impurities and MgO. The thermal decomposition of magnesium hydroxide proceeds in three stages: $Mg(OH)_2$, MgO (deformed cubic structure), and MgO (cubic structure)[58]. This sequence

allows for the identification of three temperature intervals, each corresponding to a different stage of the thermal decomposition process of $Mg(OH)_2$.

The first stage occurs between 50 °C and 250 °C and typically shows a weight variation of 1.1-1.5%, which is linked to the release of molecular water that was present in the sample, likely due to incomplete drying or the sample preparation procedure. The second stage is the main mass variation (27.1 ÷ 27.5%) that occurs between 250 °C and 500 °C, and it is associated with the decomposition of magnesium hydroxide into magnesium oxide. The third stage shows a further loss of mass (3.2 ÷ 3.7%) between 500 °C and 800 °C, probably due to the formation of a new phase following a change in the structure of the magnesium oxide or the decomposition of intermediate structures.

Overall, thermogravimetry provides valuable information for understanding the composition and behavior of various materials under different conditions.

An example of $Mg(OH)_2$ decomposition is shown below (Figure 2-9).

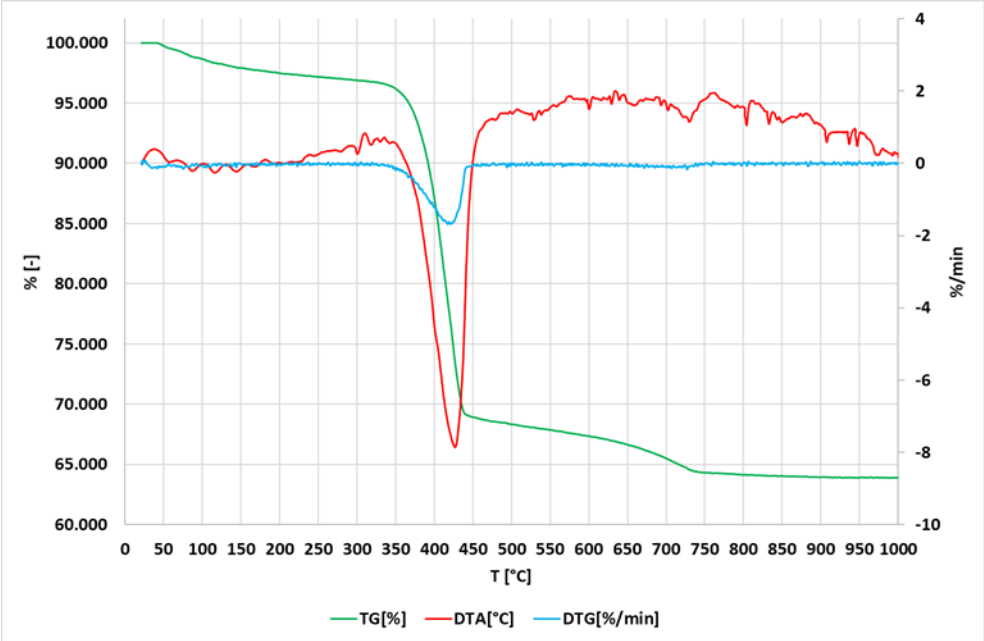

Figure 2-9: TGA spectra obtained with high purity $Mg(OH)_2$.

In thermogravimetric analysis, a graph known as the thermal decomposition curve is generated by continuously measuring the mass variation of a material over time or temperature. This curve provides valuable information about the sample's composition and the reactions it undergoes at different temperatures. The STA 449 F1Jupiter® analyzer, manufactured by NETZSCH, is a commonly used instrument for thermogravimetric analysis.

The generated graph (Figure 2-9) can be divided into three lines, each providing different information. The green line, representing the TG, shows the sample's loss in weight during heating. The red line, representing the DTA, provides data on the transformations that occurred during the heating process, such as glass transitions, crystallization, melting, and sublimation. Finally, the blue line, representing the DTG, can be used to precisely determine overlapping reactions by showing the first temperature derivative for thermal phase transitions.

The STA 449 F1Jupiter® analyzer is equipped with a precision balance that is necessary for weighing the sample. The sample, in the form of a powder, is manually inserted into a crucible, and a reference sample, such as Calcium oxalate CaC_2O_4, is present in a second crucible. The analyses are carried out at a constant heating rate of 10 ° C/min, starting from 30 ° C up to 1000 ° C, under a constant flow of high-purity nitrogen. The samples analyzed are the poor solids obtained after the cake drying formed during the filtration of the magnesium hydroxide suspensions synthesized by reactive precipitation.

The mass purity of the solids is calculated based on the results of the thermogravimetric analyzes, according to the formula:

$$Mass\ purity\ \% = \frac{m_{Mg(OH)2}}{m_{sample} - m_{H2O}} * 100 \qquad (2\text{-}16)$$

where $m_{Mg(OH)2}$ is the mass of magnesium hydroxide contained in the sample and measured based on the mass variation between 250 ° C and about 500 ° C. The m_{sample} is the sample mass weighed by the balance of the equipment used for thermogravimetric analysis and m_{H2O} is the mass of water contained in the

sample and measured by the variation in mass between about 50 ° C and 250 ° C. In particular, the mass of magnesium hydroxide contained in the sample is calculated with the equation (2-17(2.17):

$$m_{Mg(OH)2} = \frac{\Delta m_{250-500°C}}{Mw_{H2O}} * Mw_{Mg(OH)2} \quad (2\text{-}17)$$

This formula is used because, as has already been written, the mass variation in the range of 250-500 ° C is due to the loss of water due to the decomposition reaction of magnesium hydroxide into magnesium oxide.

2.3.4 X-Ray Diffraction (XRD)

X-ray diffraction is one of the most important techniques for the characterization of crystalline solids. It allows to quantify the various components of a solid sample. An X-ray beam is directed towards the sample; when X-rays interact with a crystalline phase, they are diffracted. The same substance always gives rise to the same diffraction spectrum, and in a mixture of crystalline substances, each produces its own spectrum independently of the others. Precisely because the diffraction angle is linked to the crystalline structure of the solid and its components, its measurement allows for the characterization and identification of the composition of the analyzed material and the interpretation of its structure.

Furthermore, the area underlying each peak of the diffraction spectrum obtained from the analysis is related to the amount of each component present in the sample. Therefore, from the correct spectrum interpretation, it is possible to derive the sample's composition of interest.

Figure 2-10 shows the XRD spectrum of magnesium hydroxide obtained for a real solution reported. It can distinguish two compounds: Brucite ($Mg(OH)_2$) and Calcite ($Ca(OH)_2$). This technique allows us to identify the compounds present in a sample and their relative proportions. The instrument used for the XRD is an Empyrean, Malvern PANalytical diffractometer. X-ray diffraction is

used in a variety of fields, such as materials science, geology, chemistry, and physics, to study the atomic and molecular structure of crystalline solids. It is particularly useful for identifying unknown substances and for determining the crystal structure and composition of materials. X-ray diffraction is also used to investigate the presence of defects or imperfections in crystalline solids, such as dislocations, stacking faults, and impurities.

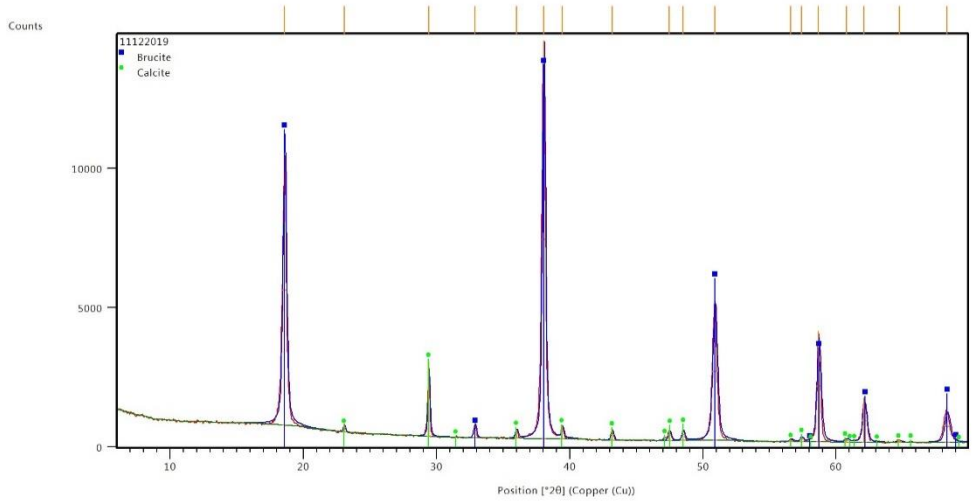

Figure 2-10: XRD patterns for magnesium hydroxides obtained by MF-PFR.

Additionally, it can be used to study the crystallographic texture of materials, which is important for understanding their mechanical and physical properties[59].

Overall, X-ray diffraction is a powerful tool for the characterization and analysis of crystalline materials, providing important information about their structure, composition, and properties.

2.3.5 Scanning Electron Microscopy

A scanning electron microscope (SEM) is a type of electron microscope that produces high-resolution images of a sample's surface. In an SEM, a small

electron probe with a diameter of 1-10 nm scans in a raster across the surface of the specimen. The specimen elastically and inelastically scatters the incident electrons, which can be used to generate images with various signals.

Elastic scattering results in large scattering angles and zigzag electron trajectories, which can cause a fraction of electrons to leave the specimen as backscattered electrons (BSE). The slowing down of electrons by inelastic scattering results in an electron range R. Electrons from the specimen atoms excited by inelastic scattering can leave the specimen as secondary electrons (SE) from a thin surface layer Asn of ca. 1-10 nm. By convention, electrons in the energy spectrum with $E \geq 50$ eV are called SE. The secondary electrons consist of (1) SE1 excited by the primary electrons; (2) SE2 excited by BSE on their path through the surface; (3) SE3 are excited when BSE strike the lower polepiece or flow (4) as SE4 through the polepiece bore.

The ionization of inner atomic shells results in either the emission of characteristic X-ray quanta (X) or Auger electrons (AE). The signal of emitted secondary electrons forms the image, backscattered electrons, Auger electrons, absorbed specimen current (SC), or X-ray quanta, which modulate the intensity of a cathode-ray tube rastered in synchronism.

Conventional SEMs work with 5-30 kV electron acceleration voltages, whereas a low-voltage scanning electron microscope (LVSEM) uses 0.5-5 kV. SEMs have a higher depth of field and better surface sensitivity than optical microscopes, making them particularly useful for studying the surface topography and composition of materials. SEMs are widely used in various fields, including materials science, nanotechnology, and biology, to name a few[59].

The ability of an alkaline solution to precipitate magnesium hydroxide from a saline solution containing Mg has been known for a long time. However, a critical aspect of this reactive crystallization process concerns the morphology of the particles and how it is influenced by the process parameters. In 2003,

Henrist et al.[60] demonstrated that magnesium hydroxide precipitates mainly in two crystal morphologies, as shown in Figure 2-11.

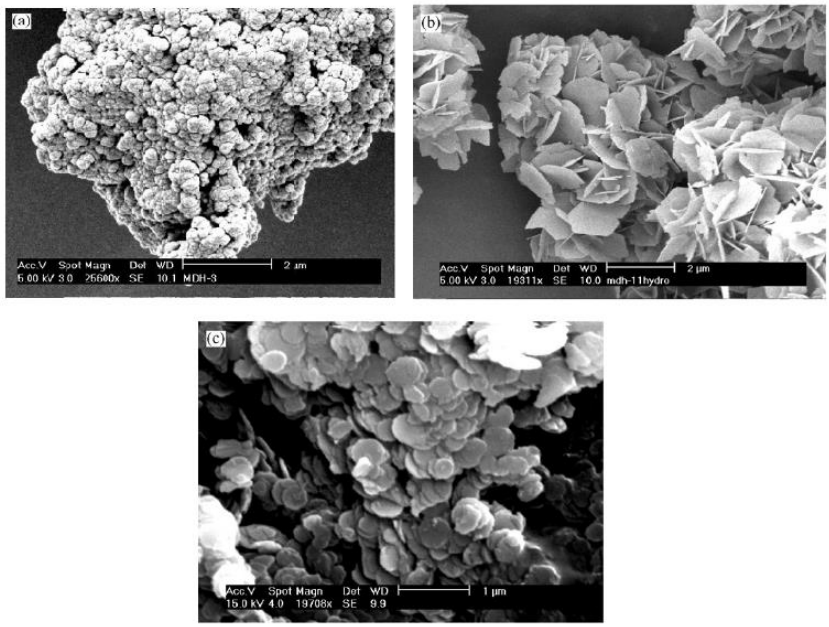

Figure 2-11: Magnesium hydroxide crystal morphology. a) globular cauliflower-like agglomerates; b) and c) platelet-shaped particles[60].

Figure 2.9a shows the typical globular cauliflower structure of magnesium hydroxide, which was also obtained with the MF-PFR. In contrast, Figures 2.9b and 2.9c show the plate-shaped particles with different aggregation states.

According to the literature, it has been demonstrated that the chemical nature of the base precipitant plays a crucial role in determining the crystal morphology. The effect of the precipitating reagent is two-fold and must be described in terms of both the pH of the crystallizing solution and the chemical nature of the cations. The pH value of the basic solution should be compared with the isoelectric point of magnesium hydroxide, which is the specific pH value that does not result in any excess charge adsorbed on the crystal surface. The isoelectric point of magnesium hydroxide has been experimentally determined to be around 12. This means that caustic soda (pH = 13) and ammonia (pH = 10)

completely reverse the sign of the adsorbed charge on the crystals. In the case of soda, the excess negative charge attracts positive ions, leading to a higher local supersaturation and nucleation increase despite the growth process.

Incorporating positive ions into the crystal lattice is a non-selective process that strongly depends on the nature of the cations in the solution. The ionic radius of the different species results in a certain steric encumbrance, leading to different impediments in adsorption compared to the magnesium ion. In the case of soda, the high mobility of the sodium ion and higher supersaturation due to excess pH near the isoelectric point cause an overabundance of nuclei. These uncontrolled growths lead to the unique globular structure of the crystalline aggregates. However, these considerations are reversed when precipitation is carried out with ammonia, resulting in lower local supersaturation and the steric impediment of the ammonium group, which enhances crystal growth, producing a more regular shape.

Temperature also has a significant effect, mainly on agglomeration behavior and particle size. The particles tend to show intergrowth at 60°C, whereas at lower temperatures, single and circular platelets are obtained, with a mean diameter depending on the synthesis and aging temperature: the lower the temperature, the higher the diameter. Varying the magnesium source modifies the chemical nature of counter-ions in the solution. Both magnesium nitrate and magnesium chloride produce the desired morphology. However, magnesium sulfate appears to promote the agglomeration of primary nuclei, and this behavior is not yet understood.

Submitting magnesium hydroxide powders in solution to a mild hydrothermal treatment has been found to induce a pronounced improvement of the morphology of the resulting particles, as well as an increase in their mean size, with a subsequent decrease in their specific surface area. Researchers Kumari et al.[61] demonstrated that $Mg(OH)_2$ microdisks, nanodisks and polyhedrons can be obtained with a hydrothermal treatment at 200 °C for 3, 12 and 48 hours,

respectively. This process can be beneficial for producing magnesium hydroxide particles with a desired morphology and size, which can impact the material's properties and functionality.

While reactive precipitation is a commonly used method for producing magnesium hydroxide, various other methods have also been proposed. These include sono-chemical, sol-gel, electrochemical, and solvo- and hydrothermal methods, as well as using microwaves, a vapor phase deposition, or the traditional use of raw minerals. Moreover, different methods have been proposed to modify the surface of magnesium hydroxide, such as using organic and inorganic compounds.

In recent years, there has been a growing interest in obtaining nanoproducts with specific particle morphologies and hydrophobic properties. This is because of the advantages that nanoscale particles can offer over larger particles, including increased surface area and reactivity, improved mechanical properties, and enhanced bioavailability.

Magnesium hydroxide with high purity and high surface specific area is particularly applicable in the pharmaceutical and nutraceutical fields. However, the morphology obtained in tests with the MF-PFR reactor is globular cauliflower (Figure 2-11 a), which is not usable as an additive in flame retardant applications. Some of the issues presented above that create globular particles are present in the reactive crystallization process from waste saltwork brine. Above all, the presence of sulfates and the use of NaOH strongly contribute to the form agglomeration of small nuclei. Understanding these factors is crucial for developing efficient and effective methods for producing magnesium hydroxide with the desired morphology and properties.

Finally, varying the magnesium source can modify the chemical nature of the counter-ions in the solution, which can affect crystal morphology. Magnesium nitrate and magnesium chloride both give rise to the desired morphology, while magnesium sulfate appears to promote the agglomeration of primary nuclei,

although this behavior is not well understood. Overall, understanding the impact of these parameters on crystal morphology is crucial for developing and controlling the synthesis of new materials with tailored properties.

2.4 Experimental procedure for precipitation test

2.4.1 Semi-batch test

The semi-batch reactor is used to carry out a preliminary study on the feasibility of recovering magnesium hydroxide. It consists of a syringe pump that injects the alkaline reagent (NaOH) into a beaker containing the brine. The solution in the beaker is stirred by a magnetic rod and a magnetic stirrer. These tests, designed to study the feasibility of magnesium recovery from complex matrix brines, were performed by recording the pH through a pH meter throughout the test.

Furthermore, the semi-batch reactor offers several advantages for the study of magnesium hydroxide recovery. The injection of NaOH into the brine allows for controlled and gradual pH adjustment, ensuring a more controlled precipitation process. The stirring of the solution using a magnetic rod and stirrer promotes homogeneity and facilitates the interaction between the reagents. The continuous monitoring of pH throughout the test provides valuable insights into the progression of the precipitation reaction and allows for precise determination of the optimal pH range for efficient magnesium hydroxide formation.

Table 2-2 and Table 2-3 summarize the operating conditions under which Test 1 with artificial solutions was carried out. Starting from solutions highly concentrated in calcium and magnesium ions, with a concentration of sodium ions equivalent to 14 g/L, it can be observed how the two alkaline earth metals can be eliminated, obtaining a good purity of the final product.

Table 2-2: recap of initial operating conditions and purity of the products obtained by semi-batch test 1.

analysis	**$[Ca^{2+}]$ in g/L**	**$[Mg^{2+}]$ in g/L**
1°(start)	23,79	2,97
2°(post filtering)	21,78	<0.10
3°(end)	<0.10	<0.10

Compounds	Purity
$Mg(OH)_2$	<97,4%
$Ca(OH)_2$	<99,8%

In fact, by repeating the same procedure with a different intermediate pH, one can see how the purity of the products increases (Table 2-3). In this case, with a final pH of 10.48, the cationic purity of the product obtained is almost total.

Table 2-3: recap of initial operating conditions and purity of the products obtained by semi-batch test 2.

analysis	**$[Ca^{2+}]$ in g/L**	**$[Mg^{2+}]$ in g/L**
1°(start)	24,12	3,08
2°(post-filtering)	22,53	<0.10
3°(end)	<0.10	<0.10

Compounds	Purity
$Mg(OH)_2$	<99,9%
$Ca(OH)_2$	<99,4%

The reaction starts from a pH value of around 6, and the 1M NaOH-water solution is slowly injected at a constant rate (60 ml/h). The pH increases quickly until a value around 9.8 (yellow point in Figure 2-12) when the magnesium hydroxide precipitation begins.

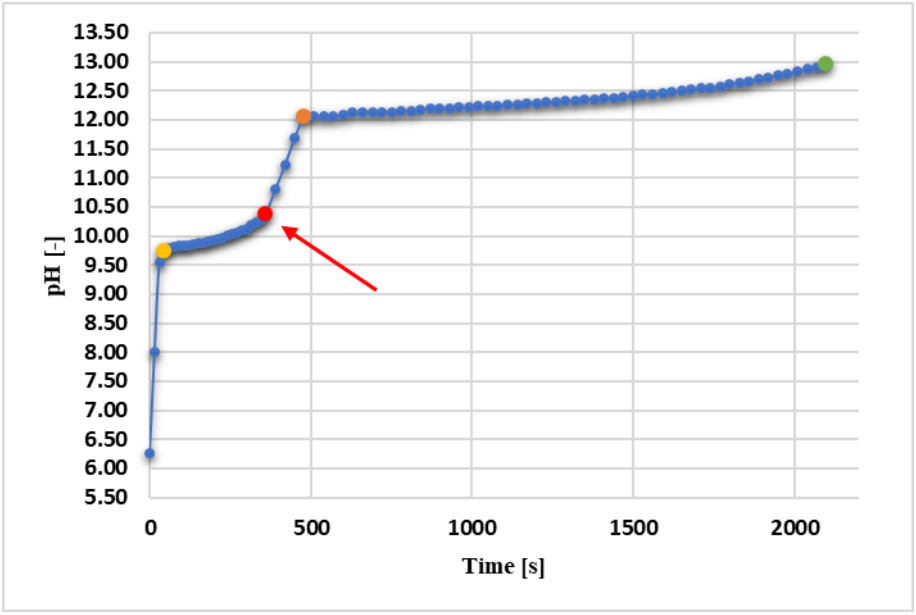

Figure 2-12: In the precipitation curve, the pH trend over time is depicted as a result of the incremental addition of a NaOH solution into a synthetic brine mimiking Zero Brine conditions.

Then, the pH rises slowly until 10.4 (red point in Figure 2-12), where magnesium can be assumed to be quantitatively precipitated. The magnesium hydroxide slurry is then filtered, and the solids are dried and analyzed. In contrast, the Mg-free filtered solution (after being analyzed) is fed to a second precipitation, where a 4M NaOH solution is used according to the same experimental procedure described above for the precipitation of $Ca(OH)_2(s)$. Also, in this case, the pH increases quickly until the value of 12.06 (orange point Figure 2-12), where calcium hydroxide precipitation starts. Afterwards, the pH rises slowly, reaching a value of around 12.4, where, theoretically, all calcium is precipitated as calcium hydroxide. The test is extended until a pH around 13 is reached (green point in Figure 2-12) to ensure that Ca^{2+} is quantitatively precipitated.

After this second precipitation step, the slurry is filtered to separate solids from the liquid and then analyzed.

The experimental results demonstrate the effectiveness of the semi-batch reactor setup in removing calcium and magnesium ions from complex matrix brines. Starting from highly concentrated solutions, the stepwise addition of NaOH at specific pH intervals results in a significant increase in the purity of the final product. By carefully controlling the pH and reaction conditions, it becomes possible to achieve nearly complete cationic purity of the magnesium hydroxide product, indicating the successful recovery of magnesium from the brine solution. After the precipitation steps, the obtained magnesium hydroxide slurry and the filtered solution containing the remaining ions are subjected to further analysis. The dried solid particles are characterized to evaluate their morphology, particle size distribution, and chemical composition.

In conclusion, the utilization of a semi-batch reactor has enabled me to conduct preliminary studies on the precipitation of magnesium hydroxide and calcium hydroxide, revealing that the process is not only feasible but also highly recommended. The results obtained from these investigations provide promising insights into the potential of this method for large-scale production. Furthermore, in the subsequent paragraphs, various analytical techniques will be employed to evaluate the quality and purity of the obtained products. Advanced characterization methods, including morphology analysis, particle size distribution measurements, and chemical composition analysis, will be utilized to assess the physical and chemical properties of the magnesium hydroxide particles. These analyses aim to ensure the high quality and suitability of the produced materials for their intended applications.

By combining the findings from the precipitation studies with the comprehensive characterization of the resulting products, a deeper understanding of the process dynamics and the optimization of operational parameters can be achieved. This knowledge will pave the way for further

advancements in the field, fostering the development of efficient and reliable production methods for magnesium hydroxide.

Overall, the successful implementation of this technology in my research has laid a solid foundation for future investigations, offering great potential for the production of high-quality magnesium hydroxide materials in various industrial applications.

2.4.2 MF-PFR test with artificial solutions: the filterability issue

Finding suitable conditions for the filtration of magnesium hydroxide is of utmost importance to enable a unit operation for separating the precipitated magnesium hydroxide from aqueous solutions. Efficient filtration plays a crucial role in the downstream processing and purification of magnesium hydroxide, allowing for its isolation and subsequent utilization in various applications.

In this part of my thesis, we not only aimed to optimize the filterability of magnesium hydroxide but also investigated the effects of different process parameters on the filtration performance. To enhance the filterability, we employed a seeding technique during the reactor start-up phase (SEED batch) or during all the process (SEED). The seeding process involved the introduction of pre-formed magnesium hydroxide particles into the reaction mixture, which acted as nuclei for crystal growth. This approach has been reported to improve the filterability of the final product by facilitating the formation of well-defined and filterable particles. Furthermore, we conducted experiments without seeding (NO SEED) to evaluate the impact of omitting the seeding step on the filtration behavior. This allowed us to compare the filterability of the slurry obtained with and without seeding, providing valuable insights into the effectiveness of the seeding technique in enhancing the filtration characteristics. To determine the optimal process conditions for filtration, we utilized the magnesium ion concentrations obtained from the ZERO BRINE project as a starting point. However, we deliberately varied the concentrations of the

precipitant (NaOH) and the flow rates to explore their influence on the filterability of magnesium hydroxide. This systematic investigation allowed us to identify the conditions that yielded the best filtration performance while considering the overall process efficiency and the desired product quality.

Subsequently, the concentrate magnesium hydroxide slurry was subjected to filtration using a Büchner filter with the same filtration cloth employed in the drum filter. The filtration cloth used in the filtration process is made of polypropylene and has a thickness of 1.9 mm. It is important to note that this specific filtration cloth is provided by NFM, a renowned supplier of filtration solutions. The polypropylene material offers excellent chemical resistance and mechanical strength, making it suitable for handling the filtration of the magnesium hydroxide slurry. Furthermore, the filtration cloth from NFM is characterized by its permeability of 5 L/dm^2/min. This parameter indicates the flow rate of liquid that can pass through the filtration cloth per unit area. The permeability value of 5 L/dm^2/min reflects the favourable porosity and hydraulic conductivity of the filtration cloth, allowing efficient liquid-solid separation during the filtration process. The filterability of the produced concentrate slurry was evaluated by measuring the filtration time and the thickness of the cake formed on the filtration cloth surface. These parameters provided valuable insights into the filtration performance and the ease of separation between the solid and liquid phases. The obtained results, summarized in Table 2-4, showcased the influence of various factors on the filterability of magnesium hydroxide. The data allowed us to assess the effectiveness of different process conditions, including seeding, in enhancing the filterability of the slurry. Additionally, we observed that an increase in the molar concentration of the alkaline solution led to longer filtration times, indicating a higher degree of particle agglomeration. This phenomenon can be attributed to the high nucleation and agglomeration rates at higher concentrations.

Table 2-4: filtration tests of 100 mL magnesium hydroxide slurry produced by MF-PFR.

test	NO SEED	SEED Batch	SEED	Mg^{2+} [g/L]	NaOH [g/l]	Q_{NaoH} [l/min]	Q_{brine} (L/min]	filtration time [s]	cake thickness [mm]
1	x			4	20	0.33	0.5	125	8
2		x		4	20	0.33	0.5	115	6.1
3			x	4	20	0.33	0.5	155	6.7
4	x			4	40	0.33	1	176	6.9
5		x		4	40	0.33	1	272	8.4
6			x	4	40	0.33	1	300	9
7	x			4	80	0.33	2	195	5.7
8		x		4	80	0.33	2	355	10.9
9			x	4	80	0.33	2	270	9.5
10	x			4	160	0.33	4	360	8.2
11		x		4	160	0.33	4	440	8.1
12			x	4	160	0.33	4	460	7.8

Understanding the relationship between process conditions, filterability, and the properties of the produced magnesium hydroxide is essential for the development of an efficient and scalable separation process. By optimizing the precipitation conditions and employing suitable filtration techniques, we can achieve high-quality magnesium hydroxide with enhanced filterability, facilitating its downstream processing and expanding its potential applications. In Figure 2-13, the relationship between the molar concentration of the alkaline solution and the filtration time is depicted.

The graph illustrates how the filtration time increases with higher concentrations of the alkaline solution. This observation suggests a correlation between the concentration of the precipitant and the filterability of the magnesium hydroxide slurry. The figure provides valuable insights into the phenomenon observed during the filtration process.

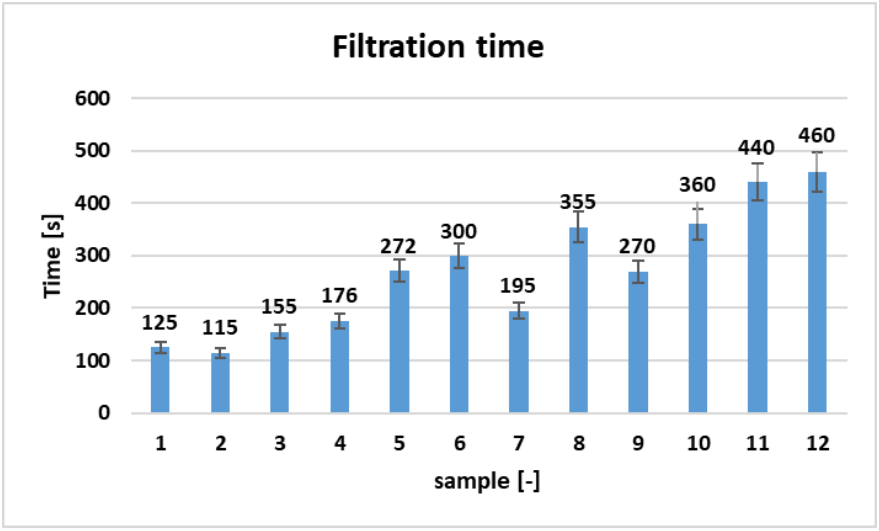

Figure 2-13: filtration time of magnesium hydroxide slurry generated by MF-PFR with industrial filter.

It indicates that a higher molar concentration of the alkaline solution leads to a longer filtration time. This phenomenon can be attributed to factors such as the nucleation rate and the agglomeration rate of the particles. The graph also highlights the importance of controlling the concentration of the alkaline solution during the precipitation process. It demonstrates that the choice of concentration significantly influences the filterability of the magnesium hydroxide slurry. By optimizing the concentration of the precipitant, it is possible to achieve improved filtration performance and enhance the overall efficiency of the separation process.

The information conveyed by Figure 2-13 provides valuable guidance for process optimization and designing filtration systems. It helps to make informed decisions regarding the selection of operating conditions to achieve the desired filterability and separation efficiency for magnesium hydroxide production. Further analysis and interpretation of the data presented in Figure 2-13, along with other experimental findings, contribute to a comprehensive understanding of the filtration behaviour of magnesium hydroxide and support the development of effective filtration strategies in industrial applications.

The results obtained from the filtration experiments, as well as the subsequent analysis of the solid product and liquid liquor, contribute to the comprehensive evaluation of the filtration process. The filtration time and the thickness of the cake formed on the filtration cloth surface serve as indicators of the ease of separation and the filterability of the magnesium hydroxide slurry. These parameters provide critical information for optimizing the filtration step and designing efficient filtration systems.

In the following sections, we will delve into the comprehensive analysis of the obtained products, focusing on parameters such as purity, particle size distribution, crystalline structure, and other relevant properties. This extensive characterization will provide valuable insights into the performance and quality of the precipitated magnesium hydroxide under different process conditions. Additionally, we will explore the potential applications of the obtained magnesium hydroxide, considering its improved filterability and purity, and discuss the implications of our findings for industrial-scale production and commercial viability.

In conclusion, the preliminary studies on the filtration of magnesium hydroxide have demonstrated the feasibility and significance of developing an efficient separation process. Through the optimization of process conditions, including seeding techniques and variations in precipitant concentrations and flow rates, we have achieved improved filterability and purity of the precipitated magnesium hydroxide. The comprehensive analysis of the obtained products using various analytical techniques will further enhance our understanding of the filtration process and enable the exploration of potential applications.

2.4.3 MF-PFR test with real solutions

Long-run experimental tests, lasting for 8 hours each, were conducted using three different feed brines obtained from different phases of ion exchange regeneration: High, Low, and Std. The High brine represented the peak phase

of releasing bivalent ions in the spent regenerant, while the Low brine represented the final phase of regeneration with lower bivalent concentrations. The Std brine, characterized by a large variability of ion concentrations, resulted from the buffering effect in the storage tank where spent regenerant was stored. The Std condition was the most commonly adopted in the experimental campaign. In Table 2 5, the average composition of three different tested brines is reported.

Table 2-5: The average composition of feed brines adopted for the precipitation tests.

Brine coming from NF	**pH**	**The concentration of main cations in solution [g/l]**				**The concentration of main anions in solution [g/l]**		
		Na^+	K^+	Ca^{2+}	Mg^{2+}	HCO_3^-	Cl^-	SO_4^{2-}
L (low TDS)	7.23	8.80	0.21	10.8	1.34	0.33	30.46	0.11
N (Std TDS)	7.03	8.29	0.24	12.6	1.76	0.11	41.21	0.55
U (High TDS)	7.00	11.49	0.24	15.8	2.51	0.14	46.38	0.65

It is worth noting that nine long-run tests were conducted with the nominal brine composition, while two spot tests were conducted with the Low and High feed brine. Detailed operative conditions for all the experiments conducted, including inlet flow-rate, outlet pH, and system performance parameters, are presented in Table 2 5 and Table 2 6. These long-run tests aimed to assess the stability and robustness of the reactor, as well as the performance of the system under different operating conditions.

Table 2-6: The Mg(OH)2(s) crystallisation experiments operational conditions.

Test run ID	**pH**	**Brine Flow Rate [l/min]**	**NaOH Flow Rate [l/min]**	**NaOH Conc. [mol/l]**
L (Low TDS 12/02/2020)	10.5	2.45	0.17	0.5

N1 (Std TDS 19/11/2019)	10.6	2.0	0.41	0.4
N2 (Nominal 21/11/2019)	10.6	2.1	0.4	0.4
N3 (Nominal 26/11/2019)	10.7	2	0.37	0.4
N4 (Nominal 28/11/2019)	10.7	2	0.37	0.4
N5 (Nominal 11/12/2019)	10.6	1.2	0.45	0.4
N6 (Nominal 13/12/2020)	10.5	1.31	0.46	0.4
N7 (Nominal 17/12/2019)	10.5	1.25	0.42	0.4
N8 (Nominal 18/02/2020)	10.35	2.66	0.38	0.5
N9 (Nominal 20/02/2020)	10.8	1.6	0.4	0.5
U (High TDS 28/02/2020)	10.25	6.1	0.34	1

The comprehensive characterization of the products obtained from the long-run experiments provides valuable insights into the system's behavior under different operating conditions. This information guides future process optimization efforts to enhance product quality, increase process efficiency, and minimize waste generation.

In subsequent sections, further analysis and evaluation of the precipitated magnesium hydroxide and calcium hydroxide products will be presented. Various analytical techniques will be employed to assess the physical, chemical, and morphological properties of the obtained solids. These analyses will

provide a more detailed understanding of the characteristics and performance of the precipitates, helping to validate the feasibility and suitability of the precipitation process. Moreover, the quality of the precipitated products will be evaluated by comparing them with desired specifications and industry standards. This assessment will aid in determining the potential applications of the obtained precipitates and their suitability for various downstream processes.

The combination of experimental data, computational analysis, and comprehensive product characterization serves as a foundation for further investigations into the optimization and scale-up of the magnesium hydroxide and calcium hydroxide precipitation process. The knowledge gained from these studies contributes to the development of sustainable and efficient strategies for the treatment and valorization of brine solutions, paving the way for their potential industrial implementation. Furthermore, it should be noted that while the concentrations of magnesium ions were taken from the ZERO BRINE project, the concentrations of the precipitant and the flow rates were modified in order to optimize the precipitation process. This customization allowed for tailoring the process parameters to achieve the desired outcomes and improve the overall efficiency of the system.

In conclusion, the successful preliminary studies on the precipitation of magnesium hydroxide and calcium hydroxide have demonstrated the feasibility and recommendation of the process. By adjusting the concentrations of the precipitant and the flow rates, it is possible to achieve favorable precipitation conditions and improve the filterability of the resulting slurry. The comprehensive characterization and evaluation of the obtained products will further contribute to understanding their properties and potential applications.

2.5 Analysis of the magnesium hydroxide

The Multiple Feed Plug Flow Reactor (MF-PFR) prototype, a cutting-edge technology, plays a pivotal role in the experimental setup for the ZERO BRINE

project. This reactor offers a comprehensive solution for conducting continuous crystallization processes, specifically targeting the precipitation of magnesium hydroxide. The MF-PFR design allows for efficient control and manipulation of various parameters, enabling the exploration of different operating conditions and their impact on the final product.

Once the solid product is obtained through filtration, washing, and drying, it is crucial to subject it to rigorous analysis. These analyses serve multiple purposes, including evaluating the purity of the solid and assessing the degree of conversion of magnesium from the initial brine into hydroxide. Additionally, the analyses provide insights into the physical, chemical, and morphological properties of the precipitates.

The analysis of the obtained products, particularly the assessment of magnesium hydroxide, becomes of paramount importance in understanding the viability of the MF-PFR prototype and the efficacy of the precipitation process. By evaluating the physical, chemical, and morphological characteristics of the precipitates, the quality and suitability of the magnesium hydroxide can be determined. This comprehensive analysis ensures that the prototype and the process meet the desired specifications and industry standards.

Furthermore, it is essential to emphasize that the true quality and performance of the products obtained from the MF-PFR prototype, after scaling up the process to nominal flow rates of 300 liters per hour and performing reactive crystallization with real solutions, remains uncertain. The complex nature of the matrix and the continuous operation of the prototype pose challenges in assessing the actual effectiveness of the process and the quality of the resulting products.

The analysis of the obtained products serves as a fundamental step in evaluating the viability of the MF-PFR and its associated process. It provides valuable insights into the purity, particle characteristics, and adherence to specifications of the magnesium hydroxide produced within the prototype. Through this

analysis, any necessary adjustments or optimizations can be identified to enhance product quality, improve process efficiency, and minimize waste generation.

In conclusion, the utilization of the MF-PFR prototype and the subsequent analysis of the obtained magnesium hydroxide products are crucial steps in the ZERO BRINE project. These efforts contribute to the development of sustainable and efficient strategies for the treatment and valorization of brine solutions. By validating the performance of the prototype and assessing the quality of the products, this research paves the way for potential industrial implementation and underscores the significance of comprehensive product analysis in optimizing and scaling up the magnesium hydroxide precipitation process.

2.5.1 Purity of precipitated magnesium hydroxide

The analysis of the precipitated magnesium hydroxide is crucial to assess the validity of the multiple feed plug flow reactor (MF-PFR) technology or prototype. As part of the ZERO BRINE project, these precipitation tests were conducted under eleven different conditions, simulating real solutions and operating with continuous flow in the prototype at a nominal flow rate of 300 l/h. However, the actual quality of the products obtained after scaling up the prototype and executing reactive crystallization with real solutions remains unknown. The complexity of the matrix and the continuous operation of the prototype make the analysis of the obtained products, specifically magnesium hydroxide, essential in understanding the effectiveness of the prototype and the process.

The purity and conversion of magnesium are key parameters that determine the commercial value of the product. High purity is desired to ensure the quality and marketability of the precipitated magnesium hydroxide. The results of Table 2-7 indicate a good purity achieved during the precipitation tests, with most cases showing purity levels exceeding 90%. However, it should be noted

that the low TDS test resulted in a precipitate with inferior purity, likely due to the co-precipitation of insoluble calcium salts.

Table 2-7: $Mg(OH)_{2(s)}$ crystallisation experiments: operating pH, purity of product and magma density.

Test run ID	pH	Mg%	Ca %	magma density [g/L]
L (Low TDS 12/02/2020)	10.5	79.3	20.7	2.7
N1 (Std TDS 19/11/2019)	10.6	91.3	8.6	2.1
N2 (Nominal 21/11/2019)	10.6	91.0	8.8	2.0
N3 (Nominal 16/11/2019)	10.7	92.6	7.3	3.1
N4 (Nominal 28/11/2019)	10.7	96.1	3.9	2.4
N5 (Nominal 11/12/2019)	10.6	93.4	6.6	3.7
N6 (Nominal 13/12/2020)	10.5	93.6	6.4	3.1
N7 (Nominal 17/12/2019)	10.5	93.1	6.9	3.8
N8 (Nominal 18/02/2020)	10.35	83.9	16.1	1.8
N9 (Nominal 20/02/2020)	10.8	88.6	11.4	3.3
U (High TDS 28/02/2020)	10.25	86.0	14.0	1.9

It is important to consider that purity refers specifically to the cationic composition of the precipitate, meaning that any other magnesium salt present, apart from magnesium hydroxide, would contribute to the overall high product purity. The co-product was identified as magnesium carbonate ($MgCO_3$) due to the formation of CO_2 bubbles during solid neutralization with HCl.

To thoroughly analyze the obtained solids, various techniques were employed. SEM analyses were performed to investigate the presence of magnesium carbonate crystals, with results indicating the absence of $MgCO_3$ crystals. However, it is worth noting that magnesium carbonate trihydrate can exhibit different morphologies depending on precipitation conditions. For instance, at room temperature and pH below 9.5, magnesium carbonate trihydrate settles in a crystalline needle-like structure, influenced by the presence of HCO_3^- ions and the viscosity of the brine[62].

The solid samples underwent preparation for ion chromatographic (IC) analysis to estimate the purity of the precipitated crystals. Subsequently, after drying, the filtrate solid was crumbled and rewashed to eliminate any soluble salts possibly precipitated from traces of brine. Then, 100 mg of each sample was weighed using an analytical balance. The samples were then mixed with 1 M hydrochloric acid (HCl) at a 10% excess over the stoichiometric ratio (3-4 mL). After allowing 2-3 hours for the solid to dissolve in HCl, each sample was transferred into a 1 L flask partially filled with ultrapure water, ensuring no loss of sample. The flask was then filled with ultrapure water, and the samples were ready for analysis using ion-exchange chromatography. Dry solids were ground using a ceramic mortar. The results of the chromatographic analysis were divided by the known dilution ratio, obtained from the sample preparation procedure for purity analysis, to determine the magnesium content of each solid sample.

The purity of the $Mg(OH)_2$ precipitate was calculated as the ratio of the concentration of magnesium or calcium ions to the sum of all cations present in the sample, using the following equation (2.18):

$$\text{Purity} = \frac{C_{Mg^{2+}\ or\ (Ca^{2+})}}{\sum_{i=1}^{N} C} \qquad (2\text{-}18)$$

The IC analysis revealed that the precipitated magnesium hydroxide samples typically contained only magnesium and calcium cations. The purity of the samples was generally above 90% for most of the tested brines, with a peak

purity of 96% observed in test N4. However, some tests showed purity values below 90%, with a minimum of 79% in test L. In all cases, the co-precipitation of calcium carbonate, as indicated by X-ray diffraction (XRD) analysis (2.5.2), influenced the purity of the magnesium hydroxide.

These comprehensive analyses, combined with the outlined sample preparation procedure, provide valuable data on the quality, composition, and consistency of the precipitated magnesium hydroxide. They play a vital role in assessing the success of the MF-PFR prototype and the reliability of the process, enabling us to make informed decisions regarding the scalability and commercial viability of the technology.

In addition to purity analysis, the magma density, defined as the grams of undissolved solids per unit volume of the suspension, was also examined. The computation of magma density involved considering the available experimental data on recovery and magnesium concentration, which were then compared with the experimental measurements. The results, along with the values for inlet magnesium concentration and recovery, can be found in Table 2-7. The computed magma density displayed a similar trend to the experimental results, with minor variations attributed to the presence of co-precipitated calcium carbonate during the magnesium precipitation process. This suggests that the magma density is not solely dependent on the inlet magnesium concentration but also influenced by the recovery. Both the computed and experimental magma densities followed the trend of recovery, underscoring its significant impact on the overall density of the precipitates.

These findings emphasize the importance of considering not only the magnesium concentration but also the recovery when assessing the magma density. By incorporating these factors into the analysis, a more comprehensive understanding of the precipitates' characteristics and behavior can be achieved.

2.5.2 XRD analysis

XRD analysis of the precipitated magnesium hydroxide samples with impurities of calcium carbonate provides valuable insights into their crystal composition. Figure 2-14 presents the XRD results obtained from the analysis. At the operating conditions of 10-15°C and a pH of 10.5, calcium was identified as the most stable species in the form of calcite. The presence of bicarbonate (HCO_3^-) in the feed brines led to the precipitation of calcium carbonate during the reactive precipitation step of magnesium hydroxide.

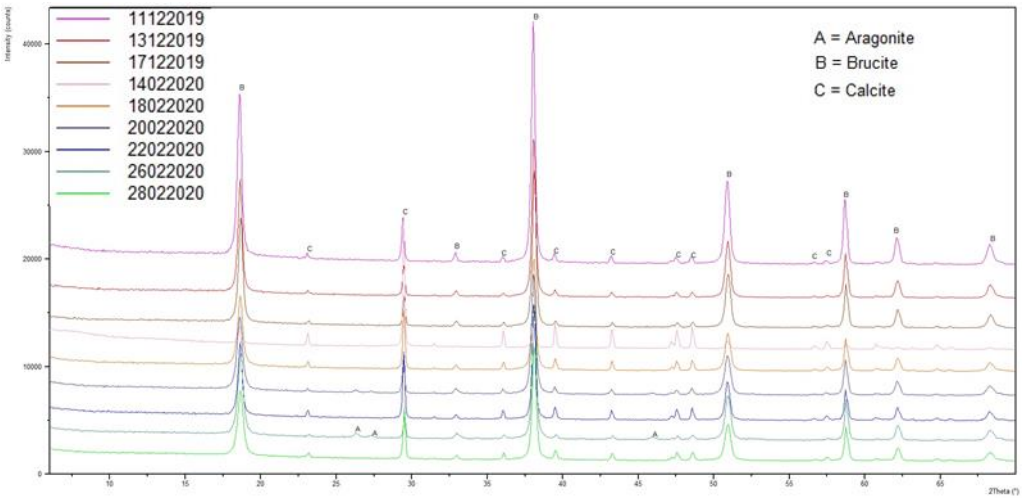

Figure 2-14: Cumulative XRD patterns for magnesium hydroxides samples from all different test-runs.

The XRD technique allows for the identification of crystalline compounds present in a sample. In this study, the washed and dried powder obtained during the precipitation of magnesium hydroxide was directly analyzed using XRD. Table 2-7 provides information on the percentage of calcium present, indicating that a higher calcium content is expected to yield different peaks compared to those of brucite. The XRD pattern depicted in Figure 2-14 supports this observation, showing the presence of additional peaks corresponding to calcite and aragonite ($CaCO_3$) in the less pure samples. This phenomenon is directly linked to the reaction between bicarbonates and the precipitating

reagent (NaOH), which results in the transformation of bicarbonates into carbonates. It is important to note that the high initial calcium percentage in the feed brines does not facilitate the precipitation of calcium carbonate as a carbonate due to the common ion effect. As observed in Figure 2-12, the precipitation curve of magnesium initiates at approximately pH 9.8 and concludes around pH 10.4. It is noteworthy that this final pH value is higher than that recorded during the fractionated precipitation test, where the pH of magnesium precipitation reached 10.4. The variation can be attributed to the complex composition of the brine, which can potentially influence the solubility of magnesium hydroxide.

The analysis of IC and XRD results demonstrates that the purity of the precipitated magnesium hydroxide is influenced by the amount of bicarbonate present in the inlet brine and the recovery of magnesium. Therefore, monitoring the recovery of magnesium is crucial, as a higher Mg recovery leads to an increased ratio between Mg and Ca at a fixed inlet brine concentration. This, in turn, results in a higher degree of purity in the produced crystals. The recovery efficiency of magnesium in the form of Mg(OH)2(s) was generally above 80% in most cases, with peaks reaching above 95%.

The XRD analysis, combined with the findings from IC, provides a comprehensive understanding of the impurities present and their impact on the purity of the precipitated magnesium hydroxide. By optimizing the reaction conditions and controlling the recovery efficiency, it is possible to minimize impurities such as calcium carbonate and achieve a higher degree of purity in the final product.

2.5.3 TGA analysis

Data was obtained using a simultaneous Netzsch STA 449 Jupiter F1 thermal analyzer, equipped with a SiC furnace and TGA DSC type S head. The TGA analysis was conducted in the temperature range of 30-900°C under a protective

gas atmosphere with minimal changes. During the TGA analysis, a small amount of the washed and dried powder of magnesium hydroxide was subjected to gradual heating up to 900°C. This technique provides valuable insights into the thermal behavior and composition of the sample. By examining the weight changes during heating, we can determine the presence of impurities, such as calcium carbonate, and evaluate the purity of the magnesium hydroxide.

The weight loss observed during the TGA analysis can be attributed to different temperature ranges. The initial weight loss, occurring between 30-200°C, is typically associated with the evaporation of moisture present in the sample. This is followed by a subsequent weight loss range of 200-550°C, which corresponds to the thermal decomposition of magnesium hydroxide according to the reaction:

$$Mg(OH)_2 \rightarrow MgO + H_2O \qquad (2\text{-}19)$$

Finally, a settling phase is observed in the temperature range of 550-900°C, attributed to the release of trapped water from the magnesium oxide bed.

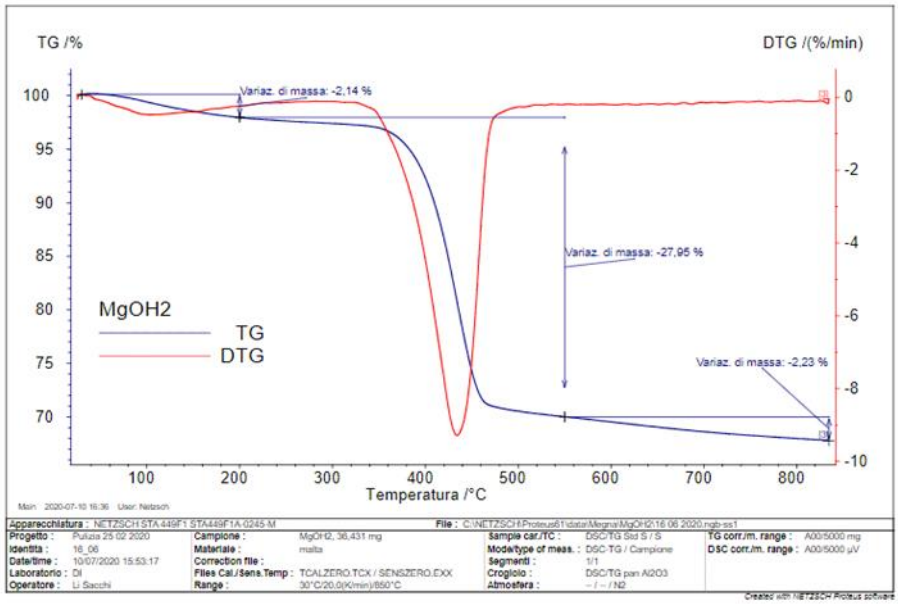

Figure 2-15: TGA spectra obtained with high purity $Mg(OH)_2$.

In samples with higher purity, only the weight loss corresponding to the decomposition of magnesium hydroxide is observed.

However, in samples with impurities, such as calcium carbonate, an additional weight loss stage is detected due to the decomposition of calcium carbonate according to the reaction:

$$CaCO_3 \rightarrow CaO + CO_2 \qquad (2\text{-}20)$$

This additional weight loss stage indicates the presence of impurities and provides further evidence of the co-precipitation of calcium carbonate during the reactive precipitation step of magnesium hydroxide.

By analyzing the stoichiometry of these reactions and considering the weight losses, it is possible to calculate the weight percentages of magnesium hydroxide and calcium carbonate in the sample. These percentages are obtained by relating the weight loss to the respective formula weights of water, magnesium hydroxide, carbon dioxide, and magnesium carbonate. This quantitative analysis allows for the determination of the mass purity of the magnesium hydroxide samples.

In Figure 2-16, the TGA spectra of two samples obtained under different conditions are depicted. These spectra provide valuable insights into the thermal behavior and composition of the samples.

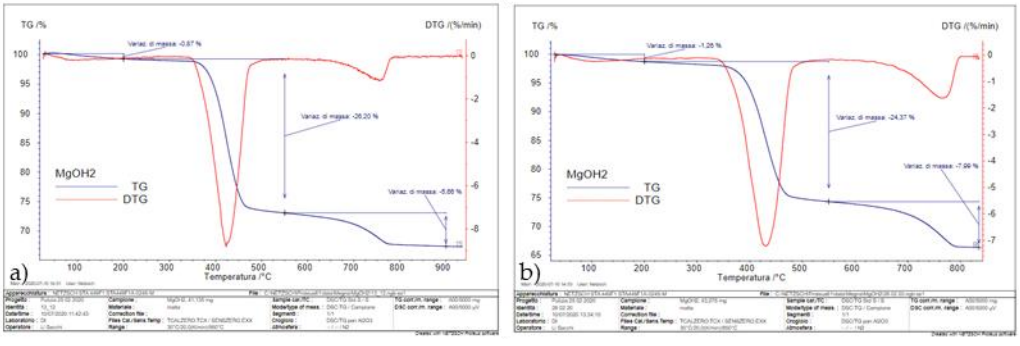

Figure 2-16: a) TGA spectra obtained with purity $Mg(OH)_2$ obtained with nominal conditions (N6); b)TGA spectra obtained with purity $Mg(OH)_2$ obtained with high concentration conditions (U).

Then, the analysis of two samples obtained under nominal concentration conditions (N6) and high concentration conditions (U) was performed. This allowed us to compare the TGA spectra of the products obtained with MF-PFR with a pure sample (Figure 2-15). This time, two distinct weight losses can be clearly observed: the first one due to magnesium hydroxide and the second one due to calcium carbonate.

The first sample (Figure 2-16a), obtained under nominal concentration conditions (N6), shows distinct weight loss patterns. The initial weight loss corresponds to the moisture content of the sample, indicated by the slight decrease in weight in the temperature range of 30-200°C. This is followed by a significant weight loss in the range of 200-550°C, attributed to the decomposition of magnesium hydroxide ($Mg(OH)_2$) into magnesium oxide (MgO) and water (H_2O) according to Equation (2.19). The second sample (Figure 2-16b), obtained under high concentration conditions (U), exhibits a similar weight loss pattern as the N6 sample. However, there are notable differences in the extent of weight loss. The initial moisture content is slightly higher in the U sample compared to the N6 sample. Additionally, the weight loss corresponding to the decomposition of magnesium hydroxide is more pronounced in the U sample, indicating a higher concentration of magnesium hydroxide.

Importantly, both samples exhibit a second weight loss in the TGA spectra, which is attributed to the presence of calcium carbonate ($CaCO_3$). This weight loss occurs at higher temperatures, typically above 600°C, and corresponds to the decomposition of calcium carbonate into calcium oxide (CaO) and carbon dioxide (CO_2) according to Equation (2.20). The presence of this weight loss peak confirms the presence of calcium carbonate impurities in the samples.

The thermogravimetric technique enables precise quantitative calculations based on the equations explained in section 2.3.3, using the weight loss during the process. By knowing the species lost during the process, these two analyses allowed us to determine the percentage of calcium present in the form of

carbonate in the N6 sample, which was found to be purer than the U sample through chromatographic analysis. The N6 sample showed a percentage of 7.4% compared to the 6.6% obtained from chromatographic analyses. On the other hand, the U sample exhibited a calcium carbonate percentage of 13.3% compared to the 14% found using chromatographic analyses.

It is important to note that these techniques provide comparable values, and more importantly, each technique complements the information provided by the others. This is because certain species may be detected by one technique but not by another.

Therefore, the TGA analysis plays a crucial role in characterizing the composition and purity of the precipitated magnesium hydroxide. It complements the XRD analysis and provides further confirmation of the presence of impurities, particularly calcium carbonate, during the precipitation process using the MF-PFR method. The combined results from XRD, chromatographic analyses, and TGA offer comprehensive insights into the thermal behavior, composition, and purity of the obtained magnesium hydroxide samples.

Ultimately, the implementation of the thermogravimetric analysis allows for a more comprehensive understanding of the obtained products and their purity characteristics. By combining the results from multiple analytical techniques, we can obtain a more complete picture of the composition and properties of the samples. This integrated approach enhances our ability to assess the purity of the products and evaluate the effectiveness of the crystallization process by MF-PFR.

2.5.4 Granulometric analysis

Previously, we discussed the analysis of purity and identification using IC, XRD, and TGA techniques. Now, let's delve into the morphological aspect, where we

can evaluate the physical and structural characteristics of the obtained magnesium hydroxide.

It is important to analyze the particle size distribution of the precipitated magnesium hydroxide crystals. Particle size plays a significant role in determining the product's physical properties, such as settling behavior, filtration efficiency, and reactivity In section 2.3.2, the instrument used and the analysis methodology were described. It is important to note that the analysis is performed on slurry samples rather than solids. This choice is made to ensure that the results reflect the nature of the compound rather than being influenced by the grinding process.

Analyzing the particle morphology provides essential insights into the physical properties of magnesium hydroxide, such as particle size, shape, and surface features. By examining the crystal size distribution (CSD) and the D values, which represent the diameter at different cumulative volume intercepts, we can gain a comprehensive understanding of the particle size distribution. Understanding the crystal size distribution is particularly important as it can significantly influence the filtration characteristics of the magnesium hydroxide.

The filtration process is favored by larger particles, as they tend to form a more porous and permeable filter cake, allowing for better liquid-solid separation and improved filtration efficiency. Conversely, smaller particles may lead to clogging and decreased filtration performance.

Another significant aspect of our analysis involved comparing the particle size distribution of test 1, test 4, test 12 obtained from the filtration tests (Table 2-4), and the flame retardant reference (Magnifin H10). This comparison, as shown in Figure 2.16, allows us to evaluate the variations in particle size among the different samples.

By examining Figure 2-17, we can observe the differences in particle size distribution among the samples. Test 4 and test 12 exhibit particle size

distributions that closely resemble that of Magnifin H10, indicating similar particle size characteristics. This suggests that the magnesium hydroxide produced under these conditions may possess comparable flame retardant properties.

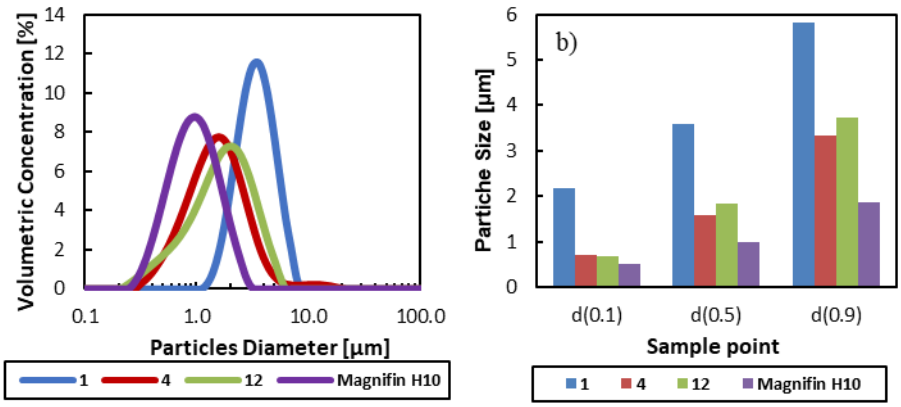

Figure 2-17: Comparison of particle size distribution between the test 1, 4, 12 and the flame retardant reference (Magnifing H10).

On the other hand, test 1 displays a distinct particle size distribution, with particles of larger dimensions compared to the other tests and Magnifin H10. These findings suggest that test 1 results in the formation of magnesium hydroxide crystals with larger sizes. While this may impact the filtration behavior, it is essential to consider the potential advantages of larger crystals in specific applications.

The comparison of particle size distribution between the different tests and the reference material provides valuable insights into the variations in particle size and their implications for the desired properties. It enables us to assess the suitability of the produced magnesium hydroxide samples for different applications, particularly in the flame retardant industry.

By combining the information obtained from particle size distribution analysis, morphological characterization using SEM, and the results from other analytical techniques, we can develop a comprehensive understanding of the composition,

structure, and properties of the magnesium hydroxide samples. This knowledge is crucial for tailoring the material to meet specific application requirements and optimizing production processes to ensure consistent quality and performance.

Overall, the morphological analysis, in conjunction with the purity assessment conducted using IC, XRD, and TGA techniques, provides a holistic understanding of the composition, structure, and properties of the precipitated magnesium hydroxide. This comprehensive characterization enhances our ability to evaluate the material's suitability for different applications, including flame retardancy and other industrial uses, and paves the way for further advancements in its production and utilization. Furthermore, the knowledge of crystal size distribution and its impact on filtration behavior provides valuable insights for optimizing process parameters and improving filtration performance.

2.5.5 SEM analysis

To further investigate the morphology and structural characteristics of the magnesium hydroxide samples obtained from the MF-PFR process. A detailed scanning electron microscope (SEM) analysis was conducted to further investigate the morphology and structural characteristics of the magnesium hydroxide samples obtained from the MF-PFR process. SEM images, shown in Figure 2.18 at magnifications of 10,000X and 50,000X, provide valuable insights into the particle structure, surface features, and aggregation patterns of the samples from tests 1, 4, and 12, as well as the commercial product Magnifin H10.

This widely utilized technique allows for the visualization and examination of the sample's microstructure by capturing images of its surface when bombarded with electrons. In the context of this study, SEM analysis provided crucial insights into the shape and form of the magnesium hydroxide particles obtained through MF-PFR, complementing the particle size distribution analysis previously discussed. While particle size distribution analysis provides

information about the overall particle dimensions, SEM allows for the observation of individual crystals.

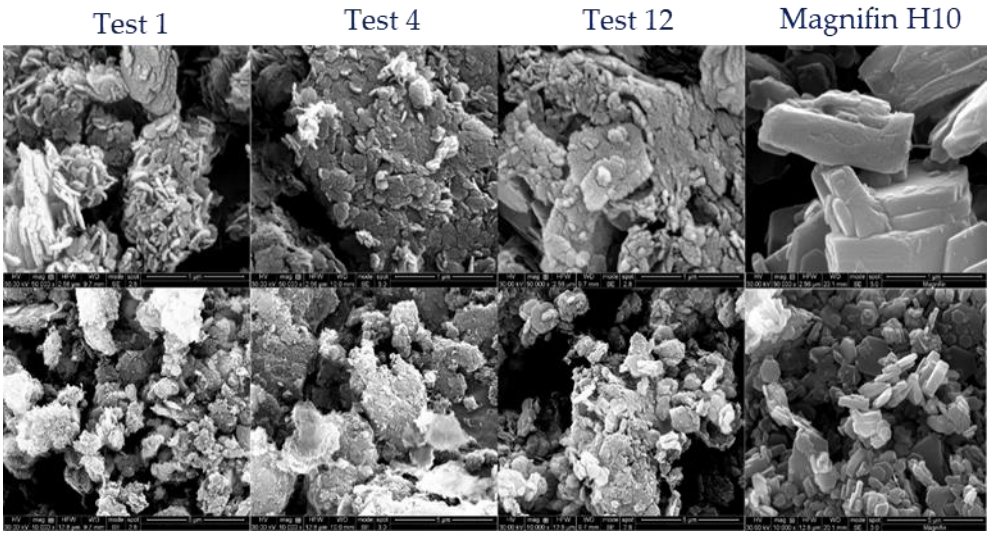

Figure 2-18: SEM images at different magnifications (10000X and 50000X) of the three samples of magnesium hydroxide (Case 1, Case 4 and Case 12) and Magnifin H10.

It was observed that under "NO SEED" conditions (Tests 1 and 4), the crystals were remarkably small, measuring less than 100 nm in diameter. The morphology of these crystals was described as cauliflower-like or globular due to the presence of numerous smaller particles. These findings were in contrast to the particle size distribution analysis, which suggested larger particle sizes on the order of micrometers.

However, these larger sizes were likely attributed to the agglomeration of the tiny crystals formed during the nucleation process. On the other hand, the SEM images of Magnifin H10, a benchmark material, revealed the presence of crystals in the range of 1-5 micrometers. Examining the sample obtained from test 12, conducted under reactor-seeded conditions, small crystals were observed to be attached to the larger Magnifin H10 crystals, indicating secondary nucleation and growth. This SEM analysis provided critical visual evidence of the crystal size and morphology variations among the different samples, shedding light on

the influence of nucleation and growth mechanisms. The obtained insights from SEM analysis, when combined with other characterization techniques, contribute to a comprehensive understanding of the composition, structure, and properties of the precipitated magnesium hydroxide samples, facilitating further optimization of the MF-PFR process and potential applications in various industries. Moreover, the SEM images also revealed important information about the aggregation behavior of the magnesium hydroxide particles. In test 12, where the MF-PFR process was conducted with the addition of seeds, the presence of small crystals attached to the larger Magnifin H10 crystals indicated a secondary nucleation process. This phenomenon suggests that the introduction of seeds facilitated the formation of new crystals, resulting in a more complex particle structure with hierarchical aggregation. This insight is valuable for understanding the nucleation and growth kinetics during the precipitation process and can aid in optimizing the process conditions to control particle size and morphology. In Figure 2.19, a higher magnification image of a sample obtained from test 12 is presented, showcasing the presence of secondary nucleation.

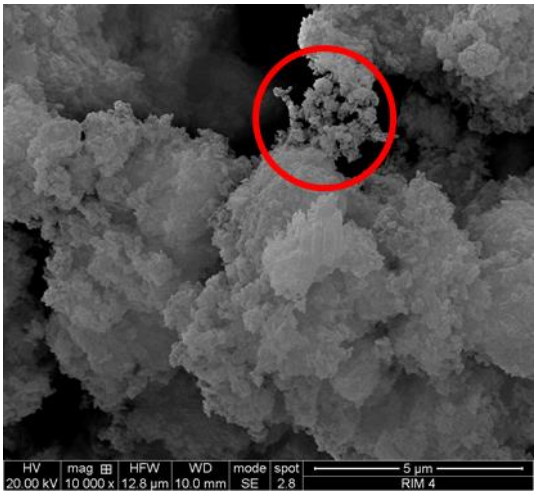

Figure 2-19: SEM image obtained at a magnification of 10,000X of test 12, highlighting secondary nucleation.

This particular sample was obtained from a reactor-seeded condition, allowing for a clear distinction of the phenomenon. Highlighted by a red oval, the image reveals the presence of small magnesium hydroxide crystals that bridge the gap between two larger Magnifin H10 crystals. The formation of these bridges, resulting from secondary nucleation, is a remarkable phenomenon that is facilitated by the high nucleation rate of magnesium hydroxide and the significant number of nuclei formed. It demonstrates the intricate connectivity and structural complexity that can arise in the synthesized samples under specific conditions.

This observation further emphasizes the role of nucleation dynamics in shaping the morphology and particle interactions within the magnesium hydroxide samples. The ability to visualize and analyze such phenomena provides valuable insights into the growth mechanisms and the potential for tailoring the material's properties through precise control of nucleation and growth conditions. By understanding and harnessing the phenomenon of secondary nucleation, researchers can potentially manipulate the morphology, particle size distribution, and aggregation behavior of magnesium hydroxide, thereby optimizing its performance for various applications. This knowledge opens up new possibilities for engineering materials with enhanced properties and tailored functionalities.

Comparing the SEM images of the samples with Magnifin H10, a commercial reference material, provided further insights. Magnifin H10 exhibited distinct characteristics with single crystals in the range of 1-5 μm. These crystals were significantly larger than those produced through the MF-PFR process, indicating differences in the nucleation and growth mechanisms. The SEM analysis also revealed that the specific filtration time increased with the NaOH molar concentration solution, suggesting a correlation between crystal size, morphology, and filtration properties. These findings highlight the importance of controlling the synthesis parameters to achieve desired particle characteristics

and optimize the filtration process. In addition, it is worth noting that researchers have explored thermal processes, such as hydrothermal treatment, as potential methods for modifying the morphology and crystal size distribution of magnesium hydroxide. By leveraging temperature, pressure, and different promoters, such as NaOH solution, Triethanolamine, Diethanolamine, etc., it is possible to tailor the properties of magnesium hydroxide to meet specific requirements for flame retardant applications. These thermal treatments can induce changes in crystal morphology, agglomeration behavior, and particle size distribution, further highlighting the potential for advanced control over the material's properties[31,35,63]. In summary, the SEM analysis provided valuable insights into the morphology, crystal size, aggregation behavior, and differences between the magnesium hydroxide samples obtained through the MF-PFR process and a commercial reference material. The obtained information contributes to a deeper understanding of the nucleation and growth mechanisms involved in the precipitation process, enabling researchers to optimize the synthesis conditions and tailor the properties of magnesium hydroxide for various applications.

In conclusion, the SEM analysis complements the granulometric analysis and offers a deeper understanding of the morphology, crystal size, aggregation behavior, and surface characteristics of the magnesium hydroxide samples obtained through the MF-PFR process. This knowledge is essential for tailoring the material's properties to specific applications and for optimizing the synthesis conditions. By combining the findings from various analytical techniques, researchers can gain comprehensive insights into the composition, purity, thermal behavior, and physical properties of magnesium hydroxide, facilitating its effective utilization in diverse fields.

3 Development and testing of a novel Crystalliser with Ion Exchange Membrane (CrIEM)

This chapter will introduce innovative technology to recover magnesium hydroxide through waste brine and alkaline industrial waste. This novel technology is the Ion Exchange Membrane Crystallizer (CrIEM), which combines the reactive and membrane crystallization, investigated to recover high purity magnesium hydroxide from multi-component artificial and natural solutions. In particular, in a CrIEM reactor, an Anion Exchange Membrane (AEM), which separates two compartments containing a saline solution and an alkaline solution, allows the passage of hydroxyl ions from the alkaline to the saline solution compartment. In this latter, the crystallization of magnesium hydroxide occurs, yet avoiding a direct mixing between the solutions feeding the reactor. In this way, it enables the use of low-cost reactants (e.g. $Ca(OH)_2$) without the risk of co-precipitation of by-products and contamination of the final crystals. An experimental campaign was carried out treating two types of feed solutions, namely: 1) an industrial waste brine from the Bolesław S´miały coal mine in Łaziska Górne (Poland) and 2) Mediterranean seawater, collected from the North Sicilian coast (Italy). The CrIEM was tested in a feed & bleed modality to operate continuously. The Mg^{2+} concentration in the feed solutions ranges from 0.7 to 3.2 g/L. Magnesium recovery efficiencies from 89 up to 100% were reached, while magnesium hydroxide purity between 94 and 98.8% was obtained.

3.1 Introduction and State of the art of the CrIEM technology

With growing attention to environmental issues and sustainability, there is an increasing focus on implementing a more efficient economic model that abandons the classic linear models to go to a circular one. The development of innovative technological solutions allows for the recovery of products with a

high added value and, on the other hand, can return diluted water suitable to be disposed of with the lowest environmental and economic impact possible. As reported in Chapter 0, magnesium hydroxide is a high added value product, and recovery from these solutions (waste solutions) represents an exciting opportunity to improve the manufacturing cycle. Because of this, a novel Ion Exchange Membrane Crystallizer (CrIEM) was developed and patented (patent) by our research group. It allows the passage of ions of interest (i.e. OH^- ions) for crystallization, without direct mixing between the two solutions, thus removing any problem of co-precipitation. It also allows the use of low cost and purity reagents or alkaline industrial waste without the risk of reducing the purity of the final product.

The Crystalliser with Ion Exchange Membrane (CrIEM) is a novel crystallization technology based on the use of ion-exchange membranes, patented by Cipollina et.al in 2015[40]. It allows to perform reactive crystallization for separation of valuable species (e.g. Mg from brines) with large flexibility in the choice of reactants. The CrIEM consists of an ionic exchange membrane separating two different solutions allowing the controlled transport of species (see Figure 3-1). In particular, an anionic exchange membrane is employed allowing the anions present in the two solution to migrate from one channel to other one, while rejecting the cations, according to the Donnan Exclusion mechanis[64]. From this perspective, it is essential to use an appropriate membrane in order to finely control the passage of species and the subsequent reactive crystallization process.

In our application, the membrane allows the passage of hydroxyl ions from an alkaline solution to the Mg-rich brine compartment, where the crystallization of magnesium hydroxide occurs, while chloride ions move in the opposite direction to comply with electroneutrality. The driving force for the movement of ions is an electro-chemical potential difference between the two channels. This

is originated from the difference in concentration and is accompanied also by the formation of Donnan potential at the solution/membrane interface[64].

Since magnesium hydroxide has a very low solubility (Ksp 5.61 10-12), the passage of hydroxyl ions lead to the increase of pH and, above 9, the supersaturation is quickly reached so that magnesium ions (Mg^{2+}) instantly react with available hydroxide ions and precipitate in the form of $Mg(OH)_2$. It is worth noting that, while the hydroxyl ions react and precipitate, thus maintaining a low concentration in the brine compartment, chlorides continuously move from the brine to alkaline compartment, thus providing an important additional driving force for the Donnan transport mechanism. Due to the membrane, the alkaline solution does not mix with the brine, thus avoiding any undesired co-precipitation of species other than $Mg(OH)_2$ (e.g. calcium sulphates and carbonates).

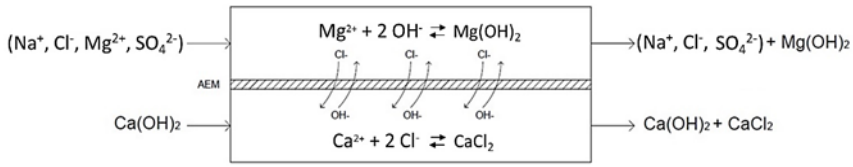

Figure 3-1: Process scheme of the CrIEM technology for the precipitation of Mg(OH)2 from Mg-rich brines.

The main innovative features of CrIEM technology are: 1) the possibility of using a low-cost reactant being unsuitable for conventional reactive crystallization processes (e.g. due to the co-precipitation of undesired products); 2) the opportunity to reduce the environmental impact by selecting the best performing and less polluting reactant; 3) the absence of moving parts, which reduces the risk of mechanical failure; 4) modularity and flexibility.

3.2 Description of the experimental set-up

The laboratory CrIEM unit adopted in the present work consists of two Plexiglas plates, each one carved with a semi-circular zig-zag shaped channel (Figure 3-2). This material was chosen in order to allow for a visual inspection of the system

during operation. The plate sizes are 535mm x 325mm x 20mm, while the channels diameter is 8.1mm. The total length of the circuit is 7180mm with a total volume of 187 ml per channel.

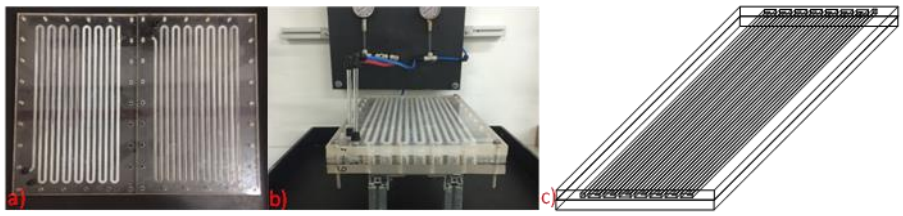

Figure 3-2: CrIEM reactor, a) disassembled; b) assembled; c) 3D scheme.

The experimental test-rig employed for the experimental campaign is reported in Figure 3-3. Two hose connectors are used to feed the solutions into the CrIEM device: only polymeric material was adopted to avoid corrosion phenomena caused by the high salinity of solutions and by the alkaline stream due to the high pH. A Fujifilm type 10 AEM was inserted between the plates, resulting in a net transfer area of about 585 cm^2.

The alkaline solution channel is connected to a storage tank, while the saline channel is connected to a buffer tank. The buffer tank consists of a cylinder with a conical frustum shape bottom, a total volume of 2750 ml and 47 mm of radius for the cylindrical part. A flexible hose fitting is located at the bottom part of the buffer tank so that the $Mg(OH)_2$ –rich suspension can be drained and stored in a separate tank. A pH meter is located within the buffer tank to check the crystallization progress. Furthermore, the upper part allows the placement of different tubes corresponding to one outlet and two inlets. One inlet and one outlet are relevant to the saline solution exiting from and entering into the CrIEM reactor, respectively; the other inlet allows the fresh saline solution make-up to the test-rig.

Two pressure gauges are positioned at the inlet of the two channels of the CrIEM in order to control the pressure drops during the process. Four peristaltic pumps (Seko Kronos 50) are used for the movement of all liquids. Two pumps were

used to recirculate saline and alkaline solution in the CrIEM from the relevant buffer tanks, while the other two pumps were used to feed the brine to its buffer tank and to drain it, respectively. The feed & bleed arrangement allows for a continuous operation mode looking at the brine stream, while a batch circulation is adopted for the alkaline solution in the buffer tank. The $Mg(OH)_2$–rich slurry stored in the tank (next to the buffer) is discontinuously sampled (after a suspension volume of about 1 litre is reached in the tank) and then filtered in a laboratory vacuum filtration system to recover the magnesium hydroxide as a solid cake.

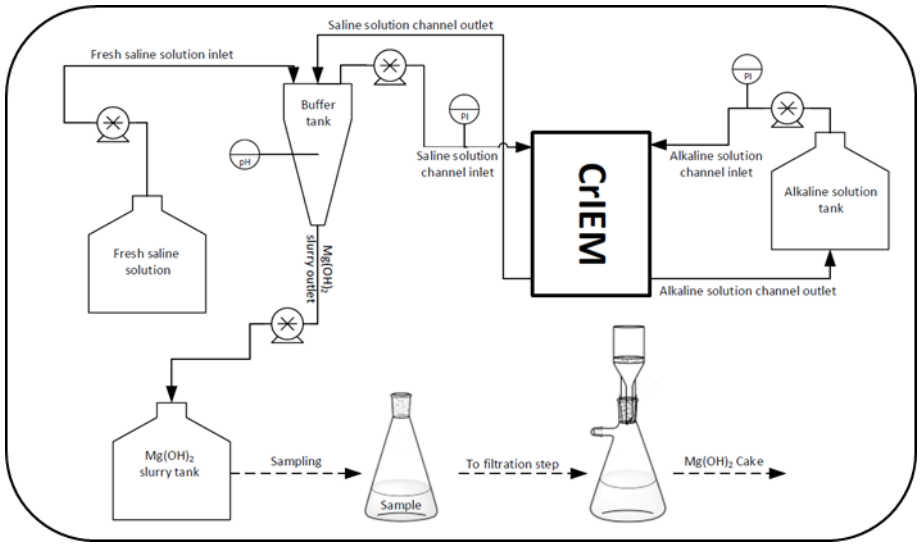

Figure 3-3: Sketch of the experimental set-up.

3.3 Materials and experimental procedures

Calcium hydroxide was chosen as alkaline reactant. It is a cheap reactant and sparingly soluble inorganic compound, generally employed in the form of suspension. Using this reactant with traditional crystallization methods, where direct mixing between reactants occur, generally provides a low-purity magnesium hydroxide. Therefore, $Ca(OH)_2$ was considered the most suitable to compare the CrIEM performance with that of traditional crystallization

methods. Moreover, the adopted $Ca(OH)_2$ suspensions could also be regarded as an attempt to mimic typical alkaline industrial wastes[65], which could be used to further promote the circular approach of the proposed technology. In all experiments, a volume of 5 litres of suspension was adopted, with a slurry concentration of 10g/l of $Ca(OH)_2$, periodically substituted in the long-run feed & bleed tests.

The experimental campaign is composed of six different tests listed in Table 3-1 and briefly described below.

In tests 1 to 4, an industrial brine deriving from the Bolesław S´miały coal mine in Łaziska Górne (Poland) was employed. The original brine was preliminarily pre-treated by Silesian University of Technology (SUT) personnel at Bolesław S´miały coal mine premises: after a decarbonization step for removal of soluble CO_2, carbonates and bicarbonates, the brine is processed in an ultrafiltration stage in order to remove completely sub-micronic coal particles. The resulting brine (TDS ~20g/l) is fed to a nanofiltration (NF) unit splitting the solution into two-streams, one NaCl-rich permeate and a second magnesium-calcium-rich retentate (TDS ~30g/l). The latter stream is used in the present experimental campaign (Tests 1 to 4) to recover $Mg(OH)_2$. In particular, tests 1 to 3 refer to three different samples (i.e. different operating days) of the real brine exiting from the NF unit. Test 4 brine results from the artificial addition of magnesium chloride hexahydrate to the brine of test 2 in order to increase the amount of dissolved Mg from 0.77 to 3.2 g/l (trying to mimic the amount of Mg contained in a typical reverse osmosis brine). Tests 5 and 6 were carried out with Mediterranean seawater as saline feed solution (sampling site: Mondello, Italy). Seawater samples were filtered with a 1 μm cartridge filter before the experiments.

In all tests a fixed volume of brine was processed (values are reported in Table 3-1).

Table 3-1: Summary of the experimental tests carried out in the present work.

Test number	Test name	Saline solution description	Volume of brine [l]	Conc. of Ca^{2+} [g/l]	Conc. of Mg^{2+} [g/l]	TDS [g/l]
1	Br-1a	Real industrial brine produced in coal mining activities after a NF step (low concentration)	1	0.70	0.74	31
2	Br-1b	Real industrial brine for reproducibility purposes	1	0.80	0.77	29
3	Br-2	Real industrial brine produced in coal mining activities after a NF step (high concentration	2	1.12	1.13	32
4	Br-3	Artificial solution mimicking a mining brine enriched in magnesium ions	1	0.80	3.20	38
5	SW-1a	Real seawater solution sampled from north coast of Sicily	2	0.49	1.47	38
6	SW-1b	Real seawater solution for reproducibility purposes	2	0.49	1.47	38

3.4 Methodology

The experimental procedure to recover magnesium from saline solution is composed of two phases: i) a start-up phase where the system is operated in batch conditions starting from a pristine brine volume, ii) a continuous operation phase where the brine loop is operated under feed & bleed mode starting from the reacted brine volume.

In the start-up step, the saline solution is recirculated from buffer tank to the CrIEM until all magnesium ions present in solution are converted into $Mg(OH)_2$. pH values in the brine buffer tank were continuously monitored by means of a digital pH meter (WTW pH-Cond 3320/SenTix® 41). As shown in Figure 3-4a, once the test starts, pH rapidly increases until a value around 9.8. Above this value, $Mg(OH)_2$ starts reacting massively with hydroxyl ions and precipitating.

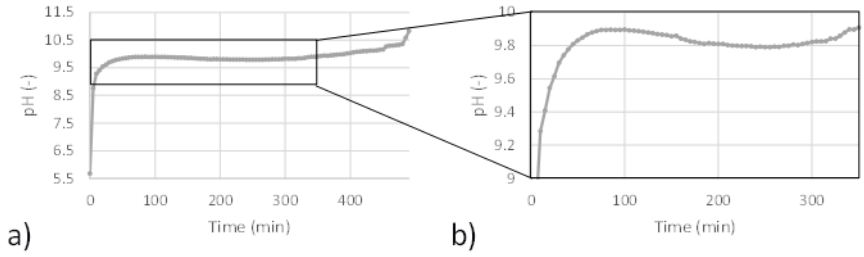

Figure 3-4: a) pH versus time trend during the start-up phase 4; b) zoom of initial pH vs time trend.

The precipitation consumes OH^- ions in solution, while a continuous passage of OH- through the membrane results in a stabilized value of the pH. When the amount of Mg ions is significantly reduced, pH starts slightly increasing up to around 10.5, when all Mg ions have reacted and pH trend starts exhibiting a sharp increase. A visual observation of the transparent reactor during experiments indicated the solution was clear up to a pH around 9.9, thus suggesting that a massive precipitation was not started yet. The slight drop of pH shown in Figure 3-4b occurs exactly when the solution starts becoming cloudy due to $Mg(OH)_2$ precipitation from a metastable slightly supersaturated

solution. The incipient formation of crystals leads to an increase in crystallization rates and a slight reduction in the pH, which then increases again until the equilibrium value.

Once pH above 10,5 was reached and all magnesium has reacted, at least 12 hours have to pass before to start the feed & bleed step. This is necessary in order to wait for the settling of magnesium hydroxide in the feed buffer tank and thus improve the bleeding of the slurry with the make-up brine, still being able to continuously remove a dense settled slurry product from the conic section on the bottom of the buffer tank.

After this step, the continuous feed & bleed operation starts, where make-up brine is fed to the buffer tank and the magnesium hydroxide slurry is drained simultaneously (see Figure 3-3).

The two inlets and the outlet of the buffer tank were accurately positioned in order to create a mixing zone in the upper part and a quiet volume in the bottom to promote the settling of particles. In fact, the make-up brine inlet is located near the surface, while the recirculated outlet from the CrIEM is injected periferically at the beginning of the conic section. The brine outlet feeding the CrIEM unit is positioned near the surface, below the make-up inlet, where the lowest particles concentration can be encountered. Finally, the dense slurry with the settled crystals was withdrawn through one peristaltic pump connected with the bottom of the buffer tank and collected in an Erlenmeyer flask.

The product slurry was sampled and then filtered by means of a laboratory vacuum filtration system. The obtained cake was flushed with distilled water to remove the trapped saline solution, then dried inside an oven at 120 ° C for at least 8 hours and subsequently analyzed. Conversely, the filtered solution is analyzed in order to calculate the conversion efficiency.

3.5 Analytical procedures and definition of performance parameters

Ionic composition of liquid and solid samples was determined by Ion Chromatography (IC) Metrohm 882 Compact IC plus and Cation Exchange column Metrosep C4-250/4.0. In order to prepare the sample for IC analysis, the filtrate was properly diluted into Milli-Q water without further pre-treatment. Conversely, 100mg of dried solids was first dissolved in a stoichiometric amount of HCl and subsequently diluted in 1000L of Milli-Q water.

Analytical measurements allowed to calculate the two main performance parameters investigated in the present work: i) magnesium recovery efficiency; ii) calcium loss and iii) magnesium hydroxide purity.

Magnesium recovery efficiency represent the % of magnesium harvested from the feed brine in the form of magnesium hydroxide. It can be calculated from the concentration of the filtered solution sampled during the test according to the following equation:

$$\frac{(C_{Mg-in}-C_{Mg-out})}{C_{Mg-in}} \times 100 \qquad (3\text{-}1)$$

where $C_{Mg\text{-}in}$ is the inlet saline solution Mg concentration, while $C_{Mg\text{-}out}$ is the Mg concentration in the sampled outlet solution, after filtration for solids separation.

Calcium loss represents the % of Calcium co-precipitated from the feed saline solution during the process. It can be calculated, similarly as the magnesium recovery efficiency, from the concentration of the filtered solution sampled during the test according to the following equation:

$$\frac{(C_{Ca-in}-C_{Ca-out})}{C_{Ca-in}} \times 100 \qquad (3\text{-}2)$$

Where $C_{Ca\text{-}in}$ is the inlet saline solution Ca concentration, while $C_{Ca\text{-}out}$ is the Ca concentration in the sampled outlet solution, after filtration for solids separation.

Magnesium hydroxide purity is defined as the % of magnesium present among all main cations detected by the IC analysis in the sampled, filtered and washed solid. Thus, it can be calculated as:

$$\frac{C^s_{Mg}}{\sum C^s_i} \times 100 \qquad (3\text{-}3)$$

where C^s_{Mg} represents the concentration of magnesium detected by ion chromatography from the dissolved solid sample, while C^s_i represent the concentration of any cation detected by ion chromatography.

3.6 Analysis of Mg^{2+} recovery in continuous feed & bleed tests

As a first observation of experimental results, it is worth analyzing the behaviour of the system in terms of pH during the whole duration of a feed & bleed continuous precipitation test. As an example, Figure 3-5 reports the pH trends for the reference tests 3 and 6.

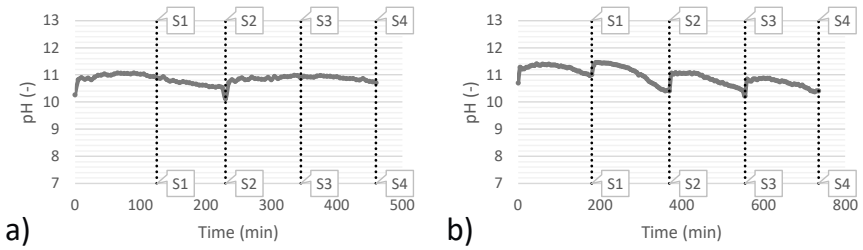

Figure 3-5: Time variation of pH during the feed & bleed tests. a) test 3; b) test 6. Vertical dotted lines indicate the time at which samples for analysis were taken (samples number is used as reference in Figure 3-6).

After all magnesium was reacted, the pH can change rapidly because no buffering agents are present. Therefore, the inlet and outlet flow rate of make-up brine and magnesium hydroxide slurry was accurately chosen. With 9 ml/min (test 3) and 5 ml/min (test 6), the optimal operating flow rate was obtained, which guarantee the pH to remain within a range 10.4 to 11.7. In fact, under pH 10.4 too many magnesium ions remain unreacted, decreasing the recovery efficiency. Conversely, above pH 11.7 the precipitation of $Ca(OH)_2$ can start. Thus, operating in this range of pH represents a good trade-off to allow for high values of magnesium recovery efficiency and low values of calcium loss, the latter being the main factor reducing the solid purity.

Focussing again on the pH trend of tests 3 and 6, small differences in behaviour can be observed, generated by the manual adjustment of flowrates but also amplified by the fact that the test n.6 has a double duration and the sampling intervals are also doubled, which generated a large variation in the pH due to the consumption of alkaline reactant. The Mg recovery efficiency (Figure 3-6a) is above 90% in all cases, with slightly larger values achieved for test n.6 (practically 100% for all samples).

Concerning Ca losses (Figure 3-6b), values recorded for test 6 are higher than for test 3, likely due to the lower initial concentration of Calcium in the feed brine, though similar amounts of Calcium were precipitated during the test (as confirmed by the similar values of purity reported in Figure 3-7).

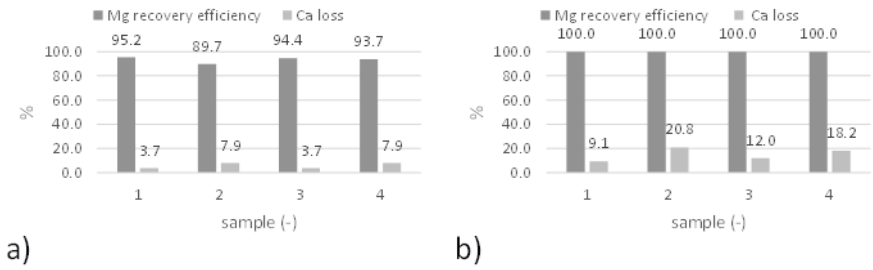

Figure 3-6: magnesium recovery efficiency and calcium loss for 4 samples collected during: a) test3; b) test 6.

When looking at the averaged values of performance parameters for all samples of each, results confirm the findings analyzed above for tests 3 and 6. In particular, magnesium recovery efficiency starts from values around 90% up to 96-97% for the tests with real brines, while reaching values around 100% for the tests with seawater. Conversely, the percentage of Calcium precipitated with the solid was higher for the test carried out with seawater (15% and 24%) than for those carried out with the industrial brine (3-6%). The cause can be twofold: 1) with industrial brines pH values are better controlled and are kept under a lower limit; 2) calcium concentration in seawater is lower than in the industrial brine, thus leading to larger percentage of precipitated calcium salts.

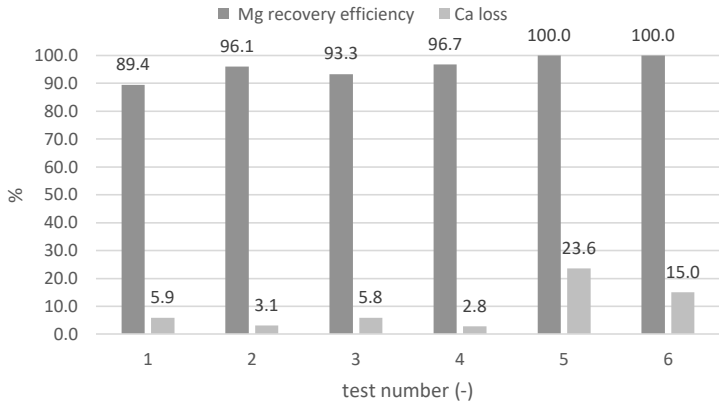

Figure 3-7: averaged values of magnesium recovery efficiency and calcium loss in all tests 1-6.

3.7 Analysis of Mg purity in the solid samples obtained in continuous feed & bleed tests

Solid samples processed and analyzed according to the above mentioned procedure have been characterized in terms of magnesium purity (against the presence of other cations, see eq. (3.3).

Also in this case, the results relevant to 4 samples of reference tests 3 and 6 are reported in Figure 3-8. In particular, the percentage of magnesium and Calcium

in the solid samples are reported, being the concentration of other cations (namely, Na^+, K^+, NH_4^+) below the IC detection limit.

In all cases, a very high purity magnesium hydroxide was produced, with a percentage of magnesium higher than 97%, exceeding 99% in many samples collected. As said above, the only impurity was related to the presence of calcium salts, with a Ca % typically below 3%. No significant variation in solid composition was observed in the 4 samples, thus indicating a fairly stable behaviour of the CrIEM reactor along the 8 to 12 hours' continuous tests.

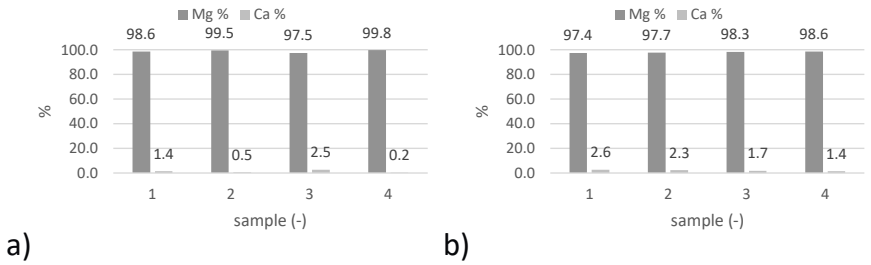

Figure 3-8: : solid purity expressed as percentage of Magnesium and Calcium ions in the 4 solid samples collected during: a) test3; b) test 6.

Looking at the averaged results for all tests performed, very good results have been confirmed, as reported in Figure 3-9. In fact, a high solid purity was obtained in all tests, with a minimum value of 94% observed for test1, while values around or above 97% have been registered for all other tests. The best performance, in terms of average solid purity, was achieved by tests 3 and 6 with average values of 99% and 98%, respectively. This indicates that, by properly controlling and optimizing the operating conditions of the CrIEM unit, a high purity product can be obtained both from an industrial brine (e.g. the coal mine brine) and form a natural saline solution such as seawater.

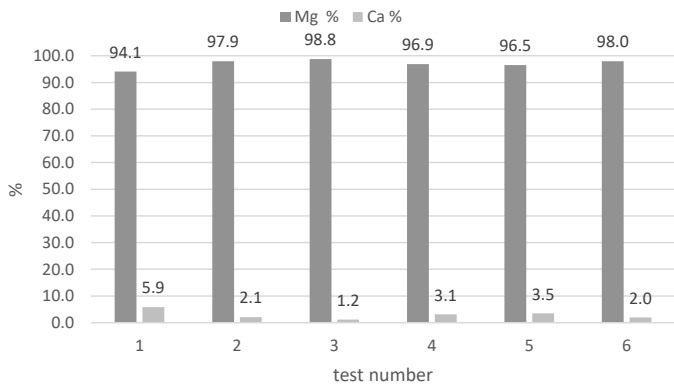

Figure 3-9: solid purity expressed as percentage of Magnesium and Calcium ions, as an average of all samples collected in all tests 1-6.

4 Saltworks Bittern: evaluation of the potential for minerals recovery

This chapter delves into the SEArcularMINE project, a research initiative centered around the valorization of by-products generated during salt processing. One such by-product is known as bittern, a highly concentrated solution rich in various salts. The aim of this chapter is to explore the potential of bittern as a valuable resource for extracting essential raw materials, specifically magnesium hydroxide and lithium. Saltworks, where seawater is evaporated to obtain salt, play a crucial role in the production of bittern. These facilities provide a unique opportunity to harness the untapped potential of by-products, thereby promoting a more sustainable and circular economy. Understanding the functioning of saltworks and the various products that can be derived or potentially derived from them is essential to unlock their full market potential.

The chapter begins by providing an overview of saltworks, including their processes, operations, and the formation of bittern as a by-product. The characteristics and composition of bittern are examined, highlighting its high concentration of salts and its significance as a potential source for valuable raw materials. By effectively utilizing bittern, it becomes possible to minimize waste generation and optimize resource utilization. To assess the potential of bittern and guide its effective utilization, a rapid and efficient method known as the brine potential test (BPT) has been developed. This methodology allows for a quick evaluation of the bittern's composition and its suitability for further processing. By identifying the specific salt content and concentration, it can be determining the feasibility of extracting valuable components such as magnesium hydroxide and lithium.

In addition, a laboratory-scale experiment was conducted to optimize lithium recovery from bittern, focusing on the production of lithium carbonate. The study investigated key parameters including temperature, initial lithium ion concentration, and reactor seeding with catalysts. The findings provide valuable insights for scaling up the recovery process in a separate work package of the SEArcularMINE project. This research aims to establish an efficient and sustainable method for extracting lithium carbonate from bittern, contributing to the development of a circular economy in the salt industry.

By harnessing the potential of bittern, this chapter explores innovative approaches to resource management and sustainability in the salt industry. It underscores the importance of considering by-products as valuable resources and highlights the economic and environmental benefits of their utilization. The SEArcularMINE project serves as an exemplary endeavor in unlocking the value of bittern and promoting a circular economy mindset within the salt processing sector. In conclusion, this chapter offers a comprehensive exploration of the SEArcularMINE project, focusing on the utilization of bittern as a valuable resource for extracting magnesium hydroxide and lithium. By understanding the functioning of saltworks, evaluating the market potential of derived products, and developing efficient methodologies for assessing and recovering valuable components, this research contributes to sustainable resource management and promotes the transition towards a circular economy paradigm in the salt industry.

4.1 Saltwork: the lifecycle from seawater to the bittern

4.1.1 Introduction to the seawater integrated cycle

Over the past two centuries, the search for new sources of raw materials has become increasingly challenging in the wake of the industrial revolution. Recognizing this pressing issue, the SEArcularMINE project has undertaken the task of identifying alternative and unconventional sources of primary resources

essential for human life, sustainable economic growth, and the development of geographic regions where conventional resources alone are insufficient to meet growing demands. One such promising avenue is the valorization of seawater, an abundant and seemingly inexhaustible source of valuable goods. Although industrial processes exist for extracting certain resources from seawater, such as salt production in saltworks and magnesium recovery, there is tremendous potential for integrating these processes into cohesive and efficient production strategies. The overarching goal is to minimize costs, reduce supply risks, and ensure a sustainable supply chain—an aspect that has become increasingly critical in assessing resource management.

Traditionally, the various market sectors involved in these industrial processes have operated independently, with limited interaction and collaboration. However, recent studies have demonstrated the immense potential of an integrated approach[16]. For example, brines generated from desalination plants can be repurposed for table salt production and mineral extraction, while Salinity Gradient Power technologies offer the possibility of generating electricity. These innovative solutions highlight the importance of exploring new avenues and maximizing the utilization of available resources. Of particular significance is the extraction of magnesium—a valuable mineral found in large quantities within seawater and brines produced during various industrial processes. Considered an essential component of "alternative mining," magnesium holds significant added value. Its extraction from seawater presents a unique opportunity to tap into a readily available and abundant source.

In this context, the present PhD thesis focuses on studying the utilization of saturated brines obtained from the final saltwork basins. These brines, which would otherwise be discarded, can be harnessed to fuel a reactive precipitation process for magnesium hydroxide production. By capitalizing on these waste streams, the project aims to create a circular economy model that optimizes

resource usage and minimizes waste generation. To facilitate the research, natural brines sourced from saltworks in Trapani, Italy, are utilized. Understanding the intricacies of the salt production process in saltworks is crucial for comprehending the environment in which the final brines are collected. This comprehensive understanding of the brine collection process forms the foundation for subsequent investigations and analyses conducted throughout the project.

In summary, the SEArcularMINE project addresses the pressing need for alternative sources of raw materials by exploring the valorization of seawater and the integration of industrial processes. The focus on magnesium extraction from brines and the utilization of saturated brines from saltworks represents a significant step toward a more sustainable and circular economy. The research conducted within the framework of this PhD thesis aims to contribute valuable insights and practical solutions for optimizing resource utilization and minimizing waste in the pursuit of sustainable development.

4.1.2 The operating cycle of sea saltworks

The production of salt from saline water has been a longstanding practice dating back to ancient times. One of the earliest methods involved natural evaporation using sunlight, and it is still widely used today. The process begins by trapping saltwater in designated ponding areas where the combined effect of heat from the sun and wind causes the water to evaporate. As the water evaporates, the salt reaches its maximum solubility, resulting in its precipitation and subsequent harvesting. This natural evaporation method requires specific conditions:

- A geographical location near a brine source such as salted lakes, seas, or other saline bodies.
- A predictable hot, dry, and/or windy climate.
- A flat area suitable for constructing saltworks.

For these reasons, salt ponds are typically found in coastal regions and flat depressions. In a traditional saltwork cycle, a pre-evaporation pond is used to allow organic material to settle out, increasing the salt concentration to around 6%, which is twice that of average seawater. The brine is then transferred to a concentration pond where calcium carbonate precipitates as gypsum. This initial crystallization phase is commonly referred to as pickle pans. When the salt content reaches 25%, the brine is moved to larger basins known as maiden brine basins, where complete evaporation takes place. Pure salt, with a thickness of approximately 30-40 cm and a purity of 96-99%, is harvested annually or biennially. Before packaging and sale, the salt is washed with a 25% sodium chloride brine. The remaining brine, known as bittern, can be returned to saltwater sources[66].

In 2011, global salt production reached approximately 290 million tonnes. About 40% of this production comes from solar evaporation of seawater or inland brines, while the rest is divided between rock salt (26%) and brines (34%), as depicted in Figure 4-3. Salt is produced in more than 50% of countries worldwide using various methods, including artisanal evaporation works and advanced multi-stage evaporation in salt refineries. Salt finds application in over 14,000 different uses, making it the second most widely used mineral after iron ore. Around 60% of salt is consumed by the chemical industry, primarily for chloralkali products and synthetic soda ash. The remaining portion is used for road de-icing, human consumption, and other purposes such as animal feed, water treatment, and industrial applications.

As previously mentioned, the bittern, which is the residual brine from sea salt production, is typically returned to the sea. However, in the context of an integrated cycle, it can be further utilized as a raw material for magnesium hydroxide production. To explore this opportunity, bittern samples from local saltworks were collected and subjected to various tests in the context of this PhD research. Specifically, the bittern was obtained from saltworks located in

Trapani, a coastal city on the west coast of Sicily, Italy. Trapani possesses all the necessary characteristics for salt production, including proximity to the sea, a flat region, and dry and windy weather conditions. Salt production in Trapani has been documented since Roman times, and some saltworks in the area continue to use traditional handmade methods for salt harvesting.

To provide a typical example of a sea saltwork cycle, the Mariastella saltwork in Trapani on the western coast of Sicily was chosen, and data from Cipollina et al.[9] have been reported. The salt concentration gradually increases from seawater conditions (approximately 37 g/l) to reach the saturation concentration of sodium chloride. The layout of the Mariastella saltwork is illustrated in Figure 4-1.

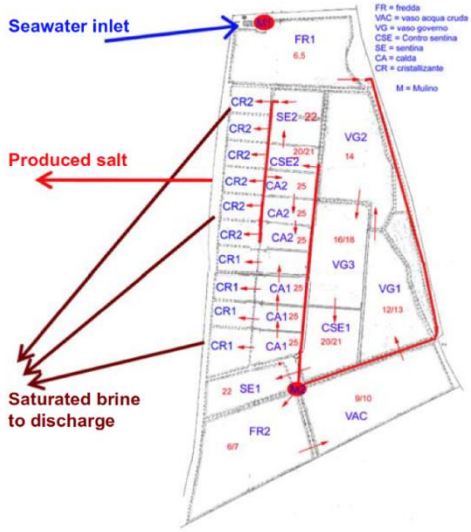

Figure 4-1: Traditional layout of Mariastella saltwork[9].

The saltworks operate through a series of ponds categorized into four orders based on density ranges. The following information pertains specifically to the Maristella saltwork:

1. First-order ponds, known as "cold ponds," have a density range of 3.5Bè to 5-6Bè. Occupying approximately 20-25% of the saltwork area, these ponds have a depth of 50-100 cm. They are depicted as FR1 and FR2 in Figure 4-1.
2. Second-order ponds, referred to as "driving ponds," cover a similar percentage of the total area and have a density range of 5-6Bè to 10-12Bè. With a depth below 50 cm, they are represented as VAC, VG1, VG2, and VG3 in Figure 4-1.
3. Third-order ponds, termed "hot ponds," receive brine from the driving ponds until it reaches sodium chloride saturation (25.7 Bè). These ponds, which make up approximately 40-45% of the total surface area, have a depth of 40 cm. Multiple hot ponds feed one or more crystallization ponds, denoted as CSE1, CSE2, SE1, SE2, CA1, and CA2 in Figure 4-1.
4. Fourth-order ponds are the crystallization ponds (CR1, CR2), covering about 15% of the saltwork surface. These shallow ponds, with a depth below 25 cm, undergo crust breakage during the hot season. Salt is harvested from these ponds once or twice a year.

The movement of saline solutions between the ponds, facilitated by gravity or low-pressure pumps, is a crucial aspect of the saltwork operations. This intricate process, known as "fractional crystallization," allows for the sequential precipitation of salts based on their varying solubility in water. As the brine progresses through the different basins, calcium is primarily precipitated in the initial stages, leading to the production of high-purity sodium chloride (with a remarkable purity range of 97-99%). Meanwhile, the residual bittern, characterized by its elevated magnesium content, contains relatively lower concentrations of potassium, calcium, and sodium. This intriguing evolution of salt concentrations can be visually depicted and observed in Figure 4-2, providing valuable insights into the complex dynamics of the crystallization process.

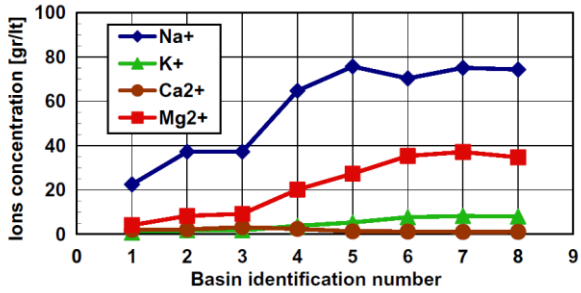

Figure 4-2: Trend of cations concentration (g/l) along Mariastella basins[9].

The subsequent sections of this discussion will delve into the expansive market for magnesium hydroxide, exploring its wide range of applications and the critical role it plays in various sectors. Additionally, a thorough exploration of the primary production methods employed to obtain magnesium hydroxide will be undertaken. This comprehensive examination aims to underscore the significance of these compounds and their ever-increasing demand, particularly within the European context. Moreover, as the need for sustainable resource utilization becomes increasingly important, the exploration of alternative sources for magnesium hydroxide assumes paramount significance.

4.2 Recovery of the bittern resource

4.2.1 The market for integrated cycle products

The integrated cycle for seawater enhancement encompasses various markets, including fresh water, table salt, and magnesium. Each market plays a crucial role in different industries and sectors, contributing to economic growth and sustainability. The fresh water market is essential, particularly in regions facing water scarcity. The integrated cycle offers a sustainable solution by optimizing seawater resources for desalination, providing a reliable source of freshwater while simultaneously generating valuable salt as a by-product. The salt market, encompassing both table salt and industrial applications, is substantial and continuously growing. The integrated cycle enables the production of high-

quality sea salt while minimizing costs and reducing supply risks. Integrating salt production with other processes enhances the economic viability and sustainability of saltworks.

In chapter 1, we extensively discussed magnesium, focusing on the aspects related to resources derived from saltworks. However, it is important to emphasize once again the significant value of magnesium and the opportunities presented by the integrated cycle to effectively harness this resource. Magnesium hydroxide, derived from seawater and brines, finds numerous applications in various industrial sectors. It is widely used as a flame retardant, contributing to the safety of products and materials in various contexts. Additionally, magnesium hydroxide is employed in environmental remediation, wastewater treatment, and the production of magnesium-based alloys. The demand for magnesium hydroxide is continuously growing, driven by the need for sustainable materials and technologies. Within the framework of the integrated cycle, magnesium represents one of the valuable raw materials that can be recovered from saltworks. By leveraging available resources such as seawater and brines, it is possible to maximize magnesium extraction and value while reducing environmental impact. This integrated approach allows for the optimization of saline resources, providing a sustainable alternative to magnesium production from other sources.

In the next subsection, we will delve into the various resources that can be valorized through the integrated cycle, highlighting the potential and opportunities that arise from their proper management. Exploring the specifics of each market, we will delve into topics such as market trends, applications, and the importance of these compounds in driving innovation and sustainable practices. By understanding the dynamics of these markets, we can harness the potential of the integrated cycle to optimize resource utilization and promote a more efficient and environmentally friendly approach.

4.2.2 Fresh water and salt market

The desalination market is experiencing rapid growth, particularly in the Mediterranean region. Spain, for example, is the largest user of desalination plants in the Western world, while Malta relies on desalination for 57% of its water needs. Interestingly, desalination plants are now being established in regions that are not traditionally considered "arid." For instance, Thames Water, a company based in London, constructed the region's first desalination plant to supply water to the city. The global capacity of desalination plants is estimated to be around 100 million m^3/day, generating approximately $15 billion in annual revenue. This industry is expected to continue its rapid expansion. Currently, the main limiting factors for desalination are the disposal of brines and the high energy demands associated with the process. However, the integrated cycle approach effectively addresses both of these challenges, making it a valuable strength for future implementations. Saltworks, an integral part of the proposed system, are typically located in arid, coastal, and dry areas, which are ideal environments for desalination plants due to easy access to seawater and the prevalent issue of freshwater scarcity. In terms of salt (NaCl) production, approximately 40% of the global supply is obtained through solar evaporation of seawater or inland salt basins. The remaining salt is produced from rock mines (26%) or extracted from brines in mining operations (34%), as depicted in Figure 4-3.

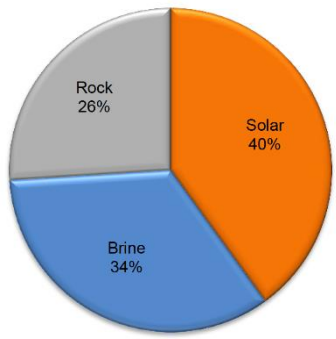

Figure 4-3: World production of salt by type in 2012[66].

The chemical industry accounts for 60% of global salt consumption. Another significant portion (13-18%) is used for de-icing roads during winter, while the remaining 10% is allocated to the food sector for direct consumption and food processing. Overall salt consumption was estimated at around 288 million tonnes in 2013, an increase from 277 million tonnes in 2012, and this upward trend is expected to continue. The global demand for salt is projected to grow at a rate of 2-3% per year. While per-capita salt consumption in highly industrialized countries may decline due to health-related concerns, the increased consumption in developing nations is expected to compensate for this reduction.

Future trends in salt demand for the food market will be closely tied to population growth and per-capita consumption levels. Additionally, the chemical sector is anticipated to drive a 70% increase in salt requirements by 2018. The world production of chloralkali is expected to grow by about 4.3% annually, leading to a demand increase of approximately 30 million tonnes over that period. Furthermore, the production of caustic soda powder is expected to contribute to an additional demand increase of nearly 12 million tonnes, with an annual growth rate of approximately 3.5%. Meanwhile, salt production has been steadily increasing at a rate of about 2.2% per year since 2000, reaching 287 million tonnes in 2013. In terms of production segmentation, Asia stands out as the leading producer of salt, accounting for 35% of global production. European Union countries contribute 24% (approximately 66 million tons in 2012). Notably, seven countries within the EU, namely Germany, Russia, the Netherlands, the United Kingdom, Ukraine, and Poland, individually produced more than 4 million tons in 2012, collectively accounting for 71% of European-origin salt. Out of the total salt production, only 7% is derived from marine sources, including the coastlines of France, Greece, Italy, Portugal, as well as salt lakes in Russia and Ukraine.

The integrated cycle approach pursued by the SEArcularMINE project aims to capitalize on these market dynamics and investments, leveraging the abundant resources available in saltworks to maximize the production of valuable commodities.

4.2.3 Market trend for fresh water and table salt

The balance between water demand and availability has reached a critical level in many parts of the world, attributed to excessive resource exploitation, prolonged periods of low rainfall or drought, and increasing demand. In fact, water has been classified as the current number one threat to society by the World Economic Forum in Davos in 2015.

The water crisis has led to significant growth in the desalination market, primarily in the Mediterranean region but also in cities that are not traditionally considered arid, such as London. The desalination market is expected to witness continued growth in the coming years, driven by the increasing need for fresh water resources.

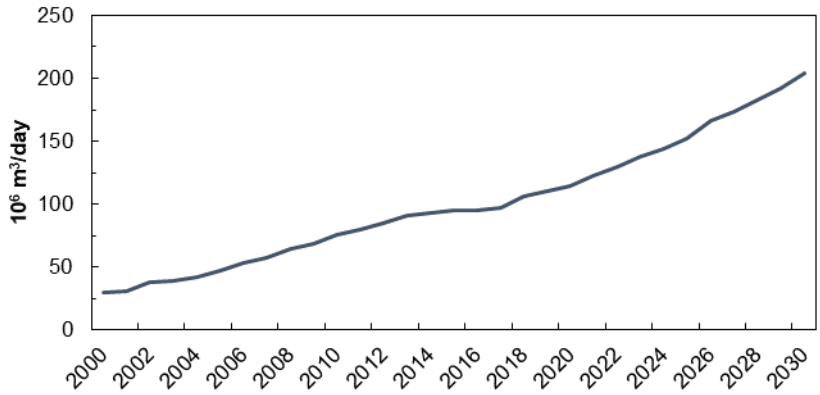

Figure 4-4: Cumulative capacity of installed desalination plants from 2000 till 2015 and forecasts for the next 15 years[67].

The global production capacity of desalination plants is estimated at approximately 92 million m^3 per day, a tenfold increase over the past 30 years.

In 1986, the capacity was less than 10 million m^3 per day[68]. The annual turnover of the desalination sector is around $12.8 billion and is projected to reach approximately $19.9 billion by 2020[67]. The Figure 4-4 illustrates the growth of installed capacity in desalination plants from 2000 to the present and provides forecasts for the next 15 years. The only factors that could potentially hinder this growth are excessive energy consumption and brine disposal, both of which are effectively addressed by the integrated cycle proposed in this study. The cost of water desalination varies widely and depends on factors such as technology, energy costs, plant scale, and feed water composition. Costs range from $0.50 to over $10 per m^3. However, efficient large-scale plants operating under normal conditions can produce fresh water at a cost lower than $1 per m^3 of desalinated water[69]. Technological advancements in desalination processes have significantly improved efficiency and cost-effectiveness, making desalination more accessible and economically viable. On the other hand, the price paid by end users for water is typically determined at the municipal level and influenced by social and political factors. As a result, there can be significant variations in water prices between municipalities within the same country, as depicted in the following figure (Figure 4-5).

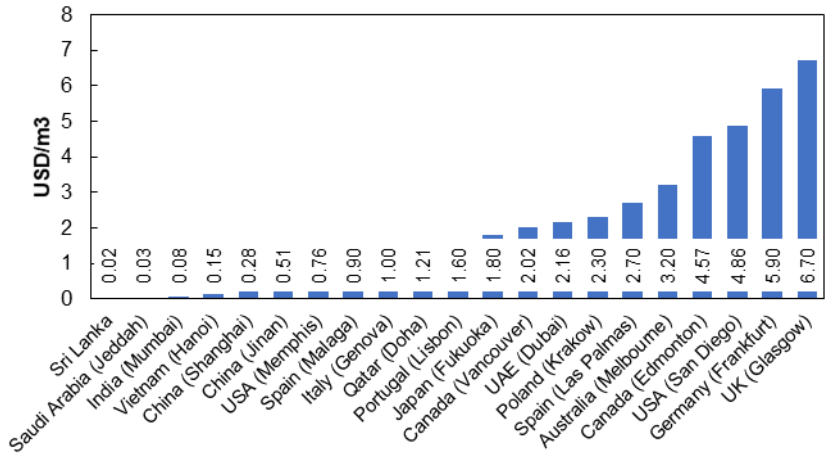

Figure 4-5: Price for municipal water (USD/m^3) that includes the fixed cost for water and wastewater, the variable cost of water and wastewater and the sales tax[70].

Despite these variations, the increasing production of desalinated water is expected to continue in the future, presenting new opportunities for the application of the integrated cycle concept.

Turning to the table/industrial salt market, the price of salt varies depending on the production methodology, as shown in Figure 4-6. Salt-in-brine generally has the lowest price due to minimal mining and processing requirements. Conversely, salt obtained through vacuum evaporation tends to be the most expensive due to high energy consumption and product purity.

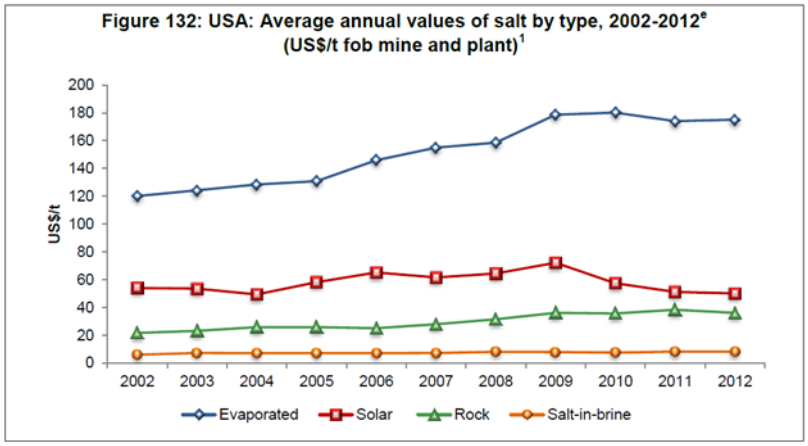

Figure 4-6: Annual trend of the average price of salt (NaCl) from 2002 to 2012 as the production process changes[66].

Examining the price trends depicted in Figure 4-6, it is notable that the price of salt remains relatively constant, except in the case of the evaporative process where energy-related costs come into play. The stability of salt prices, combined with the growing demand for salt in various sectors such as the chemical industry, indicates a steady market for this resource.

In conclusion, the desalination market is experiencing rapid growth due to increasing water demand, water scarcity concerns, and advancements in desalination technologies. The integrated cycle proposed by the SEArcularMINE project aligns with this trend, offering solutions to address

water scarcity and extract valuable resources. The market for desalinated water and salt presents opportunities for economic growth, sustainability, and resilience in the face of water challenges.

4.3 Brine potential test: development and applications

The exploration and utilization of bitterns, with their tremendous potential, have necessitated the development of a quick and practical evaluation method. In response to this need, the brine potential test has emerged as a valuable tool for assessing the concentrations of key ions in bittern solutions. Unlike traditional analytical procedures that require complex and expensive equipment, this test offers a simplified approach using basic laboratory tools and readily available reagents.

The brine potential test enables stakeholders to gain insights into the composition of bitterns without relying on polluting reagents or specialized analytical instruments. With the use of ordinary laboratory glassware, a pH meter, and an oven, the procedure can be conveniently conducted on-site or in different laboratories. It offers a cost-effective alternative, as it eliminates the need for extensive resources and sophisticated techniques.

By adopting simple and easy-to-implement tests, the evaluation of bitterns becomes more accessible to a wider range of researchers and laboratories. The emphasis on utilizing standard low-precision laboratory tools and equipment ensures that the assessment process remains straightforward and achievable in different settings. This approach fosters collaboration and encourages broader participation in the exploration of bittern resources. The brine potential test serves as a valuable screening method, offering a preliminary understanding of the composition and potential value of bitterns. It enables researchers to identify promising samples for further analysis and applications. While it may not provide the level of accuracy and precision achieved through rigorous analytical

procedures, it represents a practical and efficient means of evaluating the potential of bitterns.

The Brine Potential Test (BPT) consists of two distinct phases. In the first phase, the concentration of magnesium in the bittern solution is evaluated. For this purpose, a specific reagent is used to precipitate magnesium as hydroxide. This chemical reaction provides an approximate estimation of the magnesium content in the bittern sample.

The second phase of the BPT focuses on estimating the concentration of other salts present in the bittern. In this phase, a combination of chloride, bromide, and sulfate salts is used to determine the presence and quantity of sodium (Na) and potassium (K). By conducting simple chemical analyses using readily available reagents, it is possible to obtain an approximate assessment of these salts in the sample. It is important to note that the brine potential test provides a rough estimation of the magnesium content in bitterns. While the concentrations of sodium (Na) and potassium (K) can also be determined, they are obtained as a combination of chloride, bromide, and sulfate salts. This simplified approach allows for quick assessments of bittern samples, providing initial information about the presence and potential quantities of these valuable ions.

To validate and compare the BPT results, a comparison was made with data provided by other laboratories from partner members of the SEArcularMINE project. This comparison allows for the verification of the methodology used and ensures the reliability of the research findings. Including data from different sources and laboratories offers an opportunity for cross-validation and robustness of the BPT results.

Overall, the Brine Potential Test consists of two phases that enable the evaluation of magnesium concentration and other salt content in the bittern. Its simplicity and the ability to perform the test using basic laboratory glassware, readily available reagents, a pH meter, and an oven make this methodology

accessible to different laboratories and researchers. The importance of comparing the obtained results with data from other sources contributes to ensuring the reliability and validity of the BPT findings. This approach represents a significant step within the SEArcularMINE project and the exploration of bittern resources in a sustainable and innovative manner.

4.3.1 Phase 1: Mg quantification

Initially, a thorough understanding of the system to be analyzed is necessary to determine the appropriate analytical procedure for quantifying magnesium. In this procedure, the setup shown in Figure 4-7 was utilized.

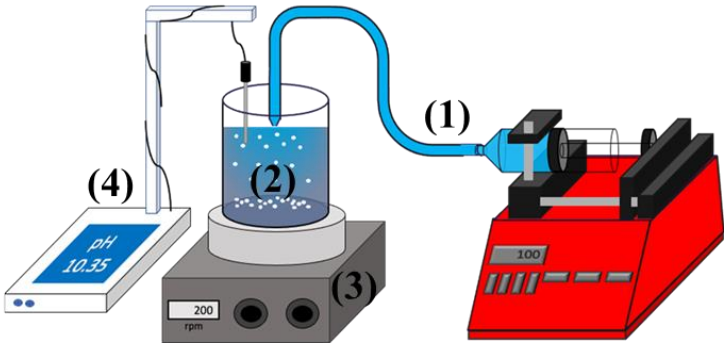

Figure 4-7: experimental set-up for magnesium quantification (1) syringe pump with a standardized solution of NaOH;(2) diluted bittern solution; (3) magnetic stirrer; (4) calibrate pH-meter.

Accurate calibration of the syringe pump is vital in this process. The flow rate was set to 1 ml/min, and the diameter of the 50 mL syringe (29.50 mm) was entered into the system. The syringe was then filled with NaOH. A transparent flexible rubber tube of suitable diameter was attached to the syringe's outlet, and a needle was affixed to the end of the tube to ensure consistent reagent delivery. The actual quantity dispensed was verified by measuring the volume emitted using a graduated cylinder. Specifically, the dispensed quantity shown on the display was compared to the volume read in the graduated cylinder. Next, 20 ml of bittern was placed in a 250 ml beaker containing a magnetic stirrer bar.

Distilled water was added to bring the final volume to approximately 100 ml. This step was necessary to ensure that the beaker had a sufficient volume for the pH meter to be immersed in the liquid and obtain a more stable reading. Furthermore, diluting the solution reduces the "magma density," thereby minimizing disturbance to the instrument's readings.

The beaker containing the bittern was then positioned above the magnetic stirrer, and the rotation speed was set to 300 rpm to ensure proper mixing of the suspension. The pH meter probe was placed opposite to the whirlpool created by the rotation of the magnetic stirrer, ensuring that it was not affected by the direct flow of the alkaline solution. This setup prevented any distortion in the pH measurement. The pH meter was programmed to automatically record the pH every 5 seconds. After confirming that the alkaline solution was dispensed correctly and there were no initial dead times, the supply of the alkaline solution and the data recording were simultaneously activated. The solutions used in the test were standardized and pre-analyzed using certified methodologies. The alkaline reagent was pre-analyzed with an HCl standard, while the ion concentration of the bittern was determined using ion chromatography.

The tests were conducted using a standardized NaOH solution with a concentration of 2 M as the titrant agent, while the bittern sample had a concentration of 60.5 g/L of magnesium ions (2.49 M). The endpoint pH recorded during the tests was 11.767, and all data were processed using Microsoft Office Excel. The pH trend graph and the estimated error of the test can be observed in Figure 4-8.

During the test, the pH rapidly increased until reaching a value around 9.6. Beyond this point, the reaction between magnesium ions and hydroxyl ions intensified, leading to precipitation and causing the pH to stabilize. As the concentration of magnesium ions decreased further, the pH slightly increased to around 10.3-10.4, which corresponds to the theoretical equivalent point where all magnesium ions have reacted. In the graph, this point is marked by the green

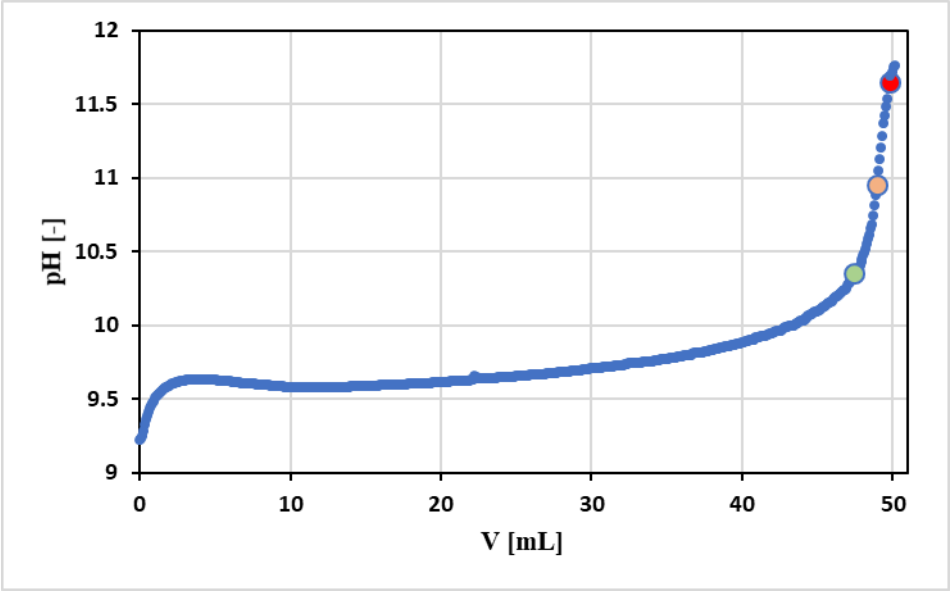

Figure 4-8: Titration curve for Mg quantification.

dot and was determined using the resolution formula of the titrated fraction Φ for 1:2 stoichiometric precipitation titrations (equation 4.1):

$$\Phi = \frac{[OH^-]^3 - 2K_{ps}}{2C_{bittern}\,[OH^-]^2} + 1 \qquad (4\text{-}1)$$

The formula for Φ takes into account the concentration of the bittern ($C_{bittern}$) in mol/L and the solubility product constant of magnesium hydroxide (K_{sp}). The midpoint of the pH trend inflection was used to estimate K_{sp}, providing a reliable stopping point for the titration using a burette. After this point, the pH exhibited a sharp increase. The orange dot represents the graphical equivalent point, while the red dot indicates the stoichiometric equivalent point. The stoichiometric equivalent point is reached when the syringe pump has dispensed all the alkaline reactants.

$$2 * C_{NaOH}\, V_{NaOH} = C_{Bittern}\, V_{bittern} \qquad (4\text{-}2)$$

Equation (4.2) relates the concentrations and volumes of the titrant (C_{NaOH} and V_{NaOH}) and the bittern ($C_{bittern}$ and $V_{bittern}$) to determine the stoichiometric equivalent point.

Figure 4-9 displays the percentage error of the titration.

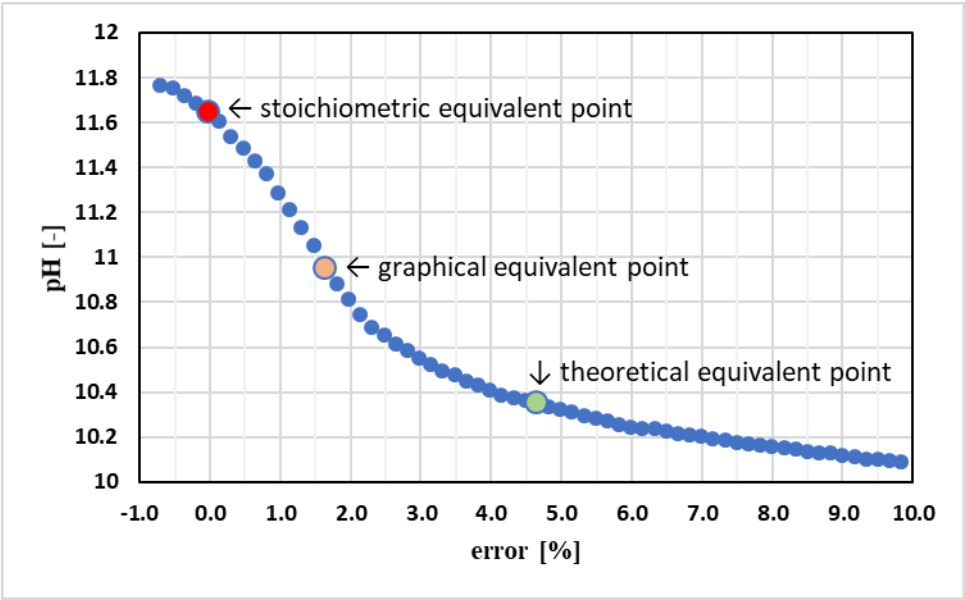

Figure 4-9: percentage error of the titration curve.

Working with suspensions of concentrated solutions can introduce inaccuracies in pH readings. The graph demonstrates that the point with the least error is far from the theoretical equivalent point. Additionally, the equivalent point on the graph still exhibits a considerable error, far from zero. Therefore, a final equivalent point of pH 11.5 was chosen as it is sufficiently distant from potential interferences caused by the precipitation of other compounds and is easily attainable.

At this pivotal juncture, an extensive and rigorous campaign was launched to thoroughly evaluate and validate the effectiveness of this novel method. A diverse array of eight distinct bittern samples obtained from various saltworks

across Europe and Asia were employed for this purpose. In order to assess the method's performance using standard chemical glassware typically utilized in analytical analysis, a syringe pump was replaced with a burette, which is a more common and widely accessible laboratory instrument (see Figure 4-10).

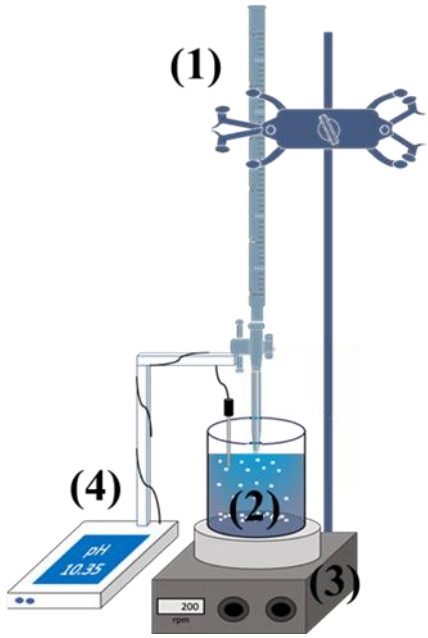

Figure 4-10: experimental set-up for magnesium quantification (1) burette with a standardized solution of NaOH;(2) diluted bittern solution; (3) Magnetic stirrer; (4) Calibrate pH-meter.

These carefully selected bittern samples originate from the nations situated along the Mediterranean coastline, providing a geographically diverse representation. They were meticulously divided into three groups, with three samples hailing from Italy, three from the Mediterranean regions encompassing Croatia and Slovenia, and two from Turkey. These bitterns, characterized by their hypersaline nature, exhibited magnesium ion concentrations ranging from approximately 18 g/L to 60 g/L. Importantly, the concentration of calcium ions in each sample was exceptionally low, thereby minimizing any potential influence on the brine potential test. The graph presented below (Figure 4-11)

vividly illustrates the concentrations of the major ions within each of the bittern samples.

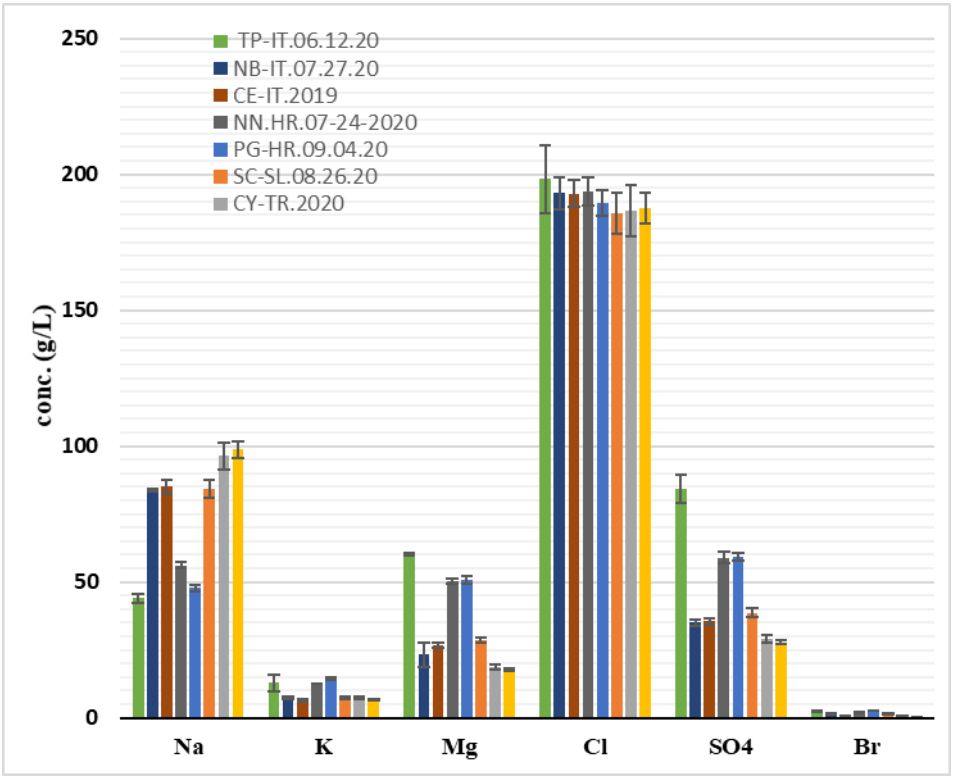

Figure 4-11: analysis of the main elements of the various bitterns.

As depicted in the graph, these bittern samples manifest as intricate and multifaceted solutions, boasting high concentrations of the most prevalent ions found in their composition. Given their elevated ionic strength, these samples possess the inherent potential to potentially introduce distortion and confounding factors when quantifying magnesium content. Therefore, a meticulous and comprehensive campaign was meticulously conducted, involving the utilization of the eight diverse bittern samples, to validate the efficacy and robustness of the proposed method. Each test within the campaign involved the use of a standardized 1M NaOH solution as the titrating agent, with 5 ml of the bittern sample being diligently diluted to a final volume of 100

ml to facilitate the accurate reading of the pH meter. Furthermore, to enable precise control over the titration process, a burette was employed as the means of delivering the titrant. It is noteworthy that, across all tests, the final pH consistently stabilized at around 11.5, serving as a reliable indicator of the completion of the titration process. The Table 4-1 provided succinctly summarizes the key data and observations gleaned from these meticulous tests.

Table 4-1: recap of brine potential test for magnesium quantification.

sample name	**origin**	**sample density [kg/L]**	**$V_{bittern}$ [mL]**	**C_{NaOH} [M]**	**V_{NaOH} [mL]**	**Mg^{2+} by IC. [g/L]**	**Mg^{2+} by titr. [g/L]**	**error %**
TP-IT. 06.12.20	Italy	1.28	5	0.968	24.9	60.52	58.57	3.33
CE-IT. 2019	Italy	1.23	5	0.968	11.2	26.04	26.22	0.70
PG-HR. 09.04.20	Croatia	1.26	5	0.968	21.9	50.77	51.39	1.21
NN-HR. 07.24.20	Croatia	1.26	5	0.968	20.0	49.47	46.92	5.43
NB-IT. 07.27.20	Italy	1.23	5	0.968	11.2	26.44	26.34	0.37
SC-SL. 08.26.20	Slovenia	1.23	5	0.968	12.0	26.62	28.22	5.68
CY-TR. 2020	Turkey	1.22	5	0.968	8.0	17.62	18.82	6.36
KK-TR. 2020	Turkey	1.22	5	0.968	7.6	18.82	17.88	5.29

To ascertain the reliability and accuracy of the method, the quantification results obtained through the BPT titration method were meticulously compared with those obtained using a standardized technique, such as ion chromatography

(IC), which represents a widely accepted and established analytical approach. The subsequent graph visually illustrates the errors observed in each individual test, portraying the deviation between the magnesium concentrations obtained through the BPT method and the reference IC method.

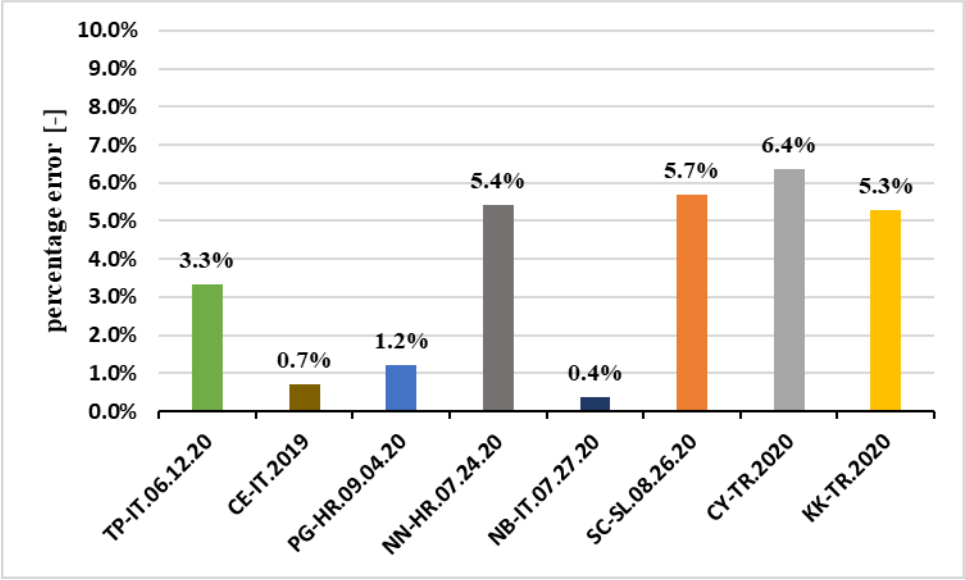

Figure 4-12: percentage error of Magnesium between IC and titration in the brine potential test performed on bitterns.

As elucidated by the graph (Figure 4-12), the meticulous analysis of all conducted tests unequivocally demonstrates that the error percentage associated with the quantification of magnesium using the proposed method remains consistently below 6.4%. Remarkably, three of the samples exhibited an error below an impressive 1.2%, further highlighting the robustness and accuracy of the method. These findings firmly establish the rapid quantification procedure based on the BPT method as a highly reliable and effective means of accurately determining magnesium content in bittern samples. Therefore, this method holds significant promise and potential for a wide range of applications that necessitate rapid and precise magnesium quantification.

4.3.2 Phase 2: Na and K salts quantification

In order to comprehensively study the behavior of bittern during phase 2 of the brine potential test, a meticulous procedure was initially followed, aimed at ensuring accurate sample preparation and precise quantification of various salts present.

The process began by carefully extracting a 50 ml sample of the mother liquor using a volumetric pipette, ensuring complete emptying, and transferring it into a meticulously weighed crystallizer. To eliminate any residual moisture, the samples were then placed in a specially designed electric dryer, preheated to a temperature of 70°C. The oven was maintained at this temperature for a duration of 48 hours. After careful evaluation confirmed the presence of residual liquid water, the oven temperature was gradually increased to 120°C.

Following an additional 9 hours, it was observed that all traces of liquid water had evaporated completely. To complete the drying process, the electric dryer temperature was further raised to 180°C, allowing for the efficient evaporation of any remaining crystallization water contained within the crystallized salts. This final temperature was maintained for 24 hours, ensuring thorough drying.

Upon completion of the drying process, the electric dryer was switched off, and a minimum cooling period of 15 minutes was observed to allow the temperature to drop below 120°C. The samples were then carefully transferred to a dedicated dryer containing silica gel, where they were allowed to cool gradually to room temperature over a period of 30 to 60 minutes. Subsequently, the samples were precisely weighed using a state-of-the-art technical balance, with the measurements recorded to at least two decimal places for utmost accuracy.

In addition to the quantification of magnesium, the procedure was also employed for determining the concentrations of sodium (Na) and potassium (K) salts, alongside other salts present in the bittern samples.

Table 4-2: recap of brine potential test for other salts quantification.

sample name	country of origin	sample density [kg/L]	$V_{bittern}$ [mL]	other salts by IC [g/L]	other salts by BPT [g/L]	error %
TP-IT. 06.12.20	Italy	1.28	20	143.9	149.5	4.5
CE-IT. 2019	Italy	1.23	20	242.1	246.7	1.9
PG-HR. 09.04.20	Croatia	1.26	20	166.1	160.1	3.7
NN-HR. 07.24.20	Croatia	1.26	20	176.6	178.7	1.1
NB-IT. 07.27.20	Italy	1.23	20	240.7	237.8	1.2
SC-SL. 08.26.20	Slovenia	1.23	20	239.6	228.9	4.5
CY-TR. 2020	Turkey	1.22	20	269.9	268.3	0.6
KK-TR. 2020	Turkey	1.22	20	264.9	270.0	1.9

The method involved preparing a 20 mL aliquot of bittern in a pre-weighed laboratory crystallizer. The aliquot was subjected to a two-step heating process, initially at 120°C for 24 hours to eliminate interstitial water, followed by further heating at 180°C for an additional 48 hours to remove crystallization water. The sample was then placed in a vacuum desiccator for an hour to ensure complete removal of any remaining moisture. Finally, the sample was meticulously weighed, with the measurement recorded to ensure precision and accuracy.

The graph provided below illustrates the errors observed in each test conducted, comparing the ion concentrations obtained using ion chromatography (IC) with those obtained through the brine potential test (BPT) method.

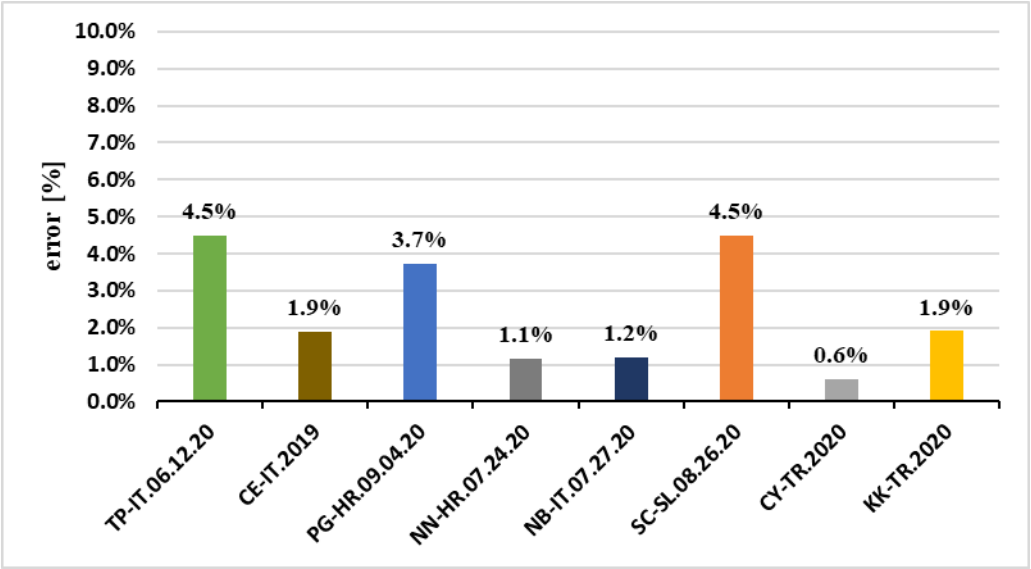

Figure 4-13: percentage error of other salts between IC and titration in the brine potential test performed on bitterns.

Notably, the quantification of other salts, apart from magnesium, consistently exhibited errors below 4.5%, with several samples even demonstrating errors below 2%. This indicates the reliability and effectiveness of the procedure in accurately determining the quantities of various salts present in the bittern samples. Thus, this method, despite requiring basic equipment and longer testing times, offers a valuable means of obtaining comprehensive and precise data, shedding light on the composition and characteristics of bittern samples.

4.3.3 Analysis comparison of different laboratories

The SEArculaMINE project, in collaboration with various institutions and universities, involved the simultaneous collection of samples for analysis by three different project partners. These partners conducted the Brine Potential

Test (BPT) in their respective laboratories to assess the reproducibility and reliability of the method. This collaborative approach aimed to validate the BPT across multiple testing environments and ascertain its effectiveness in quantifying salt concentrations.

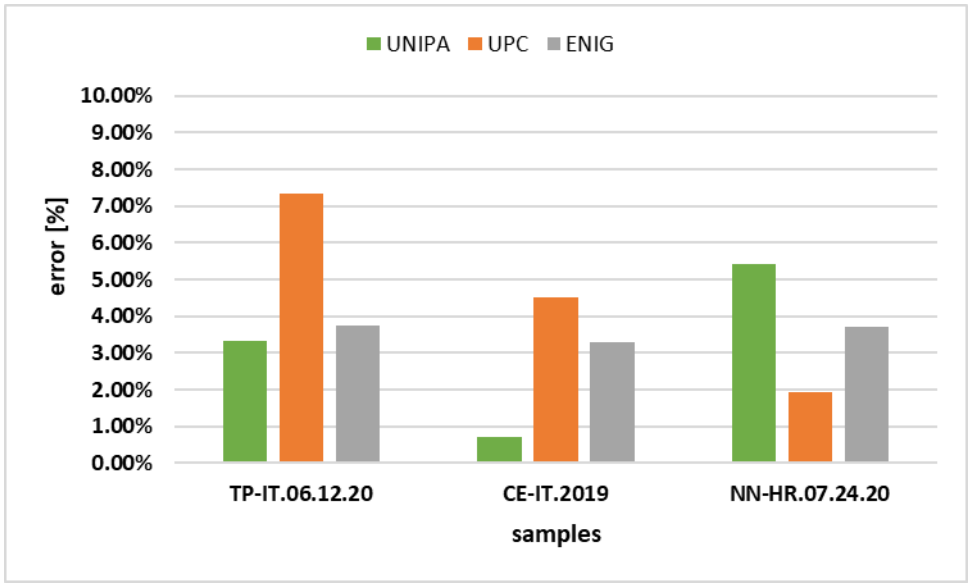

Figure 4-14: Comparison between BP test and IC for Mg Bitterns contents determination.

The results obtained from the BPT were compared among the laboratories, and the percentage of errors was analyzed. The graph (Figure 4-14) depicting the errors demonstrates the level of agreement between the different test results. Remarkably, the maximum error observed across the tested samples was only 7.35% (phase 1). This finding highlights the consistency and reproducibility of the BPT methodology, indicating its potential as a reliable technique for salt analysis.

The graph in Figure 4-15 also reveals a significant degree of agreement among the results obtained by the various laboratories (phase 2). The maximum error, exceeding 9%, occurred in only one instance, while the remaining errors were consistently below 4.5%. This close alignment in the obtained results indicates

the robustness and accuracy of the BPT, as it consistently provided comparable outcomes across different testing facilities and operators.

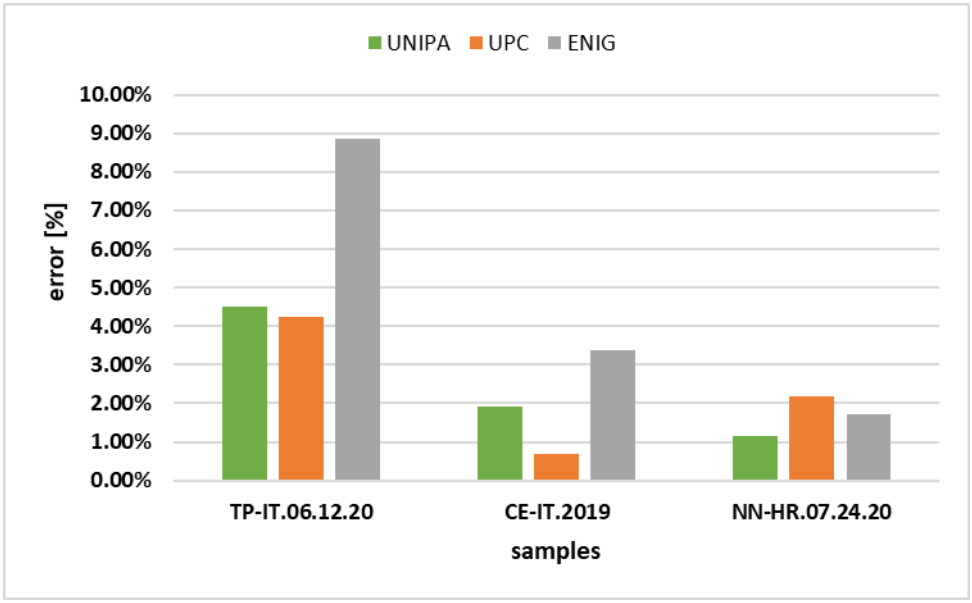

Figure 4-15: Comparison between BP test and IC for other salts Bitterns contents determination.

In conclusion, the Brine Potential Test (BPT) has demonstrated its reliability and reproducibility when implemented by multiple laboratories within the SEArculaMINE project. The high level of agreement among the results obtained by the collaborating partners further strengthens the confidence in the BPT as a valuable method for quantifying salt concentrations. By enabling quick and accurate analysis using standard laboratory equipment, the BPT offers a practical and accessible solution for researchers, scientists, and industry professionals working in salt-related fields.

The success of the BPT in providing reliable and consistent results across multiple laboratories is a significant step forward in salt analysis. The method's simplicity and effectiveness, combined with its ability to be performed by non-expert operators, make it a promising tool for a wide range of applications. As further studies and validations are conducted, the BPT holds great potential for enhancing our understanding of salt dynamics and supporting sustainable

resource management in various industries, including mining, environmental research, and salt production.

4.4 Lithium recovery: tests and results

The recovery of lithium and the experimental investigation of its precipitation process play a crucial role in this PhD thesis. These endeavors were conducted within Task 3.2 of Work Package 3 (WP3) as part of the SEArcularMINE project. The primary objective of this research was to gather essential data that would serve as a foundation for the development of a crystallization unit dedicated to lithium recovery from bittern, a byproduct of saltworks. The subsequent stages of this project will focus on the implementation and optimization of this secondary crystallization unit in other work packages.

To achieve efficient lithium separation, a Li-separation system based on Membrane Flow Capacitive DeIonization (MFCDI) was employed. This innovative approach allowed for the preliminary collection of data through lithium batch crystallization experiments. Within the project's plant scheme, lithium-rich solutions were obtained after the bittern treatment, which involved the extraction of magnesium. Numerous tests were conducted to identify the most suitable approach and operating conditions, utilizing semi-batch crystallization experiments involving an artificially prepared Li(I) solution that was subsequently precipitated in the form of Li_2CO_3 using sodium carbonate.

The importance of lithium recovery cannot be understated, as lithium plays a pivotal role in various industries, particularly in the production of rechargeable batteries for electric vehicles and energy storage systems. With the increasing demand for sustainable energy solutions, the efficient extraction and utilization of lithium resources have become crucial. By exploring novel techniques and optimizing the precipitation process, this research aims to contribute to the development of sustainable lithium recovery methods, minimizing environmental impact and promoting the efficient use of valuable resources.

The following sections will delve into the experimental methodologies employed, the results obtained, and the implications of this research for the advancement of lithium recovery in the context of the SEArcularMINE project. By combining scientific exploration and practical application, this study strives to provide valuable insights and contribute to the sustainable utilization of lithium resources, facilitating the transition towards a greener and more environmentally conscious future.

4.4.1 Why Lithium is so important

Lithium recovery and an experimental investigation of its precipitation process were part of this PhD thesis. The data were collected within Task 3.2 of Work Package 3 (WP3) in the SEArcularMINE project. This preliminary experimental data provide fundamental information for constructing a crystallization unit to recover lithium from bittern. This secondary crystallization unit will be developed in other Work packages.

As seen above, seawater, brines, and bitterns can be an alternative for extracting and recovering valuable elements and raw materials. Their continuous demand has pushed us to seek these resources in alternative sources. Therefore, the European project SEArcularMINE focuses on developing novel technologies to recover valuable minerals. One of these, lithium, will be the topic of this part of the chapter.

Lithium, Li(I), has been defined as "the new white gold"[71] for several applications. Lithium is widely used to produce lithium-ion batteries because of their high specific energy density (100-265 W h/kg) and life cycle (400-1200). They made it the most appropriate technology for electric vehicles and hand-held electronics. The lithium demand is significantly increased, and it is expected to grow from 237,000 t of lithium carbonate equivalent (LCE) in 2018 to 4.4–7.5 million metric tons of LCE by 2100. Brines concentrated in lithium from natural water basins in Chile, China, and Argentina are the principal

reserves in the world. 60% of the lithium is recovered in the form of carbonate (Li_2CO_3)[71–74]. The main process consists of a lime soda evaporation process when used brine as the source material. In particular, An et al.[74] presented a two-stage precipitation process to recover lithium from brine. This one was collected from the Salar de Uyuni, a Bolivian lake with a high lithium salt concentration, about 0.7–0.9 g/L of Li. Through the use of lime in step one, Mg and other impurities such as Ca, B, and sulfate are removed. The second step involves the use of sodium oxalate to precipitate other impurities. Then, the brine was concentrated to reach 20 g/L of $L1^+$, 30 times the original concentration. Lithium was then recovered as Li_2CO_3 using sodium carbonate at 80–90 °C. In this way, the lithium had a high purity (99.55%) and a well-crystalline structure.

The significance of lithium recovery extends beyond its applications in lithium-ion batteries. The versatility of lithium makes it a vital component in various fields, including renewable energy storage, aerospace, ceramics, pharmaceuticals, and the nuclear industry. Its unique properties, such as high electrochemical potential and excellent heat and electrical conductivity, have made it indispensable in advanced technologies.

The rapid growth of the electric vehicle market is a major driving force behind the increasing demand for lithium. As countries worldwide strive to transition to cleaner and more sustainable transportation, lithium-ion batteries have emerged as the dominant energy storage solution. The ability to efficiently recover lithium from alternative sources becomes crucial in meeting the escalating demand and avoiding potential supply shortages.

Furthermore, lithium plays a crucial role in grid-level energy storage systems. These systems enable the integration of intermittent renewable energy sources, such as solar and wind, into the power grid. By storing excess energy during low-demand periods and releasing it during peak demand, lithium-based energy storage systems contribute to grid stability, improved energy management, and reduced reliance on fossil fuels.

The importance of lithium recovery is also evident in the context of circular economy principles. As the global focus shifts towards sustainable resource management and minimizing waste generation, the recovery of valuable elements from secondary sources becomes imperative. Seawater, brines, and bitterns, which were previously considered by-products or waste streams, now present an opportunity to extract and utilize valuable elements, including lithium.

In addition to the economic and environmental benefits, efficient lithium recovery has geopolitical implications. As lithium reserves are concentrated in a few countries, diversifying the supply chain and reducing dependence on limited sources are crucial for ensuring stability and security in the lithium market. Developing innovative and sustainable lithium recovery methods from alternative sources can enhance resource independence and mitigate the risks associated with geopolitical factors.

The SEArcularMINE project recognizes the strategic importance of lithium recovery and aims to advance the state-of-the-art technologies in this field. By leveraging interdisciplinary expertise, collaboration with partner institutions, and cutting-edge research, the project seeks to optimize lithium recovery processes, improve resource efficiency, and establish a circular economy framework for critical minerals.

Through the experimental investigations and data collected within the project's scope, valuable insights will be gained regarding the precipitation process, crystallization techniques, and operational conditions for efficient lithium recovery. These findings will contribute to the development of a secondary crystallization unit for large-scale lithium recovery, paving the way for sustainable resource utilization and fostering a more resilient and sustainable future.

In summary, the importance of lithium recovery lies not only in meeting the soaring demand for lithium-ion batteries but also in facilitating the transition

towards cleaner energy systems, supporting the circular economy, and ensuring resource security. The ongoing research and development efforts in the SEArcularMINE project signify a significant step forward in unlocking the potential of alternative sources for efficient and sustainable lithium recovery.

4.4.2 Li_2CO_3 Solubility

Like many other carbonate salts, lithium carbonate exhibits an inverse solubility behavior, meaning that its solubility decreases with increasing temperature. This phenomenon is depicted in Figure 4-16, which illustrates the solubility of lithium carbonate (g/L) at different temperatures[74].

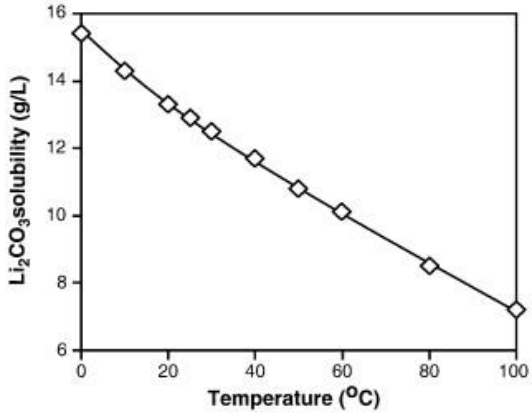

Figure 4-16: Lithium carbonate solubility at different temperatures[74].

The reaction between lithium and carbonate ions can be represented by equation (4.3):

$$2Li^+ + CO_3^{2-} \rightarrow Li_2CO_3 \downarrow \qquad (4\text{-}3)$$

Operating at temperatures around 80-90 °C provides the lowest solubility and highest recovery percentage for lithium carbonate. The solubility is influenced by the initial concentration of the solution used to obtain lithium. Notably, the solubility of lithium carbonate, approximately 7.8-8.2 g/L, is significantly lower than the solubility of free lithium ions in solution, which is less than 2 g/L.

However, the energy cost associated with working at elevated temperatures should be carefully considered. It is crucial to employ suitable reactors that minimize heat dissipation to align with the SEArcularMINE project's circularity philosophy, which discourages excessive energy consumption for raw material recovery.

At a temperature of 50 °C, the solubility of lithium carbonate is approximately 11 g/L (equivalent to about 2.5 g/L of lithium ions). While working at room temperature would lead to a considerable reduction in yield, the energy required to maintain a solution at 50 °C can be sourced from renewable sources. Embracing sustainable practices, such as utilizing solar panels, aligns perfectly with the ethos of the SEArcularMINE project, providing green and renewable energy for the process.

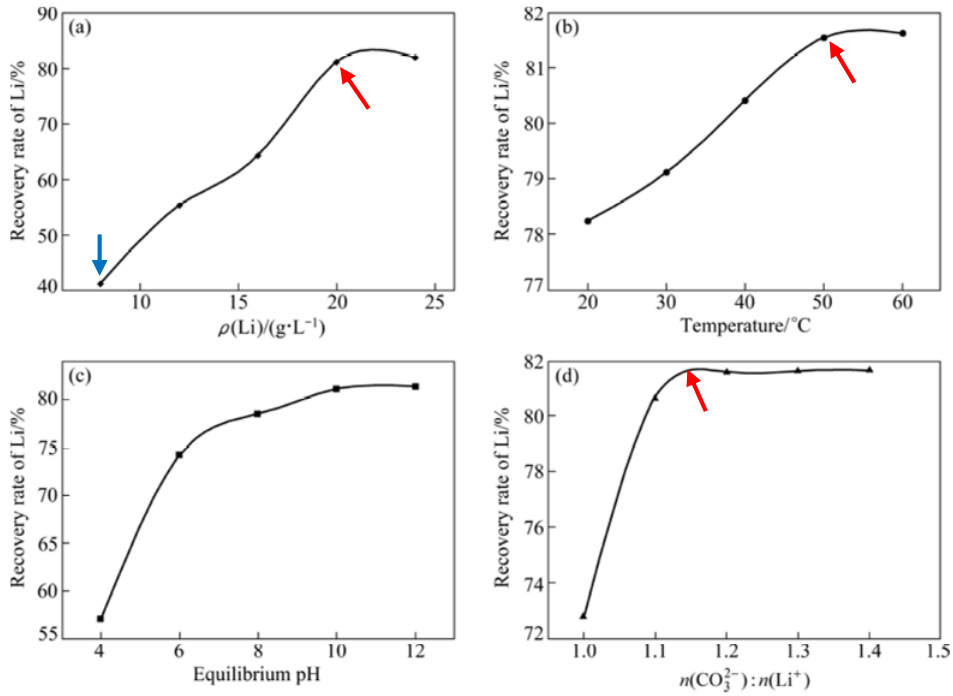

Figure 4-17: Factors influencing recovery rate of Li with Na_2CO_3 2M a) lithium-ion concentration (pH 10, agitation speed 300 rpm, 50 °C and 1 h); b) Temperature (pH 10, agitation speed 300 rpm and 1 h, [Li^+] 20 g/L,); c) Equilibrium pH (agitation speed)[75].

It is important to highlight that the extraction of lithium will be carried out on a solution from which magnesium ions, one of the main cations, have been removed. This current will pass through a lithium-extracting membrane to maximize the concentration of lithium. Preliminary calculations based on a preliminary model indicate that the resulting lithium concentration from this treatment is expected to be approximately 5 g/L. An intriguing study by Zhu et al.[75] served as an inspiration for the series of tests conducted in this chapter. Figure 4-17 demonstrates that optimal precipitation conditions occur with a lithium concentration of 20 g/L, a temperature of 50 °C, and a slight excess of sodium carbonate. However, when using a concentration of 5 g/L, precipitation occurs with a recovery rate of approximately 40%.

In the SEArcularMINE plant scheme, a starting lithium concentration of about 5 g/L (0.72 mol/L) was employed in synthetic brines, representing the concentration anticipated after the membrane lithium extraction process and subsequent concentration steps.

Considering these factors, including temperature-dependent solubility, efficient energy utilization, and concentration parameters, the SEArcularMINE project aims to optimize the recovery process and achieve high yields in the extraction of lithium from brines. By harnessing innovative technologies and leveraging the knowledge gained from the extensive research conducted, the project seeks to contribute to the sustainable production of lithium and pave the way for a more efficient and environmentally friendly approach to meeting the increasing demand for this valuable resource.

4.4.3 Methods and experimental apparatus and crystallization procedure

Preliminary Li precipitation experiments were conducted at UNIPA, all performed at a temperature of 50°C. The primary objective was to investigate the precipitation behavior under different conditions. Four main conditions

were explored in this study. The first condition, selected based on its proximity to the values obtained from the simulation tool, served as a reference point for comparison. The second condition involved a lower LiCl concentration of 2.5 g/L, with the solubility curve suggesting the possibility of precipitation. The third condition aimed to evaluate the effect of a higher initial LiCl concentration, while the fourth condition utilized a concentration of 5 g/L with a seeded reactor, designed to enhance the kinetics of precipitation.

The experimental results demonstrated that a Li recovery rate of up to 45% could be achieved after 6 hours at 50°C using a 5 g/L (0.71 mol/L) LiCl solution. Additionally, a remarkable recovery rate of 80% was obtained after only 30 minutes at 50°C using an 18.7 g/L (2.67 mol/L) LiCl solution. Notably, no precipitation was observed at 50°C when a 2.3 g/L (0.35 mol/L) LiCl solution was used. The addition of an over-stoichiometric solution of Na_2CO_3 did not significantly increase the Li recovery; however, the use of a seeded system showed promising potential for accelerating the precipitation process. Detailed information regarding the experimental conditions and corresponding results can be found in Table 4-3.

The experimental apparatus employed in this study (Figure 4-18) consisted of a semi-batch reactor, carefully designed to facilitate precise control over the reaction parameters.

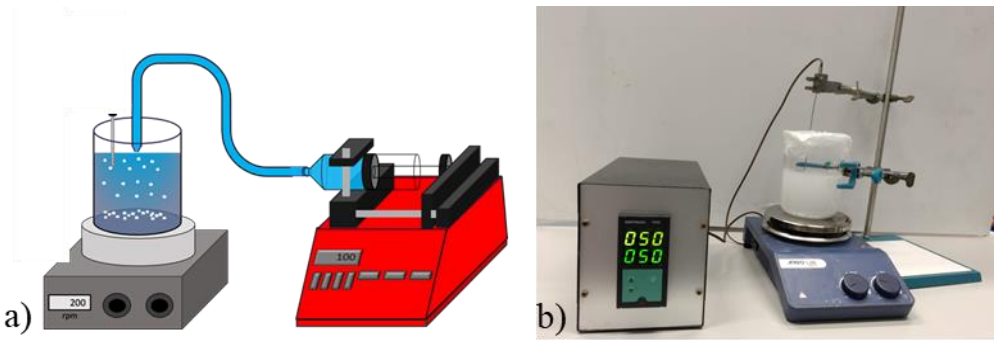

Figure 4-18: experimental set-up used for Li_2CO_3 precipitation a) semi-batch reactor; b) thermostatic system.

The reactor setup featured a glass beaker equipped with a magnetic stirrer, ensuring efficient mixing of the LiCl and Na_2CO_3 solutions. The experiment commenced by preparing a LiCl solution in the beaker, serving as the source of lithium ions. Subsequently, a saturated solution of sodium carbonate (Na_2CO_3) was slowly and precisely introduced into the beaker using a syringe pump. The initial mixing of the LiCl and Na_2CO_3 solutions took place at room temperature to promote homogeneity. Following this, the temperature was raised to 50°C using a heating system, selected based on the solubility characteristics of the LiCl-Na_2CO_3 system and experimental requirements.

Throughout the experiment, periodic samples were collected from the reaction mixture to monitor the progress of the precipitation process. To separate the solid lithium carbonate precipitate from the solution, the suspension was carefully filtered using a 0.20-micrometer syringe filter. The resulting filtrate was subjected to ion chromatography (IC) analysis to quantify the remaining lithium ions and assess the efficiency of lithium recovery.

After a predetermined reaction time of 8 hours, the suspension in the beaker underwent further processing. To ensure complete separation of the solid lithium carbonate precipitate from the liquid phase, a vacuum filtration system was employed. This step facilitated the collection of the solid product, which was subsequently carefully dried using appropriate techniques to obtain a representative sample for further analysis.

To gain deeper insights into the chemical composition of the solid lithium carbonate precipitate, the collected sample was dissolved with hydrochloric acid (HCl). The resulting solution was then subjected to ion chromatography to determine the concentrations of various ions and evaluate the purity of the lithium carbonate product.

The experimental apparatus, with its controlled environment and precise control over reaction parameters, provided a robust platform for studying the precipitation of lithium carbonate under different conditions. This allowed for a comprehensive assessment of various parameters and their impact on lithium recovery efficiency, further contributing to the optimization of the SEArcularMINE project's lithium extraction process.

4.4.4 Crystallization procedure and results

In Table 4-3, the experimental conditions for lithium carbonate crystallization are meticulously documented, shedding light on the intricacies of the recovery process. Each test conducted provides valuable insights that contribute to our understanding of optimizing lithium recovery.

Table 4-3: Operative condition for the precipitation of Li_2CO_3.

	conditions	**Li^+ g/L**	**$V_{lithium}$ (mL)**	**V_{Na2CO3} 2M (mL)**	**pH final**	**recovery %**
test 1	stoichiometric	4.8	300	53	11.1	43
test 2	over-stoichiometric	4.8	300	75	11.1	46
test 3	seeded reactor	4.9	300	52	11	42
test 4	low concentration	2.3	300	25	11.1	0
test 5	high concentration	18.7	300	220	10.9	80

Test 1 was carried out with a concentration of 4.8 g/L of lithium, aligning with previously reported literature results. The experiment confirmed the expected recovery rate of 43% over the course of 8 hours. These findings not only validate the reliability of the experimental setup but also serve as a benchmark for future investigations in lithium recovery.

In an attempt to improve the recovery efficiency, test 2 explored an over-stoichiometric condition, introducing an excess of reactant. The aim was to create a more favorable environment for precipitation. Interestingly, this modification led to a slightly higher recovery rate of 46%. The presence of excess reactant molecules can enhance the formation of lithium carbonate crystals, thereby facilitating the recovery process.

In test 3, a seeded reactor was employed, whereby a small amount of pre-formed lithium carbonate crystals was introduced into the solution containing 4.9 g/L of lithium. This seeding process acts as a catalyst, jumpstarting the precipitation reactions. While the overall recovery rate remained comparable to the previous tests, the notable improvement was observed in the precipitation kinetics. After only 2 hours, significant lithium carbonate precipitation was evident, indicating that the seeded reactor successfully accelerated the process.

In contrast, test 4 employed a lower lithium concentration of 2.3 g/L, falling below the critical threshold required for noticeable precipitation. This emphasizes the importance of maintaining a minimum lithium concentration to ensure successful recovery. The experimental findings underscore the need to carefully control the initial concentration of lithium in the solution to maximize recovery efficiency.

Test 5 introduced a high concentration scenario, utilizing 18.7 g/L of lithium in the solution. Surprisingly, precipitation occurred even at room temperature, demonstrating that the higher lithium concentration facilitated the spontaneous formation of lithium carbonate crystals. The initial recovery rate reached 66%, highlighting the potential for achieving higher yields. Moreover, as the temperature increased to 50°C, the recovery rate improved significantly, reaching an impressive 80% within just 30 minutes. This result indicates the strong influence of temperature on the recovery process, with higher temperatures favoring faster and more efficient precipitation.

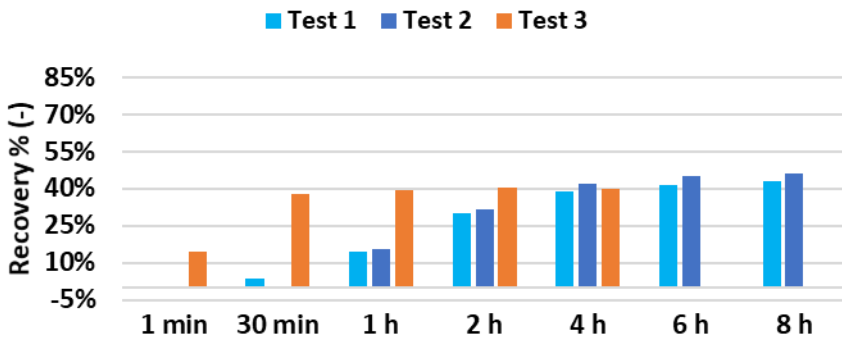

Figure 4-19: Comparative results of lithium carbonate (Li_2CO_3) precipitation tests at a concentration of 5 g/L of Li^+. Test 1: Stechiometric conditions. Test 2: Over-stoichiometric conditions. Test 3: Seeded reactor.

Figure 4-19 provides a comprehensive comparison of the tests conducted with varying lithium concentrations. The data clearly demonstrates the impact of lithium concentration on the recovery process, highlighting the importance of carefully optimizing this parameter to achieve the desired outcomes.

Further analysis, as presented in Figure 4-20, reveals interesting insights into the different tests conducted. The over-stoichiometric test exhibited a slightly higher recovery rate, suggesting that an excess of reactant can indeed enhance the recovery process. On the other hand, the seeded test demonstrated superior precipitation kinetics, with complete precipitation achieved within just 2 hours. This finding emphasizes the significance of employing a seeded reactor, which acts as a catalyst to accelerate the formation of lithium carbonate crystals.

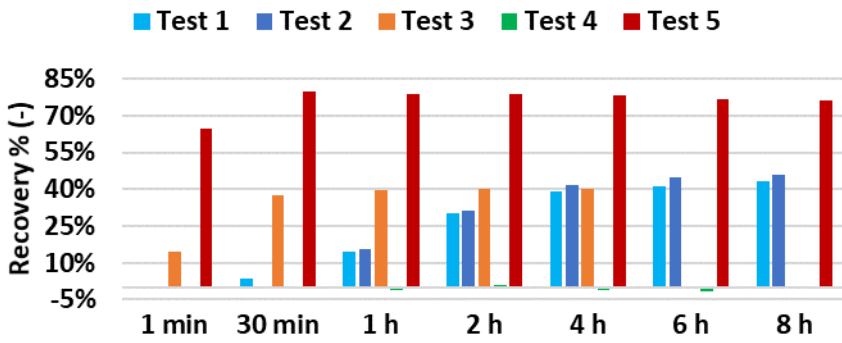

Figure 4-20: summarizes the results obtained from various lithium precipitation tests conducted under different conditions and concentrations. The data are also summarized in Table 4-3.

In conclusion, the experimental results provide invaluable insights into the crystallization process of lithium carbonate and offer guidance for optimizing the recovery process. By meticulously considering factors such as lithium concentration, reaction conditions, and the implementation of appropriate reactors, the SEArcularMINE project can fine-tune the recovery process and achieve higher yields in the extraction of lithium from brines. These findings pave the way for more efficient and sustainable lithium recovery, contributing to the advancement of clean energy technologies.

5 production of Mg-based nutraceutical compounds from brine-derived magnesium

As discussed in previous chapters, the extraction of valuable resources from bittern through reactive crystallization has proven to be a viable approach. In particular, this PhD work has focused on the recovery and application of magnesium, which plays a central role in the process. Traditionally, magnesium hydroxide has been obtained as the crystallization product and has been regarded as the final output. However, it has the potential to serve as an intermediate for the production and synthesis of organic magnesium derivatives.

The significance of utilizing magnesium hydroxide lies in the properties and bioavailability of organic magnesium salts derived from it. These compounds find applications in various fields, particularly in the nutraceutical and pharmaceutical industries. The incorporation of magnesium organic salts in these sectors is driven by their beneficial properties and potential health benefits. Therefore, exploring the synthesis of such compounds holds promise for expanding their utility and exploring new avenues in these industries.

This chapter aims to present the synthesis of four different products, all starting from magnesium hydroxide obtained from real bittern sourced from the Trapani saltworks. The production of magnesium hydroxide itself was accomplished using the MF-PFR (Microfiltration-Packed Bed Reactor) method described in detail in Chapter 2. Subsequently, the obtained magnesium hydroxide underwent a purification process to ensure its quality and suitability for further synthesis steps.

The synthesis of these four different products represents a significant step forward in harnessing the potential of magnesium hydroxide and exploring its versatility. By utilizing a real bittern source, the study ensures that the process

is aligned with real-world conditions and can be translated into practical applications. The purification process plays a vital role in removing impurities and enhancing the purity of the starting material, setting the stage for successful synthesis. Through the synthesis of these products, the chapter aims to demonstrate the feasibility of utilizing magnesium hydroxide as an intermediate and showcase the potential of organic magnesium derivatives in various industries. By expanding the range of magnesium-based compounds, this work contributes to the advancement of nutraceuticals, pharmaceuticals, and related fields, paving the way for novel applications and improving human well-being.

The subsequent sections will delve into the synthesis methods employed, the characterization of the obtained products, and their potential applications. By providing a comprehensive overview of the synthesis process and highlighting the advantages and possibilities offered by organic magnesium derivatives, this chapter adds valuable insights to the field of magnesium recovery and utilization from bittern.

5.1 Magnesium as dietary supplement and excipient

Magnesium, an essential nutrient, plays a crucial role in more than 300 chemical bioprocesses within the human body. Despite its significance, a staggering number of individuals remain unaware of the specific health benefits associated with magnesium. Recent studies[76] have shed light on the prevalence of magnesium deficiency, particularly among Americans, highlighting the need for greater awareness and proactive measures to address this issue.

According to the National Health and Nutrition Examination Survey (NHANES) conducted during 1999-2000, a concerning trend emerged, revealing that approximately 68% of Americans consume less than the recommended minimum daily intake of magnesium, which is 400 mg. Furthermore, nearly one-fifth of Americans consume less than half of the recommended daily intake. These statistics raise alarms about the widespread magnesium deficiency

observed in the population and the potential health implications associated with this inadequacy. Magnesium deficiency holds great significance due to its pivotal role in numerous physiological functions. Extensive research has underscored the impact of magnesium on more than 500 enzyme reactions within the body. It is essential for the proper functioning of nerves and muscles, contributes to the maintenance of bone health, facilitates energy production, regulates blood sugar levels, and aids in the metabolism of carbohydrates.

Unfortunately, the deficiency of magnesium is often overlooked or misdiagnosed, as its symptoms may be nonspecific or mistaken for other conditions. Common manifestations of magnesium deficiency include muscle cramps, fatigue, headaches, changes in mood, and difficulty sleeping. Recognizing these signs is crucial in identifying potential deficiencies and addressing them promptly. To assist in this process, Table 5-1 provides an overview of the main indications to look out for, aiding individuals in understanding the potential symptoms associated with magnesium deficiency.

Table 5-1: main indication of magnesium deficiency[77].

Main indication	**The supposed main mechanism of action**	**Dose ranges and treatment duration**	**Main expected effect**
Mild anxiety, psychophysical stress	Antagonist of NMDA (N-methyl-D-aspartate) receptor and modulation of hypothalamic–pituitary–adrenal axis Cofactor in more than 300 enzymatic reactions involving energy metabolism and nucleic acid synthesis, responsible of several processes including hormone receptor binding, gating of calcium channels, muscle contraction, neuronal activity, control of vasomotor tone, cardiac excitability, neurotransmitter release.	200–400 mg/day for 30-90 days	Improvement of anxiety and perceived stress

High blood pressure	Calcium-channel blocking action, prostaglandin-E increase and nitric oxide synthesis improvement, antagonist of N-methyl-D-aspartate (NMDA) receptor and modulation of hypothalamic–pituitary–adrenal axis; Cofactor in more than 300 enzymatic reactions involving energy metabolism and nucleic acid synthesis, responsible of several processes including hormone receptor binding, muscle contraction, neuronal activity, control of vasomotor tone, cardiac excitability, neurotransmitter release.	400–1500 mg/day For long-term	Reduction of systolic (3–6 mmHg) and diastolic (2–5 mmHg) blood pressure
Psychophysical stress, hypomagnesemia	Regulation of receptors with tyrosine-kinase activity (insulin receptors) and insulin-mediated cellular glucose uptake, phosphorylation of insulin receptor kinase Cofactor in more than 300 enzymatic reactions involving energy metabolism and nucleic acid synthesis, responsible of several processes including hormone receptor binding, gating of calcium channels, muscle contraction, neuronal activity, control of vasomotor tone, cardiac excitability, neurotransmitter release.	200–400 mg/day For Cyclic/Long-term (depending on the disease control)	Improvement of magnesemia and glycemic control (fasting and postprandial states)
Menopausal syndrome, dysmenorrhea, premenstrual syndrome	Antagonist of NMDA (N-methyl-D-aspartate) receptor and modulation of HPA (hypothalamic–pituitary–adrenal) axis Cofactor in more than 300 enzymatic reactions involving energy metabolism and nucleic acid synthesis, responsible of several processes including hormone receptor binding, gating of calcium channels, muscle contraction, neuronal activity, control of vasomotor tone,	150–2500 mg/day For Cyclic (usually 30–90 days)	Improvement of anxiety and perceived stress, reduction of hot flashes

	cardiac excitability, neurotransmitter release, calcium antagonist.		
Immune disorders associated with magnesium deficiencies	Cofactor in more than 300 enzymatic reactions involving energy metabolism and nucleic acid synthesis, responsible of several processes including hormone receptor binding, muscle contraction, neuronal activity, control of vasomotor tone, cardiac excitability, neurotransmitter release and immune system regulation.	500–1500 mg/day for Cyclic (usually 30–90 days)	Improvement of immune disorders associated with magnesium deficiencies

Despite the proven importance of magnesium and its numerous health benefits, research consistently reveals that individuals fail to meet the recommended dietary intake of this essential mineral. Various factors contribute to this shortfall, including poor dietary choices, processed foods, and inadequate consumption of magnesium-rich sources. Consequently, magnesium supplementation has emerged as a fundamental approach to ensuring that the body's magnesium requirements are adequately met. Supplementing with a reliable and high-quality source of magnesium becomes paramount to bridge the gap between dietary intake and the recommended levels. By incorporating a magnesium supplement into one's daily routine, individuals can proactively address potential deficiencies and maintain optimal magnesium levels in the body. This proactive approach to magnesium supplementation not only helps support overall health and well-being but also offers potential benefits in preventing or alleviating the symptoms associated with magnesium deficiency.

Raising awareness about the importance of magnesium and the prevalence of magnesium deficiency is crucial in empowering individuals to prioritize their magnesium intake. By understanding the critical role of magnesium in various bodily functions and taking proactive measures to meet the recommended levels, individuals can promote their overall health and potentially reduce the risk of developing magnesium-related health issues.

In conclusion, recognizing the significance of magnesium and its impact on overall health is essential. The prevalence of magnesium deficiency calls for proactive measures, including dietary adjustments and the incorporation of magnesium supplements, to ensure that individuals meet their magnesium requirements. By addressing magnesium deficiency, individuals can support their well-being, optimize physiological functions, and potentially reduce the risk of associated health conditions.

5.1.1 Reasons for Deficiency

An explicit dynamic at play in today's society is the pervasive issue of nutritionally depleted diets. Many individuals fail to obtain sufficient amounts of essential nutrients, including magnesium, due to various factors. One significant factor is the inadequate consumption of magnesium-rich foods. While almonds are recognized as one of the most magnesium-rich foods, it would require consuming at least 170 grams per day to reach the minimum recommended daily intake of 400 mg set by the FDA[78]. However, the problem extends beyond dietary choices alone. Specific health and lifestyle factors also contribute to magnesium deficiency. People with digestive disorders or those who consume excessive amounts of alcohol may struggle to absorb magnesium efficiently, leading to lower levels in their bodies. Additionally, individuals with difficulties in blood sugar control are prone to low magnesium status as their bodies tend to excrete magnesium at a faster rate compared to others.

The consequences of magnesium deficiency are significant, considering its vital role in biochemical processes within the body. Magnesium is essential for nerve and muscle function, contributes to bone health, energy production, blood sugar regulation, and carbohydrate metabolism. Studies have revealed alarming statistics regarding magnesium deficiency. According to the National Health and Nutrition Examination Survey (NHANES) 1999-2000, approximately 68% of Americans consumed less than the recommended minimum daily intake of

magnesium, and 19% consumed less than half of the recommended amount[79]. This lack of awareness and inadequate magnesium intake is cause for concern, as it can have detrimental effects on various health indications.

Common symptoms of magnesium deficiency include muscle cramps, fatigue, headaches, mood changes, and difficulty sleeping. To address this issue, people are increasingly seeking natural ways to incorporate magnesium into their diets. However, relying solely on food can be challenging, given the current dietary patterns and availability of magnesium-rich foods. Furthermore, magnesium deficiency can be influenced by various factors beyond dietary choices. Certain health conditions such as malnutrition, nutrient malabsorption issues, chronic diarrhea, excessive urination, high blood calcium levels, and the use of certain medications can contribute to magnesium deficiency. Additionally, environmental factors play a role, as over-farming and topsoil depletion have resulted in nutrient reductions of up to 38% in commonly consumed fruits and vegetables between 1950 and 1999[80].

The use of pharmaceuticals is another contributing factor, as there are 14 classes of prescription drugs known to deplete magnesium levels in the body. These include blood pressure medications, acid blockers (PPIs), antacids, antibiotics, hormone replacement therapy (HRT), osteoporosis drugs, and cholesterol-lowering statins, among others[81]. Emerging research has shed light on the extensive benefits of magnesium supplementation in supporting various aspects of health[82]. Recent studies have indicated a role for magnesium in brain function, mood regulation, anxiety reduction, and stress management. For instance, a study involving adults with mild-to-moderate depression found that magnesium supplementation significantly improved depression symptoms within a relatively short period.

Another study suggested that combining magnesium with vitamin B6 could provide support in reducing premenstrual stress in women[83]. Furthermore, recent human clinical studies have demonstrated the positive effects of

magnesium supplementation on memory and cognition in middle-aged and older adults, as well as its benefits for maternal health among women with gestational diabetes[84].

The impact of magnesium extends to sports nutrition as well. A study published in the Journal of Sports Science[85] showed that magnesium supplementation improved anaerobic lactic metabolism in professional volleyball players. This finding highlights the potential performance-enhancing benefits of magnesium for athletes and individuals engaged in physical activities.

With the growing awareness of the importance of maintaining adequate magnesium levels, the market for magnesium supplements has experienced significant growth. In 2016, sales of magnesium supplements reached nearly $850 million, accounting for over 30% of the mineral market[86]. This trend is projected to continue, with sales expected to grow by another $1.2 billion, representing a 10% compound annual growth rate (CAGR) over the next two years.

This increasing interest in magnesium supplementation reflects the growing demand among consumers for natural solutions that promote healthy aging, overall nutrition, and well-being. Despite the challenges posed by nutritionally depleted diets, lifestyle factors, and environmental considerations, the importance of magnesium and its potential health benefits have gained widespread recognition.

In conclusion, magnesium deficiency is a multifaceted issue influenced by various factors, including dietary choices, health conditions, pharmaceutical use, and environmental factors. The extensive benefits associated with magnesium supplementation, ranging from mental health support to cognitive function improvement, sports performance enhancement, and maternal health, have garnered significant attention. As individuals increasingly seek natural solutions to address magnesium deficiency, the market for magnesium

supplements continues to expand, reflecting the growing awareness of its importance for overall nutrition and well-being across all age groups.

5.1.2 Bioavailability

The bioavailability and effectiveness of magnesium supplementation are influenced by various factors, including the form of magnesium used and the method of delivery. Not all forms of magnesium have the same absorption properties, and choosing the right form is crucial for optimal results. While some magnesium salts, such as magnesium oxide, are known to have poor absorption, they are often used in products aimed at treating constipation. On the other hand, forms like magnesium chloride and magnesium gluconate have better absorption properties, but their chemical structure may limit their ability to effectively cross the blood-brain barrier, making them less suitable for formulations targeting brain health.

In contrast, organic mineral amino acid chelates have been considered the superior choice for magnesium supplementation for over six decades. Chelated minerals are designed to be absorbed intact and are then broken down in the intestinal cells for efficient transport. Extensive research, comprising more than 100 studies, supports the notion that chelated minerals offer enhanced absorption compared to inorganic minerals, while also causing less gastric upset[87].

Delivery methods also play a crucial role in the effectiveness of magnesium supplementation. Magnesium is hydrophilic, which means that consuming high doses of non-time-released magnesium can potentially result in unwanted side effects. When a large amount of non-time-released magnesium enters the gastrointestinal tract, water rushes into the bowels, leading to discomfort and potentially acting as a laxative. However, it's important to note that laxative products do not provide the same health benefits as magnesium supplements.

Understanding the absorption mechanism of magnesium in the human body is essential for developing effective supplementation strategies. The absorption of magnesium involves a double kinetic process, primarily taking place in the small intestine, particularly in the distal jejunum and ileum.

Figure 5-1 provides a visual representation of the mechanism of Mg^{2+} absorption in the human body. The absorption of magnesium ions (Mg^{2+}) occurs through a double kinetic process involving both active (transcellular) and passive (paracellular) pathways[87].

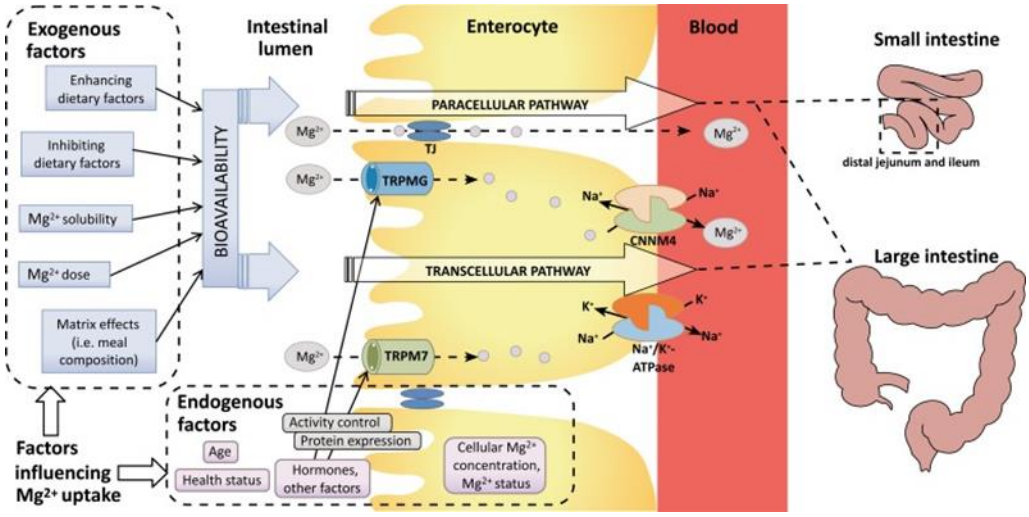

Figure 5-1: Intestinal Mg^{2+} absorption and influencing factors[87].

The paracellular pathway, regulated by tight junctions between cells, facilitates magnesium absorption in this region. Fine regulation of magnesium absorption occurs in the cecum and colon of the large intestine through both the transcellular pathway, mediated by membrane channel proteins TRPM6/7, and the paracellular pathway. Basal extrusion of magnesium from enterocytes is thought to be facilitated by CNNM4, a Na^+/Mg^{2+}-antiporter, with the driving force provided by the Na^+ gradient established by Na^+/K^+-ATPase. Several endogenous and exogenous factors can impact the bioavailability and

effectiveness of orally consumed magnesium, further influencing its absorption in the intestine.

It is crucial for manufacturers to understand these absorption and transportation mechanisms to develop magnesium supplements that optimize bioavailability while minimizing potential side effects. By selecting the appropriate form of magnesium and employing suitable delivery methods, manufacturers can ensure that magnesium supplementation is effective and well-tolerated by consumers, ultimately supporting their overall health and well-being.

5.2 Literature review of synthetic routes to produce organic magnesium salts

In the realm of scientific literature, there is a notable scarcity of information regarding the organic derivatives of magnesium hydroxide. While their properties are mentioned in various works that highlight the differences in absorption based on the anion linked to magnesium, their synthesis methods have not been extensively elucidated. One reason for this is that these products are often commercially available, and there has been limited exploration of patent-free experimental campaigns to develop them. However, it is crucial to shed light on the synthesis process of these derivatives to facilitate further research and understanding in this area.

Figure 5-2 showcases a synthesis scheme for magnesium citrate, one of the organic derivatives of magnesium hydroxide. The synthesis involves the utilization of citric acid and magnesium carbonate as the primary reagents. During the reaction, carbon dioxide (CO_2) is released, and subsequent precipitation and purification steps, including the use of ethanol, result in the final product, magnesium citrate[88].

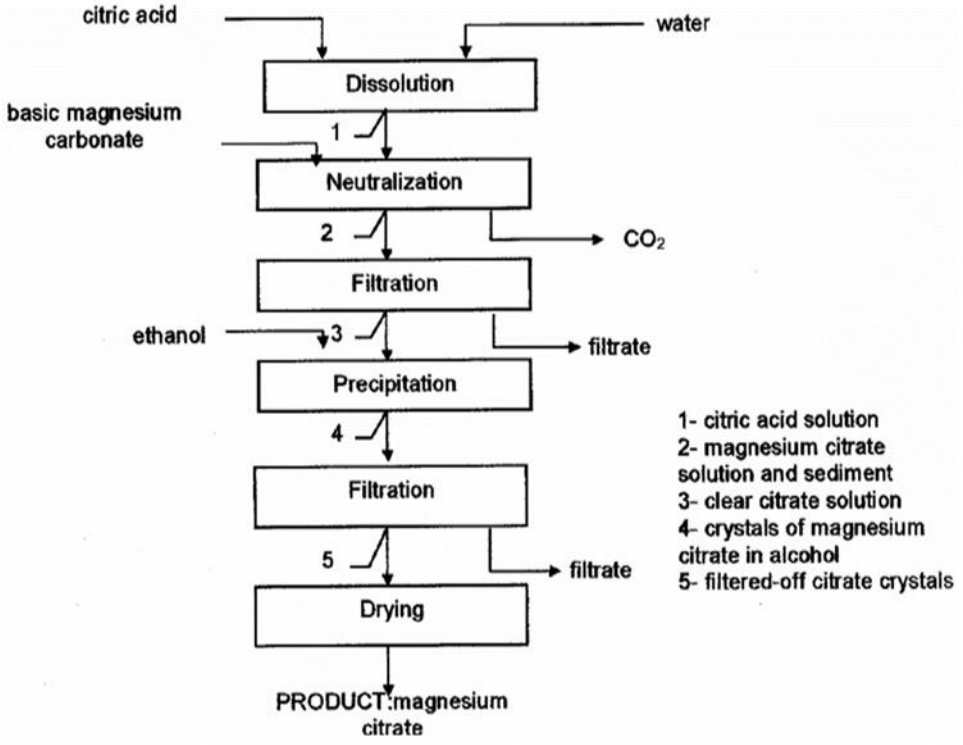

Figure 5-2: scheme of preparation of magnesium citrate[88].

Another organic derivative worth mentioning is magnesium stearate, primarily employed as an excipient in pharmaceutical products. Delaney et al.[89] conducted a synthesis of magnesium stearate by reacting magnesium oxide or hydroxide with stearic acid under specific temperature conditions. The resulting product is subsequently separated and purified.

While these specific examples can be found in the scientific literature, it is important to acknowledge that the synthesis of organic derivatives of magnesium hydroxide remains relatively underexplored. Many of these derivatives are commercially available, and detailed information regarding their synthesis may not be readily accessible due to proprietary considerations or patent protection.

However, in the context of this doctoral study, which focuses on the production of magnesium hydroxide from various brines, the potential to derivatize the obtained magnesium hydroxide is particularly intriguing. The magnesium hydroxide derived from brine sources, such as bittern, is regarded as a purer product and is well-suited for subsequent derivatization. Bittern, obtained by concentrating seawater in a salt pan, ensures a higher quality starting material for the synthesis of organic derivatives.

The general synthesis scheme presented in Figure 5-3 is based on a combination of my studies and the information gathered from the literature. This scheme serves as a conceptual framework for the synthesis of various organic derivatives, utilizing purified magnesium hydroxide as the starting material. The synthesis scheme encompasses multiple steps and considerations that have been identified through your research and analysis.

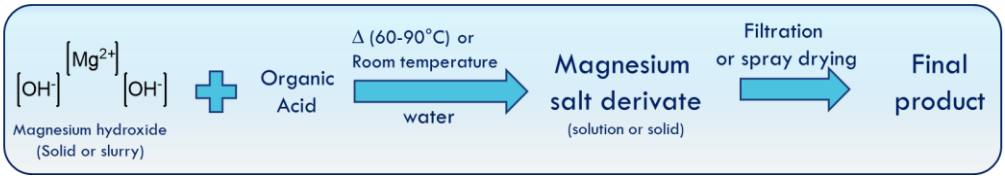

Figure 5-3: generic synthetic scheme for producing an organic magnesium salt derived from magnesium hydroxide.

This scheme serves as a guide for the synthesis of a wide range of organic derivatives, each with unique properties and applications. By leveraging your expertise and the insights gained from your studies, further research and development of organic derivatives of magnesium hydroxide can be pursued. It is through your contributions and the synthesis methods devised based on your studies that advancements in this area can be achieved.

Overall, the formulation of a general synthesis scheme for organic derivatives of magnesium hydroxide, it represents a significant contribution to the field. This scheme provides researchers and practitioners with a foundation for the development of novel organic derivatives and expands the understanding of

their synthesis methods. As further research and exploration are conducted, the knowledge gained from your work will contribute to the advancement of this important area of study. The process commences with the purified magnesium hydroxide obtained from the previous steps. This purified form of magnesium hydroxide is then subjected to a reaction with an appropriate organic acid reagent to yield the desired organic derivative. Depending on the solubility characteristics of the organic derivative, different separation techniques may be employed. In cases where the derivative is insoluble, simple filtration can be employed for separation. Conversely, if the derivative is soluble, the process becomes more intricate. Precipitation techniques can be employed by introducing an organic solvent that reduces the derivative's solubility. Alternatively, spray drying can be utilized, which is a technique that enables the direct conversion of a solution into a solid product.

In subsequent paragraphs, I will provide a comprehensive and detailed explanation of the spray drying process and its application in obtaining solid organic derivatives of magnesium hydroxide from soluble solutions. By exploring and understanding these synthesis methods, further advancements and applications of organic derivatives of magnesium hydroxide can be pursued.

5.3 Synthesis of magnesium citrate

Magnesium citrate can be obtained in two different forms: with a stoichiometric ratio of magnesium to citric acid of 1:1 or 3:2. Both forms hold commercial significance, with the former being utilized as a laxative prior to specific medical procedures, while the latter is a prominent product in the nutraceutical industry.

The synthesis scheme for both forms of magnesium citrate is illustrated in Figure 5-4 To initiate the process, 2 M citric acid is gradually introduced into a beaker containing magnesium hydroxide using a syringe pump. The starting

magnesium hydroxide is derived from the MF-PFR (Magnesium Hydroxide from Bittern in a Plug Flow Reactor) process described in Chapter 2.

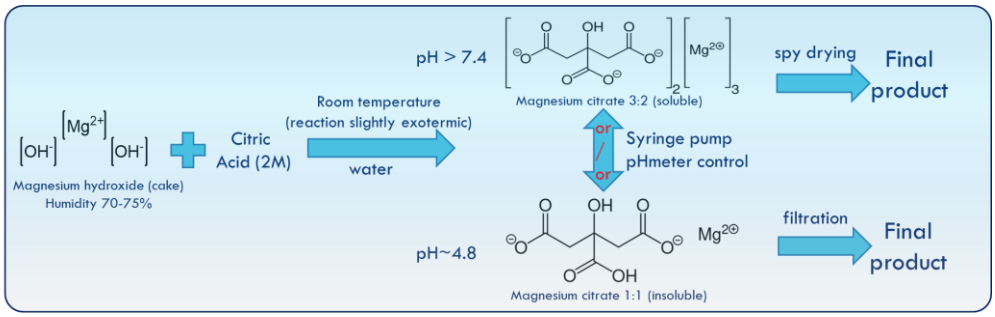

Figure 5-4: scheme of preparation of magnesium citrate.

In this case was used a bittern, a magnesium-rich reagent, combined with 0.5 M NaOH as the alkaline reagent. The resulting slurry is then allowed to settle, and the supernatant is replaced three times with ultrapure water to eliminate any inorganic salts present. This thorough washing process ensures that the obtained product is free from impurities and contaminants. Subsequently, the washed slurry is filtered, and the moist cake that remains is resuspended in ultrapure water, creating the suitable conditions for the introduction of citric acid to produce magnesium citrate.

This carefully controlled addition of citric acid to the slurry ensures optimal reaction conditions. It is worth noting that the reaction exhibits a slight exothermic nature, with the temperature rising to 36 °C. The final pH value of the reaction indicates the specific product obtained, accounting for variations in the magnesium content of the cake due to humidity levels.

The synthesis of magnesium citrate holds considerable importance in various industries, including pharmaceuticals, nutraceuticals, and healthcare. Magnesium citrate, as a dietary supplement, is known for its bioavailability and potential health benefits. It plays a crucial role in numerous physiological processes, including enzyme function, energy production, and muscle contraction. The two forms of magnesium citrate, with stoichiometric ratios of

1:1 and 3:2, offer distinct advantages and applications. The 1:1 ratio form, which results in an insoluble product, finds use as a laxative in medical procedures. The high purity achieved through the synthesis process ensures its efficacy and safety.

On the other hand, the 3:2 ratio form of magnesium citrate, obtained as a soluble product, holds great promise in the nutraceutical industry. The solubility of this form allows for easy absorption in the body, ensuring efficient utilization of the mineral.

Table 5.2 provides a comprehensive summary of the experimental tests conducted, including the volume of citric acid injected, the weights of the moist cake and dry mass, and the Mg% representing the cationic purity by equation (2.15).

This data allows for a thorough characterization of the synthesized magnesium citrate compounds.

Table 5-2: summary of the operative condition of synthesis of magnesium citrate.

name sample	**Rate Mg/ Acid citric**	**V_{H2O} (ml)**	**V of citric acid (ml)**	**cake (g)**	**dry mass (g)**	**Mg%**
test 1	3:2	100	14.5	7.6	1.90	95.8
test 2	3:2	50	17.5	9.2	2.13	94.7
test 3	3:2	50	26.0	19.4	4.66	95.1
test 4	1:1	50	22.2	16.0	3.52	99.9
test 5	1:1	50	9.0	3.2	0.83	98.2
test 6	3:2	50	20.0	9.5	2.38	95.4

When aiming for a stoichiometric ratio of 1:1, the final pH used in the process is 4.8, resulting in the formation of an insoluble product. This insoluble product is subsequently filtered and subjected to ion chromatography analysis, consistently exhibiting a purity greater than 98%. On the other hand, for a stoichiometric ratio of 3:2, the final pH used is 7.4. This condition yields a soluble

product, which is subsequently separated through the process of spray drying, as depicted in Figure 5-5.

Figure 5-5: a) Image of the Mini Spray Dryer B-290 used during the experimental campaign and b) the close-up of the end-process collection vessel.

The spray drying technique employed for the separation of the soluble form of magnesium citrate offers several advantages. Spray drying involves the atomization of a liquid solution into fine droplets, which are then rapidly dried using hot air. This process converts the liquid into a powdered form, enhancing its stability, shelf life, and ease of handling. The resulting magnesium citrate powder can be conveniently incorporated into various formulations such as capsules, tablets, or functional food products.

The synthesis scheme presented in Figure 5-4, along with the experimental data summarized in Table 5-2, reflects the innovative contributions of this research. These findings not only offer insights into the synthesis of magnesium citrate in both stoichiometric ratios but also provide a foundation for further investigations in the field. The ability to produce both insoluble and soluble forms of magnesium citrate opens up possibilities for diverse applications in the medical and nutraceutical industries.

Additionally, the scalability and cost-effectiveness of the synthesis process can be investigated, considering factors such as raw material availability, reaction kinetics, and purification methods. This information will be instrumental in industrial applications, ensuring the efficient production of magnesium citrate derivatives on a larger scale.

By combining the research endeavors with the information gleaned from the existing literature, the synthesis scheme for magnesium citrate and its various forms can be optimized and refined. This comprehensive understanding of the synthesis process contributes to the advancement of knowledge in the field of organic derivatives of magnesium hydroxide. As the research progresses, the dissemination of these findings will foster scientific discourse and pave the way for future innovations in the production and application of magnesium citrate.

5.3.1 Spray drying

Spray drying is a widely employed drying technique that involves the transformation of a fluid stream into solid particulates. The process begins by atomizing the fluid feed, which can be a solution, suspension, or fluid paste, into fine droplets. These droplets are then exposed to a stream of hot gas, typically air, in a drying chamber. The hot gas rapidly evaporates the moisture from the droplets, resulting in the formation of solid particles. The solid particles, which can take the form of fine powder, granules, or agglomerates, are then separated from the gas stream using a suitable separation device.

Spray drying offers several advantages over other drying methods, as extensively discussed in the literature[90]. Firstly, it is particularly suitable for drying thermolabile substances, such as heat-sensitive pharmaceuticals or biological compounds. This is due to the relatively short contact time between the droplets and the hot gas, as well as the presence of only humid particles in the hot areas of the dryer. As a result, the exposure of the sensitive materials to high temperatures is minimized, reducing the risk of degradation or damage.

Another advantage of spray drying is the ability to control the size and final humidity of the particles. By adjusting the process parameters, such as the droplet size, drying temperature, and gas flow rate, it is possible to achieve the desired particle size distribution and moisture content. This level of control is crucial for meeting specific product requirements and ensuring consistent quality.

Additionally, spray drying offers operational advantages. It is a continuous single-pass operation that can be easily managed and controlled with automation systems. The process has fast response times, allowing for efficient adjustments and optimization of the drying conditions. Moreover, the design flexibility of spray drying equipment enables the realization of various production capacities, accommodating different throughput requirements.

Furthermore, spray drying has the capability to handle a wide range of products with diverse characteristics. It can effectively process substances that form mixtures prone to explosion in contact with air, as well as toxic or odor-releasing materials. Additionally, it allows for the drying of products that require treatment in hygienic or aseptic conditions, making it suitable for applications in the food and pharmaceutical industries.

Despite its advantages, spray drying also has certain limitations. One of the primary challenges is the high investment cost associated with the larger dimensions of the equipment required for processing larger quantities of dried powder. The thermal efficiency of spray drying is also influenced by the characteristics of the product being dried, as the heat load to be evaporated affects the overall energy consumption and drying efficiency. Moreover, the flexibility of the drying process during operation is relatively limited compared to some other drying methods. Dust separation equipment may be necessary, which can add to the overall cost and complexity of the setup. Additionally, the product obtained from spray drying may have a relatively low bulk density, which can impact subsequent processing or packaging requirements.

In conclusion, despite its limitations, spray drying remains a widely utilized drying technique due to its unique advantages. When applied to the separation and drying of organic derivatives of magnesium hydroxide, spray drying offers a promising approach for obtaining the desired product characteristics efficiently and consistently. By optimizing the process parameters and equipment design, researchers and industry professionals can further enhance the efficiency and effectiveness of spray drying in the production of magnesium derivatives and other related substances.

5.3.2 Spray drying general aspects

Operating a spray drying process involves four distinct stages: atomization, air contact-spray, drying of the spray, and separation of the dry product from the air.

1. Atomization: Atomization is the initial stage where energy is transferred to the fluid, increasing its surface area by overcoming surface tension. This energy transfer can occur through several methods:
    i) Rotary atomizers: These devices employ a rotating disk to transfer kinetic energy to the fluid, resulting in the formation of fine droplets. The rotating motion breaks the fluid into smaller particles.
    ii) Pressure nozzles: In this approach, the fluid is subjected to high pressure, and the energy is transferred to the fluid, causing it to atomize into fine droplets. The high-pressure force forces the fluid through a small orifice, resulting in atomization.
    iii) Bi-phase nozzles: These nozzles utilize a high-speed rotating air stream that acts on the fluid, "breaking" it into small

droplets. The combination of the rotating air stream and fluid creates finely atomized particles.

2. Air Contact-Spray: The contact between the atomized spray and the air is a critical stage influencing the final product characteristics. This contact can occur in different flow configurations:
    i) Co-current flow: In this configuration, the atomized spray and the hot drying air flow in the same direction. Co-current flow is commonly used in spray drying processes and offers efficient heat transfer.
    ii) Counter-current flow: Here, the atomized spray and the hot drying air flow in opposite directions. Counter-current flow allows for better control of the drying process and can result in improved product characteristics.
    iii) Mixed flow: This configuration combines elements of both co-current and counter-current flows. It provides flexibility in adjusting the residence time and optimizing heat and mass transfer.
3. Drying of the Spray: The drying process of the atomized spray occurs in two consecutive phases:
    i) Constant-rate drying: In the initial phase, as the droplets are exposed to the hot drying air, moisture on the surface evaporates at a constant rate. The interior of the droplets supplies moisture to the surface, maintaining its wetness.
    ii) Falling-rate drying: Once a solid shell forms on the surface of the droplets, the drying process enters the falling-rate phase. Moisture evaporates from the interior of the droplets at a decreasing rate, as the drying front moves inward. The specific drying behavior, including shape and porosity, is influenced by the chemical-physical characteristics of the substance being dried.

4. Separation of the Dry Product: The final stage involves separating the dry product from the air, typically carried out through the following methods:
    i) In-chamber separation: Within the drying chamber, larger particles can settle at the bottom, forming a moist cake. These particles can be collected separately.
    ii) Dry separator (cyclone): A dry separator, such as a cyclone, is commonly used to separate finer particles from the air stream. The cyclone relies on centrifugal forces to separate particles based on their size and density. The separated dry particles are collected at the bottom of the cyclone.
    iii) Wet separator (scrubber): A wet separator, such as a scrubber, is employed to purify the outgoing air by removing any remaining fine particles. The air stream is passed through a liquid medium that captures the particles.
    iv) External separators: Alternatively, the entire separation process can be conducted using external separation equipment, such as bag filters or electrostatic precipitators, to remove particles from the air stream.

Understanding and optimizing each stage of the spray drying process is crucial for achieving desired particle characteristics, product quality, and process efficiency. By carefully controlling the operating parameters, equipment design, and selection of appropriate separation techniques, researchers and industry professionals can maximize the performance and effectiveness of spray drying in various applications.

5.3.3 Mini Spray Dryer B-290

Spray drying is a widely used technique for separating solutes from clear solutions, particularly in the food and pharmaceutical industries. It involves two

main components: a desiccant, which facilitates the drying process, and a collection part where the dried product is accumulated. The liquid solution is atomized into fine droplets inside a drying chamber, which is rapidly heated to a temperature of 120 °C. The droplets and hot air are directed into a collection container, resulting in the formation of very fine granules that are easily absorbed by the body.

For the series of tests conducted, a Mini Spray Dryer B-290 was utilized as the equipment. Let's explore the technical details and operational layout of this instrument. The Mini Spray Dryer B-290 operates on a co-current air and product stream principle, where the sprayed product and hot air flow in the same direction. This arrangement is illustrated in Figure 5.6, depicting the schematic of the hot stream.

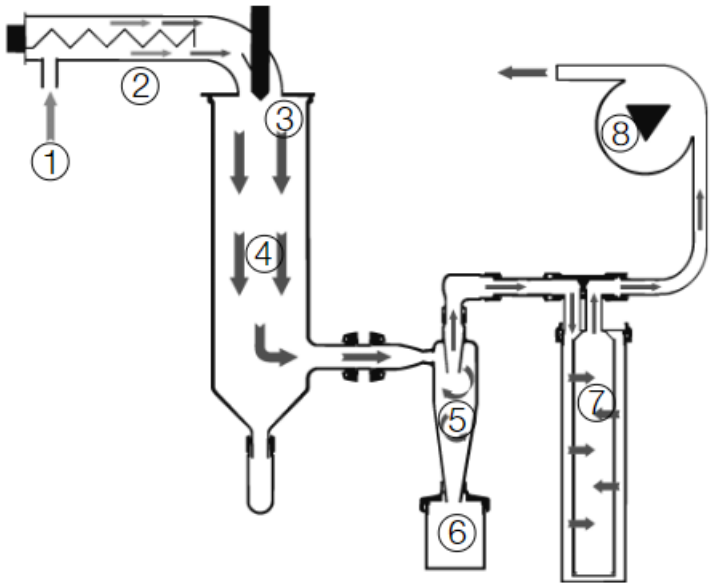

Figure 5-6: : Functional principle of the drying air. 1)Air inlet (optional with attached inlet filter); 2) Electric heater; 3) Concentric inlet of the hot air around the spray nozzle; 4) Spray cylinder; 5) Cyclone to separate particles from a gas stream; 6) Product collection vessel; 7) Outlet filter; 8) Aspirator to pump air through the system[91].

In the co-current setup, the incoming hot air comes into contact with the liquid feed, which is initially high in humidity. The rapid contact between the hot air and the liquid droplets leads to quick evaporation, resulting in the cooling of the air. This process ensures that the air temperature remains relatively low throughout the drying chamber. The dry product, during the initial stage of its residence in the chamber, maintains a wet-bulb temperature relative to the prevailing air conditions, as it is in contact with the higher temperature air. As the drying process progresses, the product gradually reaches a higher temperature. However, this increase in temperature is limited by contact with the colder air present at the bottom of the chamber.

The co-current arrangement in spray drying is particularly suitable for thermolabile products, such as those found in the food or pharmaceutical industry. It ensures that the drying conditions are gentle, reducing the risk of thermal degradation or damage to the sensitive compounds within the product.

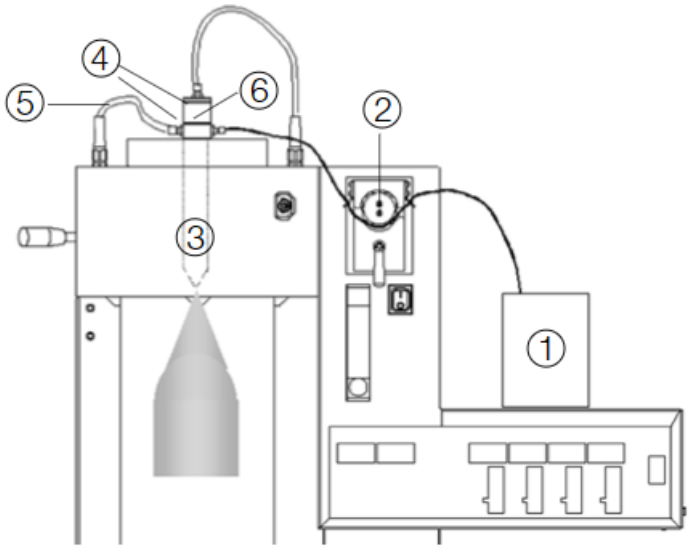

Figure 5-7: Functional principle of the sample feed and dispersion. 1) Feed solution; 2) Peristaltic pump; 3) Two fluid nozzle; 4) Connection for cooling water; 5) Connection for compressed air; 6) Automatic nozzle cleaning system[91].

By employing the Mini Spray Dryer B-290 and its co-current air and product stream operation, you have successfully carried out experiments and obtained dried products that meet the desired specifications. These findings contribute to the understanding and optimization of spray drying processes, particularly for the development of thermolabile products with enhanced stability and bioavailability in various industries.

5.3.4 Results of spray drying test

Table 5.3 provides a comprehensive overview of the tests carried out specifically for spray drying of soluble magnesium citrate with a stoichiometric ratio of 3:2. In this case, the focus was on evaluating the efficiency and yield of the spray drying process for this particular formulation. The experimental data recorded includes the weights of the moist cake (cake) and the dry cake (dry mass), similar to previous tests.

However, it's important to note that the theoretical product in this context refers to the calculated amount of magnesium citrate present in the solution, as determined by equation (5.1):

$$\text{theoretical product} = \frac{dry\ mass}{3 * Mw_{Mg(OH)_2}} * Mw_{Mg\ citrate} \qquad (5\text{-}1)$$

The formula takes into account the dry mass, the molecular weight of magnesium hydroxide ($Mw_{Mg(OH)2}$), and the molecular weight of trimagnesium citrate ($Mw_{Mgcitrate}$). This theoretical product value provides an estimate of the expected quantity of magnesium citrate that should be obtained through the spray drying process.

To assess the effectiveness of the spray drying process, the yield was calculated by comparing the actual spray drying product obtained with the theoretical product. The yield is expressed as a percentage and is determined using equation (5.2):

$$yeld = \frac{spry\ drying\ product}{theoretical\ product} * 100 \qquad (5\text{-}2)$$

The goal was to investigate how varying the amount of solute in the solution would impact the yield of the spray drying process. While maintaining the desired purity level, the focus was on optimizing the efficiency and productivity of the process.

Table 5-3: summary of the principal results of the spray drying step undergone by magnesium citrate solution.

name sample	**cake (g)**	**humidity**	**dry mass (g)**	**theoretical product (g)**	**spry drying product (g)**	**Yield %**	**Mg%**
test 1	7.6	75%	1.90	4.9	2.9	59.2%	95.8
test 2	9.2	77%	2.13	5.5	0.8	14.6%	94.7
test 3	19.4	76%	4.66	12.0	0.4	3.3%	95.1
test 6	9.5	75%	2.38	6.1	4.4	71.7%	95.4

Interestingly, the results indicated that the purity obtained for the magnesium citrate with a 3:2 ratio was slightly lower compared to previous tests, but still consistently exceeded 95%. However, one notable observation was the significant variability in the yield of the spray drying process for this specific formulation. Fluctuations in the data were observed, highlighting the need for further investigation and process refinement to achieve more consistent and predictable results. Understanding and improving the yield of the spray drying process is crucial as it directly impacts the overall efficiency and cost-effectiveness of large-scale production. The variability observed in the data suggests the presence of influencing factors that require careful consideration and control.

By analyzing and optimizing the spray drying process for magnesium citrate with a 3:2 ratio, it becomes possible to enhance the yield and minimize fluctuations. These findings contribute to the broader understanding of spray drying techniques for organic derivatives, paving the way for further advancements in the production and application of magnesium citrate in various industries.

5.3.5 FT-IR analysis of magnesium citrate

Fourier Transform Infrared (FT-IR) spectroscopy is a powerful analytical technique widely used in chemical and material science research. It provides valuable insights into the molecular structure, functional groups, and chemical composition of substances. FT-IR spectroscopy operates based on the principle of measuring the absorption of infrared radiation by a sample[92].

In this technique, an infrared beam is directed onto the sample, and the resulting interaction between the radiation and the sample's molecules leads to the absorption of specific frequencies of infrared light. The absorbed frequencies correspond to the vibrations of different chemical bonds and functional groups within the molecules, providing a unique fingerprint for each compound. FT-IR spectroscopy offers several advantages over conventional dispersive spectroscopy methods. It utilizes a Fourier transform algorithm to convert the time-domain signal into a frequency-domain spectrum, resulting in higher sensitivity and improved signal-to-noise ratio. This enables precise and accurate measurements of even weak infrared signals. The obtained FT-IR spectra consist of a series of peaks and bands that correspond to specific molecular vibrations. These spectra can be analyzed and compared to reference spectra in databases to identify unknown compounds and verify the presence of specific functional groups. Additionally, FT-IR spectroscopy allows for the quantitative analysis of compounds, making it a valuable tool in various fields, including chemistry, pharmaceuticals, polymers, and environmental science.

In the context of the research conducted on the synthesis of magnesium citrate, FT-IR spectroscopy plays a crucial role in confirming the successful formation of the desired compounds. By comparing the obtained IR spectra with reference spectra, it becomes possible to identify characteristic peaks associated with the carbonyl group and observe changes in their position and shape due to the presence of magnesium. This information aids in the characterization and quality assessment of the synthesized compounds.

Figure 5-8 provides a detailed analysis of the infrared (IR) spectra for the obtained compounds, as well as the citric acid reagent. The IR spectra offer valuable information about the chemical structure and functional groups present in the compounds, enabling their identification and comparison with existing scientific literature.

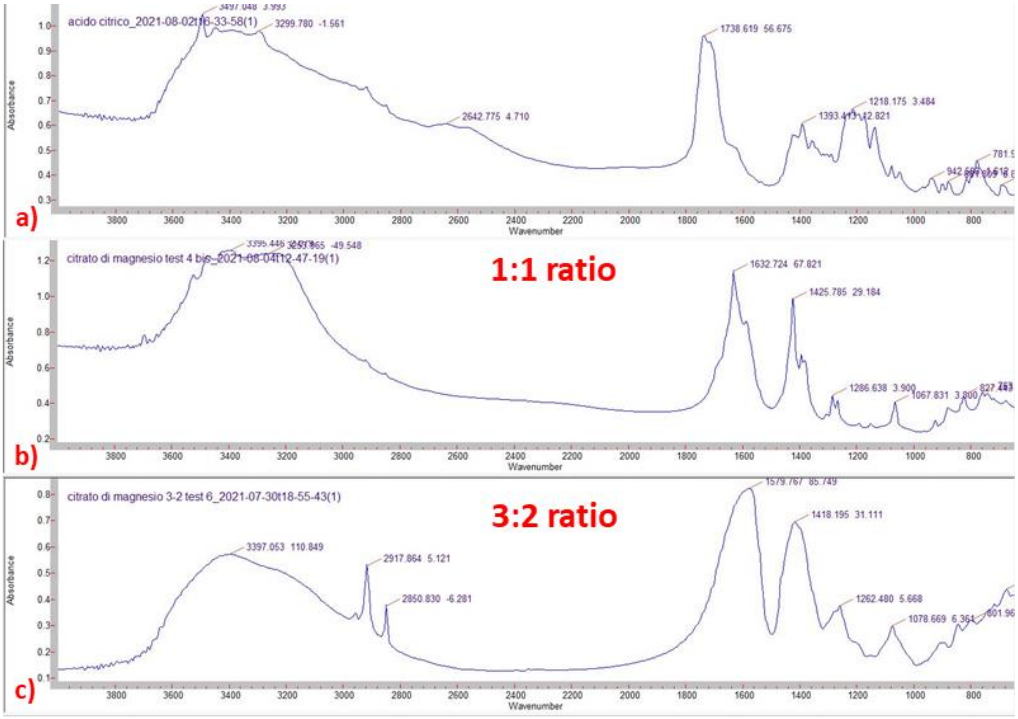

Figure 5-8: IR spectrum of a) citric acid, b) magnesium citrate (1:1) and magnesium citrate (3:2).

Initially, the IR spectrum of citric acid, the starting reagent, exhibits a characteristic narrow peak above 1700 wavenumbers, corresponding to the carbonyl group. However, after the synthesis process, notable changes occur in the position and shape of the carbonyl peak. Both compounds obtained, regardless of the stoichiometric ratio (1:1 or 3:2), display a shift towards lower wavenumbers, indicating a modification in the carbonyl group's environment. In the obtained compounds, the carbonyl peak is observed below 1600 wavenumbers, consistent with previous literature reports. This shift can be attributed to the formation of magnesium citrate compounds, where the presence of magnesium alters the electronic properties of the carbonyl group, leading to the observed change in wavenumber.

Interestingly, the influence of magnesium is also evident in the widening of the carbonyl peak. While the compound with a 1:1 ratio exhibits a relatively narrow peak, the compound with a 3:2 ratio shows a significantly broader peak. This broadening effect can be attributed to the interaction between the magnesium cation and the carbonyl oxygen atom, which affects the vibrational energy and results in a wider peak. These observations are in accordance with the information available in the Spectrabase database and confirm the successful synthesis of magnesium citrate compounds[93,94].

By comparing the obtained compounds' IR spectra with the literature data, it is evident that the compounds can be easily distinguished from the citric acid reagent based on their characteristic peaks. The shift in the carbonyl peak position and the widening effect induced by the presence of magnesium provide clear indications of the successful formation of the desired magnesium citrate compounds.

The analysis of the IR spectra not only validates the effectiveness of the synthesis process but also enhances our understanding of the chemical properties of the compounds. This information is crucial for ensuring the quality and consistency of the synthesized compounds in the nutraceutical and pharmaceutical

industries. Moreover, the obtained IR spectra serve as a valuable reference for future research and development of magnesium citrate derivatives, facilitating their characterization and identification in various applications.

The application of FT-IR spectroscopy in the analysis of the magnesium citrate synthesis process not only highlights its effectiveness but also emphasizes the importance of spectroscopic techniques in understanding the chemical properties and structural characteristics of organic compounds. By harnessing the power of FT-IR spectroscopy, researchers can gain valuable insights into the composition and behavior of compounds, paving the way for further advancements and applications in various scientific disciplines.

5.4 Synthesis of magnesium stearate

Magnesium stearate, a compound widely used as an excipient in pharmaceutical formulations, plays a crucial role in the production of solid dosage forms such as tablets and capsules. Apart from its functionality as a lubricant and flow enhancer, magnesium stearate also aids in the prevention of sticking and capping during tablet compression.

The synthesis of magnesium stearate involves the reaction between stearic acid, a long-chain fatty acid, and magnesium hydroxide. The synthesis scheme for magnesium stearate is depicted in Figure 5-9. By combining these two components, a salt known as magnesium stearate is formed. This process is typically carried out in a controlled environment to ensure the desired reaction kinetics and product quality.

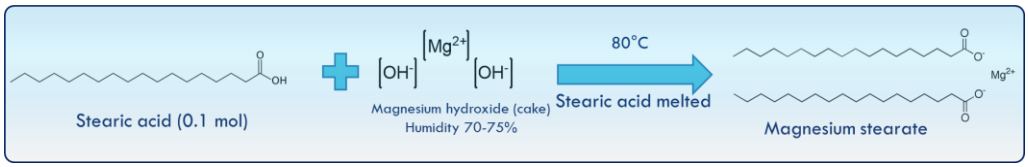

Figure 5-9: scheme of preparation of magnesium stearate.

During the synthesis, the molten stearic acid provides the fatty acid component necessary for the reaction, while the magnesium hydroxide acts as the magnesium source. It is important to note that the absence of water in this reaction is intentional, as the hydrophobic nature of magnesium stearate makes it less reactive in the presence of moisture. This choice of reaction conditions ensures optimal conversion and purity of the product.

Table 5.4 summarizes the results of various tests conducted to synthesize magnesium stearate. Stoichiometric amounts of stearic acid and magnesium hydroxide were used in most cases, except for test 1, which aimed to evaluate the impact of different reactant ratios on the yield. By employing stoichiometric quantities, the synthesis process aims for maximum conversion of the reactants into magnesium stearate.

Table 5-4: summary of the operative condition of synthesis of magnesium stearate.

test	stearic acid (g)	magnesium hydroxide (g)	final mass (g)	theoretical final mass (g)	yield	Mg (%)
1	14.22	1.46	15.55	15.68	99.1%	87.5
2	14.22	5.83	19.39	20.05	96.7%	96.9
3	14.22	5.83	19.32	20.05	96.3%	98.9

The theoretical final mass is calculated as the sum of the reagents: stearic acid and magnesium hydroxide by equation (5.3):

$$\text{theoretical final mass} = \text{stearic acid} + \text{magnesium hydroxide} \qquad (5\text{-}3)$$

The yield, expressed as a percentage, represents the ratio of the final mass obtained after the synthesis to the theoretical final mass by equation (5.4):

$$yeld = \frac{final\ mass}{\text{theoretical final mass}} * 100 \qquad (5\text{-}4)$$

Following the completion of the reaction, the resulting product is a viscous solid with a melting point of 88.5 °C. To ensure thorough completion of the reaction

and to eliminate any residual impurities, the product is subjected to further processing. This involves transferring the product to an oven and maintaining it at a temperature of 85 °C for an extended period, typically overnight. These additional steps help enhance the purity and consistency of the final magnesium stearate product.

To verify the successful synthesis of magnesium stearate, Fourier Transform Infrared (FT-IR) spectroscopy is employed. FT-IR spectroscopy provides valuable insights into the molecular structure and functional groups present in a compound. In this case, the FT-IR spectra of stearic acid, magnesium stearate, and magnesium hydroxide are compared.

Figure 5-10 displays the comparison between the spectra of stearic acid and magnesium stearate.

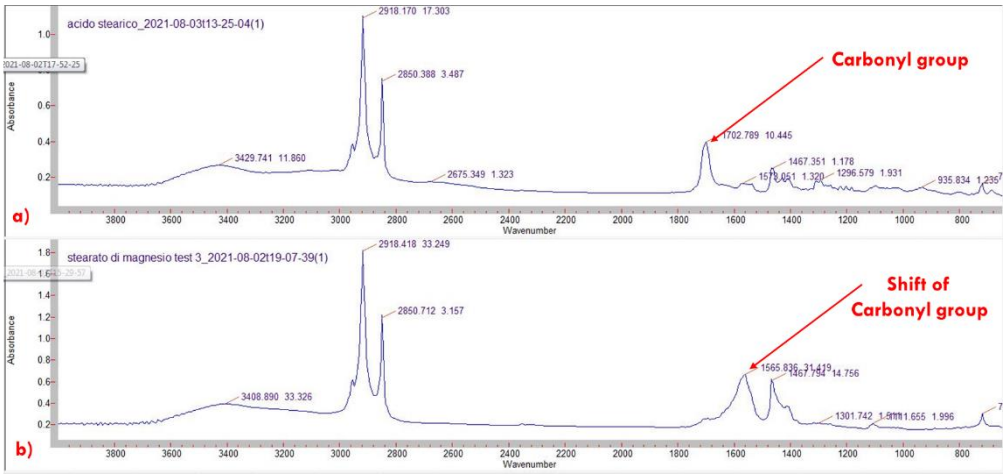

Figure 5-10: IR spectrum of a) stearic acid, b) magnesium stearate.

It is evident from the spectra that the presence of magnesium in the magnesium stearate sample causes a significant shift in the carbonyl signal compared to stearic acid. The carbonyl peak in stearic acid appears at approximately 1702 wavenumbers, while in magnesium stearate, it shifts to around 1565 wavenumbers. This shift in the carbonyl peak is attributed to the coordination of magnesium with the carboxylate group of stearic acid. These findings align

with the data available in the Spectrabase database, further supporting the successful synthesis of magnesium stearate[95,96].

Furthermore, Figure 5-11 presents a comparison between the spectra of magnesium stearate and magnesium hydroxide.

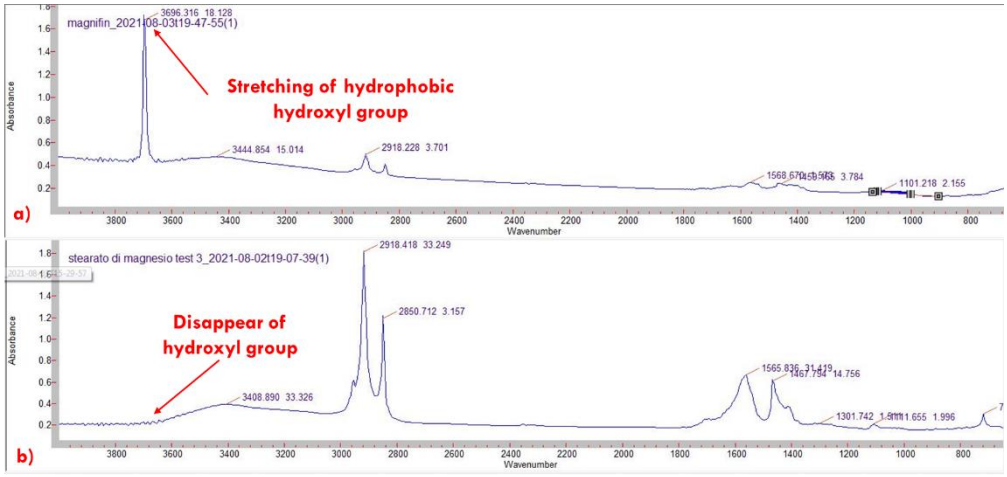

Figure 5-11: IR spectrum of a) magnesium hydroxide, b) magnesium stearate.

Magnesium hydroxide is characterized by a distinctive hydroxyl peak in the region of 3600-3700 wavenumbers. However, in the spectrum of magnesium stearate, this hydroxyl peak is absent. The absence of the hydroxyl peak confirms that the reaction between stearic acid and magnesium hydroxide has been completed, and the hydroxide is no longer present in the final product.

In conclusion, the synthesis of magnesium stearate involves the reaction between stearic acid and magnesium hydroxide under controlled conditions. The resulting product is a vital excipient widely used in pharmaceutical formulations. The use of FT-IR spectroscopy provides valuable evidence of the successful synthesis, demonstrating the chemical transformation and absence of starting materials in the final magnesium stearate product. These findings support the suitability and quality of magnesium stearate for various pharmaceutical applications.

5.5 Synthesis of magnesium aspartate

Magnesium aspartate, an organic salt composed of L-aspartate and magnesium, holds significant importance as a widely used compound in excipients and food supplements. It is worth noting that magnesium deficiency can contribute to various diseases, underscoring the significance of introducing dietary supplements for individuals with such deficiencies. Researchers, like Schmidbaur et al.[97] in the 1990s, have advocated for the formation of magnesium-based supplements using natural amino acids. By combining the use of a compound with high nutritional value, such as L-aspartic acid, with the addition of magnesium, a synergistic effect can be achieved.

Following the general synthesis scheme discussed in Section 5.2, the synthesis of magnesium aspartate follows a similar approach. Figure 5-12 provides a summary scheme, which is a modification of the scheme reported by Grigoryan et al.[98] While Grigoryan et al. used magnesium oxide, this modified scheme utilizes a stoichiometric amount of aspartic acid added to a slurry of magnesium hydroxide.

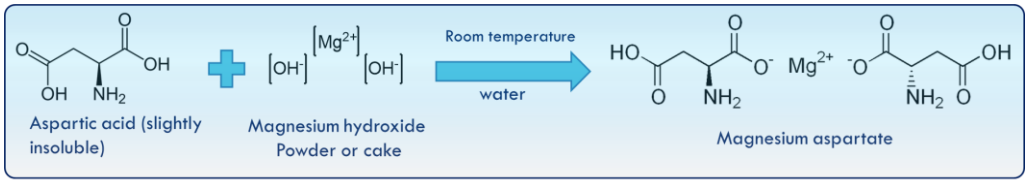

Figure 5-12: scheme of preparation of magnesium aspartate.

Aspartic acid, although slightly soluble, exhibits higher solubility compared to magnesium hydroxide. The reaction takes place in batches at room temperature, and over time, the initially cloudy suspension becomes clearer, indicating the formation of magnesium aspartate. To remove any unreacted compounds, the solution is filtered using a vacuum filtration system before further analysis and treatment.

Table 5 summarizes the results of the tests carried out during the synthesis of magnesium aspartate. In order to obtain magnesium aspartate powder, the evaporation method was employed. However, due to the magma density of the resulting product being below the standards for spray drying, an alternative approach was adopted. The solution was evaporated using a rotavapor, ensuring a quantitative yield. Subsequent analyses were then conducted to quantify and characterize the compound.

Table 5-5: summary of the operative condition of synthesis of magnesium aspartate.

test	acid aspartic (g)	magnesium hydroxide cake (g)	water (ml)	magnesium aspartate in solution (g/L)	recovery (%)	Mg (%)
1	10.57	5.03	100	42.18	99.1	96.9
2	10.57	5.03	100	39.39	98.9	99.7
3	10.57	5.03	100	44.30	99.5	99.5
4	12.44	6.15	100	41.24	99.0	99.4
5	12.44	6.15	100	43.55	99.3	98.7

Characterization of the synthesized magnesium aspartate involves several analytical techniques. Ion chromatography is employed to determine the concentration of magnesium ions present in the solution, which allows for the evaluation of the magnesium aspartate concentration. It is important to note that magnesium and aspartate are present in a stoichiometric ratio of 1:2.

Furthermore, FT-IR analysis (Figure 5-13) is conducted to gain insights into the formation of the desired product. Comparing the FT-IR spectra of aspartic acid and magnesium aspartate, significant differences are observed. Aspartic acid exhibits several intense peaks within the range of 800-1700 wavenumbers, with peaks near 1700 wavenumbers corresponding to the carbonyl group, while others correspond to carbon-carbon and carbon-oxygen stretching vibrations. In contrast, the FT-IR spectrum of magnesium aspartate demonstrates a noticeable

shift in the carbonyl peak to a lower wavenumber (around 1600), indicating the successful formation of the desired compound.

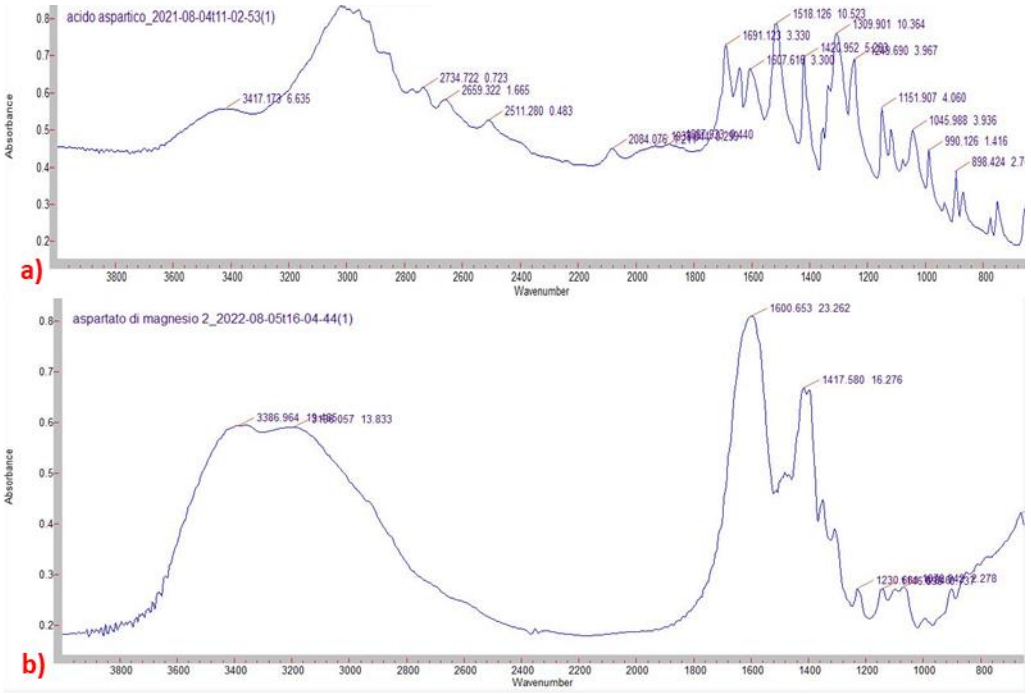

Figure 5-13: IR spectrum of a) aspartic acid, b) magnesium aspartate.

Notably, the spectrum of magnesium aspartate does not exhibit the narrow and deep peak characteristic of magnesium hydroxide, which typically appears around 3700 wavenumbers. These findings align with the existing literature, including the Spectrabase database[99].

To summarize, the synthesis of magnesium aspartate involves the reaction between aspartic acid and magnesium hydroxide, resulting in the formation of a stoichiometrically balanced organic salt. The characterization of the product through ion chromatography and FT-IR spectroscopy confirms the successful synthesis of magnesium aspartate, showcasing its potential use as a dietary supplement. The utilization of natural amino acids, such as L-aspartic acid, in combination with magnesium, offers a beneficial approach for the development of nutritional supplements to address magnesium deficiency effectively.

5.6 Final remarks

Magnesium plays a crucial role in human health, and its deficiency can lead to the development of various pathologies. As highlighted by numerous scientific studies and literature, supplementing magnesium is essential to address this deficit and improve overall health. The non-toxic nature of magnesium also makes it an excellent candidate for producing excipients used in pharmacological products, such as magnesium stearate. The interest in utilizing magnesium hydroxide to develop nutraceutical supplements is well-founded. The source of magnesium in this case has a natural origin, derived from bitterns, which are concentrated seawater solutions. This natural source of magnesium offers a sustainable and environmentally friendly option for supplement production.

In our laboratory-scale synthesis experiments, we followed the available literature sources and employed batch reactors. The results have been promising, yielding high-purity compounds suitable for nutraceutical applications. However, further research and development are needed to scale up the synthesis process. Integrating magnesium obtained from natural sources with organic acids derived from natural or waste sources would be the next step in our pursuit. This approach aligns with the principles of a circular economy, where waste materials can be transformed into valuable resources. The transformation of magnesium hydroxide into nutraceutical supplements holds great potential in addressing magnesium deficiency and promoting human health. By utilizing magnesium from natural sources, such as concentrated seawater, we can reduce dependence on finite resources and promote sustainable utilization. Moreover, integrating organic acids derived from natural or waste sources into the synthesis process contributes to the principles of a circular economy. This approach not only leads to the production of high-quality magnesium-based supplements but also aligns with broader goals of environmental conservation and resource efficiency.

As we embrace a circular economy perspective, we not only address the nutritional needs of individuals but also contribute to the sustainable development of our society. The conversion of magnesium hydroxide into nutraceutical supplements exemplifies how scientific research and innovation can create synergies between human health, environmental sustainability, and resource conservation. It offers a pathway towards a more resilient and balanced future.

In conclusion, the transformation of magnesium hydroxide into nutraceutical supplements represents a promising avenue for addressing magnesium deficiency and promoting human health. Leveraging magnesium from natural sources, such as concentrated seawater, and integrating it with organic acids derived from natural or waste sources offers a sustainable approach to supplement production. By embracing the principles of the circular economy, we can not only improve individual well-being but also contribute to the long-term conservation of resources and environmental sustainability. Continued research and development in this field are essential for realizing the full potential of magnesium-based supplements and advancing our understanding of their benefits to human health.

6 Conclusions

This thesis work has focused on the recovery of raw materials with a high added value from waste saline streams, always in line with the principles of circular economy. By viewing waste as an opportunity to obtain valuable resources, the aim was to minimize environmental impact and create an integrated cycle of resource utilization. The successful implementation of this approach not only reduces waste generation but also conserves natural resources, thus promoting sustainable practices.

Two European projects, Zero Brine and SEArcularMINE, played a significant role in validating the concept of waste recovery. These projects specifically targeted the recovery of raw materials from waste solutions, such as brines and bitterns. The concentration of these solutions, exceeding that of seawater, made them ideal for the extraction of valuable compounds like magnesium hydroxide.

The Zero Brine project focused on two industrial processes: water softening and coal extraction. The brines generated during these processes were utilized as feed streams. The synthesis of magnesium hydroxide was successfully achieved using different equipment and several operating conditions. Comprehensive characterization, including SEM, laser scattering, XRD, and TGA, confirmed the high purity and suitable morphological properties of the obtained magnesium hydroxide solids. The purification process resulted in products with purity levels of up to 96%.

In the case of brine from coal extraction, the recovery of magnesium was carried out using a patented prototype based on membrane crystallization technology known as CrIEM. This innovative approach allowed the recovery of magnesium using calcium hydroxide as a cheap but “interacting” alkaline reagent. Laboratory-scale tests demonstrated that the CrIEM process could produce magnesium hydroxide with purities of at least 94%. The ability to recover high-

purity products from challenging waste streams showcased the potential of this technology for future industrial applications.

In a second phase of the thesis, the work also focused on the recovery of valuable trace elements, with lithium being a key target. A preliminary study conducted within the SEArcularMINE project explored the recovery of lithium from bitterns. By simulating the process and conducting laboratory-scale tests, the optimal conditions for lithium recovery were determined. The findings indicated that a temperature of at least 50°C and a minimum concentration of 5 g/L of lithium ions were necessary to achieve a recovery rate of 40% in the form of lithium carbonate (Li_2CO_3). This research opens room for further investigation into the scalable recovery of lithium and other trace elements from waste solutions.

Furthermore, a quick test, called the brine potential test (BPT), for evaluating the potential of bitterns as a source of valuable resources has been developed and validated with real bitterns from sea saltworks. The BPT provided a simplified and low-error method for screening bittern samples, enabling rapid decision-making in resource recovery operations. The validation of the BPT through comparison with standardized analytical methods, such as ion chromatography, confirmed its reliability and suitability for industrial applications.

In the final phase of the thesis, the attention was posed to the synthesis of Magnesium organic derivatives using magnesium hydroxide recovered from bitterns. By reacting the high-purity magnesium hydroxide with organic salts like citric acid, stearic acid, and aspartic acid, the desired organic derivatives were obtained. FT-IR analysis played a crucial role in confirming the successful transformation of reagents into the desired products. These preliminary syntheses, supported by scientific literature, demonstrated the feasibility of utilizing magnesium hydroxides from waste streams for the production of nutraceutical and pharmaceutical compounds.

In conclusion, the thesis work showcased the significant potential of waste brines valorization within a circular economy framework. The successful implementation of novel magnesium recovery schemes, alongside the development of characterization techniques and the brine potential test, contributed to advancing knowledge, technology, and best practices in raw material recovery from birnes.

This research represents a contribution towards a sustainable and resource-efficient future, where waste brine is no longer seen as a problem but as a valuable resource for economic, environmental, and societal benefits. Continued research and collaboration in this field are vital for widespread adoption of circular economy principles and the realization of a more sustainable and resilient society.

7 Nomenclature

C_{sat} Equilibrium concentration (mol/L)

C^*_{sat} Maximum conventional solubility (mol/L)

ΔC Difference of the current solute concentration and the equilibrium concentration (mol/l)

a Activity (mol l^{-1})

Ac Crystal area (m^2)

b Nucleation rate order with respect to supersaturation (-)

B° Nucleation speed (# s m^{-3})

C Molar concentration (mol/L)

C^{Mg}_{Brine} Magnesium concentration in the brine (mol/l)

d10 Diameter at the intercepts for 10% of cumulative volume (µm)

d50 Diameter at the intercepts for 50% of cumulative volume (µm)

d90 Diameter at the intercepts for 90% of cumulative volume (µm)

f Void fanning friction factor [-]

F^{Brine}_{in} Inlet volume flow-rate of brine (l/min)

F^{NaOH}_{in} Inlet volume flow-rate of sodium hydroxide (l/min)

g Growth rate order with respect to supersaturation (-)

G Linear growth rate (m/s)

k_g Growth rate coefficient (µm s^{-1})

k_n Nucleation rate coefficient (# s^{-1} $g_{crystal}^{-1}$)

L Particle length (m)

m Molal concentration (mol kg^{-1})

M_w^{Mg}	Molecular weight of magnesium (kg/mol)
$M_W^{Mg(OH)_2}$	Molecular weight of magnesium hydroxide (kg/mol)
N	crystals concentration
n	Population density (# m^{-3} m)
R_G	Growth rate (kg m^2 s)
S	Supersaturation degree (-)
V	volume (mL)
vf	Volume crystal factor (-)

Greek letters

γ	Activity coefficient (-)
β	Form crystal factor (-)
ρ	solution density [kg m^{-3}]

Acronyms

AEM	Anion exchange membrane
CSD	crystal size distribution
ED	Electrodialysis
CrIEM	Crystallizer with Ion Exchange Membrane
CRWs	critical raw materials
CSD	Crystal size distribution
CSTR	Continuous-flow Stirred-Tank Reactor
EU	European Union

FDA	Food and Drug Administration
IC	Ion chromatography
ICP-AES	Inductively coupled plasma atomic emission spectroscopy
IEM	Ion exchange membrane
IXE	Ion exchange resins
LCE	lithium carbonate equivalent
MD	Membrane distillation
MED	Multiple effect distillation
MDC	Membrane Distillation Crystallization
MFCDI	Membrane Flow Capacitive DeIonization
MF-PFR	Multiple Feed – Flow Reactor
MSF	Multi-Stage Flash
MSMPR	Mixed-suspension, mixed-product-removal
NaCl	sodium chloride
NF	nano-filtration
NHANES	National Health and Nutrition Examination Survey
RO	Reverse osmosis
SEM	Scanning electron microscope
SUT	Silesian University of Technology
TDS	Total Dissolved solids
TGA	Thermogravimetric analysis
TU-Delft	Delft University of Technology
UNIPA	Università degli Studi di Palermo

WPs	work packages
X	X-ray quanta
XRD	X-ray crystallography

8 References

1. Roberts, D. A., Johnston, E. L. & Knott, N. A. Impacts of desalination plant discharges on the marine environment: A critical review of published studies. *Water Res.* **44**, 5117–5128 (2010).

2. Mavukkandy, M. O., Chabib, C. M., Mustafa, I., Al Ghaferi, A. & AlMarzooqi, F. Brine management in desalination industry: From waste to resources generation. *Desalination* **472**, 114187 (2019).

3. Jones, E., Qadir, M., van Vliet, M. T. H., Smakhtin, V. & Kang, S. mu. The state of desalination and brine production: A global outlook. *Sci. Total Environ.* **657**, 1343–1356 (2019).

4. Panagopoulos, A., Haralambous, K. J. & Loizidou, M. Desalination brine disposal methods and treatment technologies - A review. *Sci. Total Environ.* **693**, 133545 (2019).

5. Chang, J. S. Understanding the role of ecological indicator use in assessing the effects of desalination plants. *Desalination* **365**, 416–433 (2015).

6. Mavukkandy, M. O., Chabib, C. M., Mustafa, I., Al Ghaferi, A. & AlMarzooqi, F. Brine management in desalination industry: From waste to resources generation. *Desalination* **472**, 114187 (2019).

7. Garrote-Moreno, A. *et al.* Plant water relations and ion homoeostasis of Mediterranean seagrasses (Posidonia oceanica and Cymodocea nodosa) in response to hypersaline stress. *Mar. Biol.* **162**, 55–68 (2015).

8. Loganathan, P., Naidu, G. & Vigneswaran, S. Mining valuable minerals from seawater: A critical review. *Environ. Sci. Water Res. Technol.* **3**, 37–53 (2017).

9. Cipollina, A. *et al.* Integrated production of fresh water, sea salt and magnesium from sea water. *Desalin. Water Treat.* **49**, 390–403 (2012).

10. Turek, M., Dydo, P. & Klimek, R. Salt production from coal-mine brine in NF - evaporation - crystallization system. *Desalination* **221**, 238–243 (2008).

11. Quist-Jensen, C. A., Macedonio, F. & Drioli, E. Membrane crystallization for salts recovery from brine—an experimental and theoretical analysis.

Desalin. Water Treat. **57**, 7593–7603 (2016).

12. Turek, M., Mitko, K., Chorzewska, M. & Dydo, P. Use of the desalination brines in the saturation of membrane electrolysis feed. *Desalin. Water Treat.* **51**, 2749–2754 (2013).

13. Steele, J. H., Thorpe, S. A. & Turekian, K. K. *Encyclopedia Of Ocean Sciences 2nd Edition*. *Elsevier Ltd* **4**, (2011).

14. Shahmansouri, A., Min, J., Jin, L. & Bellona, C. Feasibility of extracting valuable minerals from desalination concentrate: A comprehensive literature review. *J. Clean. Prod.* **100**, 4–16 (2015).

15. Mg, G. *et al.* 2016 Market Research Report on Global Mg (OH) 2 Industry Chapter One Mg (OH) 2 Industry Overview. (2016).

16. QYR Chemical & Material Research Center. Europe Magnesium Hydroxide Industry 2016 Market Research Report. 65 (2016).

17. Nishihama, S., Onishi, K. & Yoshizuka, K. Selective recovery process of lithium from seawater using integrated ion exchange methods. *Solvent Extr. Ion Exch.* **29**, 421–431 (2011).

18. Ryu, J. *et al.* Strontium ion (Sr2+) separation from seawater by hydrothermally structured titanate nanotubes: Removal vs. recovery. *Chem. Eng. J.* **304**, 503–510 (2016).

19. Naidu, G., Nur, T., Loganathan, P., Kandasamy, J. & Vigneswaran, S. Selective sorption of rubidium by potassium cobalt hexacyanoferrate. *Sep. Purif. Technol.* **163**, 238–246 (2016).

20. Drioli, E., Criscuoli, A. & Curcio, E. Integrated membrane operations for seawater desalination. *Desalination* **147**, 77–81 (2002).

21. Reig, M., Farrokhzad, H., Van der Bruggen, B., Gibert, O. & Cortina, J. L. Synthesis of a monovalent selective cation exchange membrane to concentrate reverse osmosis brines by electrodialysis. *Desalination* **375**, 1–9 (2015).

22. Macedonio, F. & Drioli, E. Hydrophobic membranes for salts recovery from desalination plants. *Desalin. Water Treat.* **18**, 224–234 (2010).

23. Ezugbe, E. O. & Rathilal, S. Membrane technologies in wastewater

treatment: A review. *Membranes (Basel).* **10**, (2020).

24. Curcio, E., Criscuoli, A. & Drioli, E. Membrane crystallizers. *Ind. Eng. Chem. Res.* **40**, 2679–2684 (2001).

25. Drioli, E., Di Profio, G. & Curcio, E. Progress in membrane crystallization. *Curr. Opin. Chem. Eng.* **1**, 178–182 (2012).

26. Di Profio, G., Salehi, S. M., Curcio, E. & Drioli, E. 3.11 Membrane Crystallization Technology. *Compr. Membr. Sci. Eng.* **3**, 297–317 (2017).

27. Rahman, M. *et al.* Production of slow release crystal fertilizer from wastewaters through struvite crystallization – A review. *Arab. J. Chem.* **7**, 139–155 (2014).

28. Lu, H. *et al.* Crystallization techniques in wastewater treatment: An overview of applications. *Chemosphere* **173**, 474–484 (2017).

29. Rubio, J. & Tessele, F. Removal of heavy metal ions by adsorptive particulate flotation. *Miner. Eng.* **10**, 671–679 (1997).

30. Suzuki, K., Tanaka, Y., Osada, T. & Waki, M. Removal of phosphate, magnesium and calcium from swine wastewater through crystallization enhanced by aeration. *Water Res.* **36**, 2991–2998 (2002).

31. Pilarska, A. A., Klapiszewski, Ł. & Jesionowski, T. Recent development in the synthesis, modification and application of Mg(OH)2 and MgO: A review. *Powder Technol.* **319**, 373–407 (2017).

32. Ren, M., Yang, M., Li, S., Chen, G. & Yuan, Q. High throughput preparation of magnesium hydroxide flame retardant: Via microreaction technology. *RSC Adv.* **6**, 92670–92681 (2016).

33. Hsu, J. P. & Nacu, A. Preparation of submicron-sized Mg(OH)2particles through precipitation. *Colloids Surfaces A Physicochem. Eng. Asp.* **262**, 220–231 (2005).

34. Song, X., Tong, K., Sun, S., Sun, Z. & Yu, J. Preparation and crystallization kinetics of micron-sized Mg(OH)2in a mixed suspension mixed product removal crystallizer. *Front. Chem. Sci. Eng.* **7**, 130–138 (2013).

35. Li, X. *et al.* Preparation of magnesium hydroxide flame retardant from light calcined powder by ammonia circulation method. *Powder Technol.*

260, 98–104 (2014).

36. Cipollina, A. *et al.* Reactive crystallisation process for magnesium recovery from concentrated brines. *Desalin. Water Treat.* **55**, 2377–2388 (2015).

37. Jaskula, B. B. W. 2012 Minerals Yearbook, Magnesium Compounds. *Geol. Surv. Reston, VA, USA, 2013* 1–5 (2013).

38. Mohammad, A. F., El-Naas, M. H., Al-Marzouqi, A. H., Suleiman, M. I. & Al Musharfy, M. Optimization of magnesium recovery from reject brine for reuse in desalination post-treatment. *J. Water Process Eng.* **31**, 100810 (2019).

39. Dong, H., Unluer, C., Yang, E. H. & Al-Tabbaa, A. Synthesis of reactive MgO from reject brine via the addition of NH4OH. *Hydrometallurgy* **169**, 165–172 (2017).

40. Cipollina, A. *et al.* Reattore e procedimento per effettuare reazioni selettive, IT patent: 102015000042831, 2015. 2–5 (2015).

41. Etal, H. A. R. US2405055-Patent-Magnesium hydroxide from seawater. (1943).

42. La Corte, D. *et al.* A novel ionic exchange membrane crystallizer to recover magnesium hydroxide from seawater and industrial brines. *Membranes (Basel).* **10**, 1–14 (2020).

43. Vassallo, F. *et al.* A pilot-plant for the selective recovery of magnesium and calcium from waste brines. *Desalination* **517**, 115231 (2021).

44. Mullin, J. W. Crystallisation, 4th Edition By J. W. Mullin. 2001. Butterworth Heinemann: Oxford, UK. 600 pp. £75.00. ISBN 075-064-833-3. Organic Process Research & Development6, 201–202 (2002).

45. Alamdari, A., Rahimpour, M. R., Esfandiari, N. & Nourafkan, E. Kinetics of magnesium hydroxide precipitation from sea bittern. *Chem. Eng. Process. Process Intensif.* **47**, 215–221 (2008).

46. Wu, J. S., Du, J. & Gao, Y. M. Crystal growth morphology of magnesium hydroxide. *Turkish J. Chem.* **38**, 402–412 (2014).

47. Barba, D., Brandani, V., Di Giacomo, G. & Foscolo, P. U. Magnesium

oxide production from concentrated brines. *Desalination* **33**, 241–250 (1980).

48. Wulandari, W., Brooks, G. a, Rhamdhani, M. a, Monaghan, B. J. & Sciences, I. Magnesium : Current and Alternative Production Routes. *Chemeca 2010 Eng. Edge; 26-29 Sept. 2010, Hilt. Adelaide, South Aust.* 347 (2008). doi:10.1002/hrdq.1020

49. Baird, T., Braterman, P. S., Cochrane, H. D. & Spoors, G. Magnesium hydroxide precipitation as studied by gel growth methods. *J. Cryst. Growth* **91**, 610–616 (1988).

50. Lu, L. *et al.* Reactive Crystallization Kinetics of Magnesium Hydroxide in the Mg(NO3)2–NaOH System. *Cryst. Res. Technol.* **53**, 1–10 (2018).

51. Vassallo, F., La Corte, D., Cipollina, A., Tamburini, A. & Micale, G. High purity recovery of magnesium and calcium hydroxides from waste brines. *Chem. Eng. Trans.* **86**, 931–936 (2021).

52. Bevacqua, M. *et al.* A continuous plug flow reactor for magnesium recovery from concentrated brine. *Desalin. Water Treat.* 10–14 (2015).

53. Vassallo, F. *et al.* A simulation tool for ion exchange membrane crystallization of magnesium hydroxide from waste brine. *Chem. Eng. Res. Des.* **173**, 193–205 (2021).

54. Al Mutaz, I. S. & Wagialia, K. M. Production of magnesium from desalination brines. *Resour. Conserv. Recycl.* **3**, 231–239 (1990).

55. Liu, W., Xu, H., Shi, X., Yang, X. & Wang, X. Improved Lime Method to Prepare High-Purity Magnesium Hydroxide and Light Magnesia from Bischofite. *Jom* **71**, 4674–4680 (2019).

56. M., Y. & E., R. Ion Exchange Chromatography - An Overview. *Column Chromatogr.* 1–30 (2013). doi:10.5772/55652

57. Malvern. Mastersizer 2000 essentials. (2007).

58. No, L. Thermal Taichi Decomposition of Magnesium Hydroxide NAKAMURA SATO , Shuji IKOMA , Fusaji OZAWA and Takato (Department of Applied Chemistry , Faculty of Engineering , Shizuoka University). **181**, (1982).

59. A, D. A. S. F. J. H. S. R. C. D. M. W. C. L. . *Skoog and West's Fundamentals of analytical chemistry*. (2014).

60. Henrist, C., Mathieu, J. P., Vogels, C., Rulmont, A. & Cloots, R. Morphological study of magnesium hydroxide nanoparticles precipitated in dilute aqueous solution. *J. Cryst. Growth* **249**, 321–330 (2003).

61. Kumari, L., Li, W. Z., Vannoy, C. H., Leblanc, R. M. & Wang, D. Z. Synthesis, characterization and optical properties of Mg(OH)2micro-/nanostructure and its conversion to MgO. *Ceram. Int.* **35**, 3355–3364 (2009).

62. Zhang, Z. *et al.* Temperature- And pH-dependent morphology and FT-IR analysis of magnesium carbonate hydrates. *J. Phys. Chem. B* **110**, 12969–12973 (2006).

63. Chen, Y. *et al.* A novel preparation of nanosized hexagonal Mg(OH)2as a flame retardant. *Particuology* **24**, 177–182 (2016).

64. H. Strathmann. *ION-EXCHANGE MEMBRANE SEPARATION PROCESSES*. *Elsevier Ltd* **9th ed**, (2004).

65. Gomes, H. I., Mayes, W. M., Rogerson, M., Stewart, D. I. & Burked, I. T. Alkaline residues and the environment: A review of impacts, management practices and opportunities. *J. Clean. Prod.* **112**, 3571–3582 (2016).

66. Net, M., Id, L. & User, A. S. Roskill Information Services Ltd. Salt: Global Industry Markets and Outlook. (2014).

67. Virgili, F. GWI Q4 Desalination Market Review and Forecast Points to Some Improvement in Contracted Capacity. IDA News(2015).

68. Ghaffour, N., Bundschuh, J., Mahmoudi, H. & Goosen, M. F. A. Renewable energy-driven desalination technologies: A comprehensive review on challenges and potential applications of integrated systems. *Desalination* **356**, 94–114 (2015).

69. Loutatidou, S., Chalermthai, B., Marpu, P. R. & Arafat, H. A. Capital cost estimation of RO plants: GCC countries versus southern Europe. *Desalination* **347**, 103–111 (2014).

70. Gude, V. G. Desalination and sustainability - An appraisal and current perspective. *Water Res.* **89**, 87–106 (2016).

71. Alsabbagh, A., Aljarrah, S. & Almahasneh, M. Lithium enrichment optimization from Dead Sea end brine by chemical precipitation technique. *Miner. Eng.* **170**, 107038 (2021).

72. Meng, F., McNeice, J., Zadeh, S. S. & Ghahreman, A. Review of Lithium Production and Recovery from Minerals, Brines, and Lithium-Ion Batteries. *Miner. Process. Extr. Metall. Rev.* **42**, 123–141 (2021).

73. Ambrose, H. & Kendall, A. Understanding the future of lithium: Part 1, resource model. *J. Ind. Ecol.* **24**, 80–89 (2020).

74. An, J. W. *et al.* Recovery of lithium from Uyuni salar brine. *Hydrometallurgy* **117–118**, 64–70 (2012).

75. Zhu, S. G. *et al.* Recovery of Co and Li from spent lithium-ion batteries by combination method of acid leaching and chemical precipitation. *Trans. Nonferrous Met. Soc. China (English Ed.* **22**, 2274–2281 (2012).

76. King, D. E., Mainous, A. G., Geesey, M. E. & Woolson, R. F. Dietary Magnesium and C-reactive Protein Levels. *J. Am. Coll. Nutr.* **24**, 166–171 (2005).

77. Cicero, A. F. G. & Colletti, A. *Handbook of Nutraceuticals for Clinical Use*. (2018). doi:10.1007/978-3-319-73642-6

78. Jung, K. *et al.* Effect of Oral Intake of Lactiplantibacillus plantarum APsulloc. **331261**, (2022).

79. DiNicolantonio, J. J., O'Keefe, J. H. & Wilson, W. Subclinical magnesium deficiency: A principal driver of cardiovascular disease and a public health crisis. *Open Hear.* **5**, (2018).

80. Davis, D. R., Epp, M. D., Riordan, H. D. & Davis, D. R. Changes in USDA Food Composition Data for 43 Garden Crops, 1950 to 1999. *J. Am. Coll. Nutr.* **23**, 669–682 (2004).

81. Thomas, D. R. Vitamins in aging, health, and longevity. *Clin. Interv. Aging* **1**, 81–91 (2006).

82. Tarleton, E. K., Littenberg, B., MacLean, C. D., Kennedy, A. G. & Daley,

C. Role of magnesium in the treatment of depression. *PLoS One* **12**, 1–15 (2017).

83. McCabe, D., Lisy, K., Lockwood, C. & Colbeck, M. The impact of essential fatty acid, B vitamins, vitamin C, magnesium and zinc supplementation on stress levels in women: A systematic review. *JBI Database Syst. Rev. Implement. Reports* **15**, 402–453 (2017).

84. Asemi, Z. *et al.* Magnesium supplementation affects metabolic status and pregnancy outcomes in gestational diabetes: A randomized, double-blind, placebo-controlled trial. *Am. J. Clin. Nutr.* **102**, 222–229 (2015).

85. Setaro, L. *et al.* Magnesium status and the physical performance of volleyball players: effects of magnesium supplementation. *J. Sports Sci.* **32**, 438–445 (2014).

86. Vantage Market Research & Consultancy Services. All rights reserved. Magnesium Supplements Market Global Industry Assessment & Forecast (2016-2020).

87. Schuchardt, J. P. & Hahn, A. Intestinal Absorption and Factors Influencing Bioavailability of Magnesium- An Update. *Curr. Nutr. Food Sci.* **13**, 260–278 (2017).

88. Staszczuk, P. & Pekalska, J. Methods of Preparation of Magnesium Organic Compounds from Natural Dolomite. *Physicochem. Probl. Miner. Process.* **37**, 149–158 (2003).

89. Delaney, S. P. *et al.* Characterization of Synthesized and Commercial Forms of Magnesium Stearate Using Differential Scanning Calorimetry, Thermogravimetric Analysis, Powder X-Ray Diffraction, and Solid-State NMR Spectroscopy. *J. Pharm. Sci.* **106**, 338–347 (2017).

90. *Selvamuthukumaran, M. (Ed.). (2019). Handbook on Spray Drying Applications for Food Industries (1st ed.). CRC Press. https://doi.org/10.1201/9780429055133*.

91. Net, M., Id, L. & User, A. S. Operation Manual 93001 en B-290. 1–5 (2018).

92. Spectrometric Identification of Organic Compounds, 8th Edition Robert M. Silverstein, Francis X. Webster, David J. Kiemle, David L. Bryce; ISBN: 978-0-470-61637-6 September 2014.

93. Net, M., Id, L. & User, A. S. John Wiley & Sons, Inc. SpectraBase; SpectraBase Compound ID=lgXutBXIrF SpectraBase Spectrum ID=2fYCi7nfg0n citric acid https://spectrabase.com/spectrum/2fYCi7nfg0n. 1–5 (2018).

94. Wesolowski, M., Leyk, E. & Szynkaruk, P. Detection of magnesium compounds in dietary supplements and medicinal products by DSC, Infrared and Raman techniques. *J. Therm. Anal. Calorim.* **116**, 671–680 (2014).

95. Net, M., Id, L. & User, A. S. John Wiley & Sons, Inc. SpectraBase; SpectraBase Compound ID=vNzE0k9wS0 SpectraBase Spectrum ID=F522xY4dg4i Magnesium Stearate https://spectrabase.com/spectrum/F522xY4dg4i. 1–5 (2018).

96. Net, M., Id, L. & User, A. S. John Wiley & Sons, Inc. SpectraBase; SpectraBase Compound ID=7kH3z5zFF2C SpectraBase Spectrum ID=BZ8lc4t5qQm Magnesium hydroxide https://spectrabase.com/spectrum/BZ8lc4t5qQm. 1–5 (2018).

97. Schmidbaur, H., Classen, H. G. & Helbig, J. Aspartic and Glutamic Acid as Ligands to Alkali and Alkaline-Earth Metals: Structural Chemistry as Related to Magnesium Therapy. *Angew. Chemie Int. Ed. English* **29**, 1090–1103 (1990).

98. Grigoryan, I. V & Kompantseva, E. V. DEVELOPING METHODS OF PREPARATION AND QUANTITATIVE ANALYSIS OF MAGNESIUM ASPARTATE. **39**, 548–550 (2005).

99. John Wiley & Sons, Inc. SpectraBase; SpectraBase Compound ID=28np88IEo07 SpectraBase Spectrum ID=GujBgGXb76n Aspartate magnesium salt dihydrate https://spectrabase.com/spectrum/GujBgGXb76n. 1–5 (2018).